

1-1-1985

Thermodynamics of deformation.

Richard E. Lyon

University of Massachusetts Amherst

Follow this and additional works at: https://scholarworks.umass.edu/dissertations_1

Recommended Citation

Lyon, Richard E., "Thermodynamics of deformation." (1985). *Doctoral Dissertations 1896 - February 2014*. 945.
https://scholarworks.umass.edu/dissertations_1/945

This Open Access Dissertation is brought to you for free and open access by ScholarWorks@UMass Amherst. It has been accepted for inclusion in Doctoral Dissertations 1896 - February 2014 by an authorized administrator of ScholarWorks@UMass Amherst. For more information, please contact scholarworks@library.umass.edu.

312066 0278 5146 5

FIVE COLLEGE DEPOSITORY

THERMODYNAMICS OF DEFORMATION

A Dissertation Presented

By

RICHARD E. LYON

Submitted to the Graduate School of the
University of Massachusetts in partial fulfillment
of the requirements for the degree of

DOCTOR OF PHILOSOPHY

May 1985

Polymer Science and Engineering

Richard E. Lyon

©

All Rights Reserved

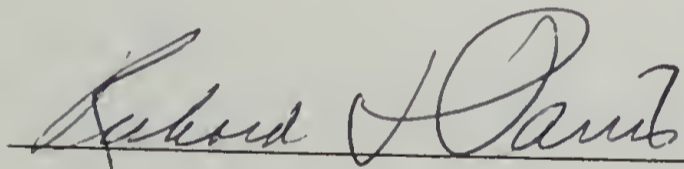
THERMODYNAMICS OF DEFORMATION

A Dissertation Presented

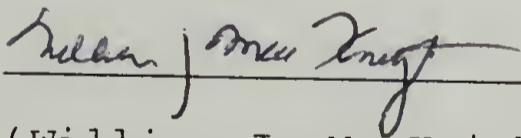
By

RICHARD EVAN LYON

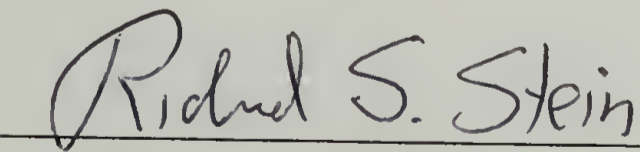
Approved as to style and content by:



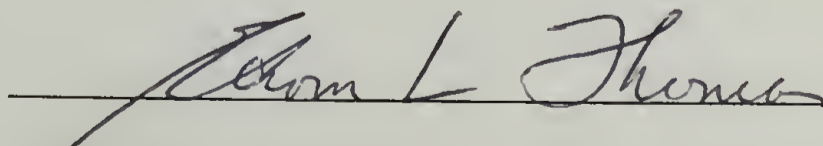
(Richard J. Farris), Committee co-Chairman



(William J. MacKnight), Committee co-Chairman



(Richard S. Stein), Member



(Edwin L. Thomas), Department Head
Polymer Science and Engineering Department

This thesis is dedicated to the memory of my parents Mary Dina and Richard John who started this whole thing, and to my wife Virginia and daughter Blair who saw it through to the end.

Acknowledgement

I would like to thank the DuPont Corporation and the Materials Research Laboratory of the University of Massachusetts for partial support for this project. In particular I would like to thank Richard J. Farris for his continued help and guidance throughout my graduate career, and William J. MacKnight for his moral support. I am also indebted to Richard S. Stein for many helpful discussions.

Abstract

The thermodynamics of uniaxial solid deformation was studied experimentally for a number of polymeric solids, including two polyurethane-urea elastomers, natural rubber, a thermoplastic elastomer and low density polyethylene. A deformation calorimeter was developed to measure the heat and work of uniaxial solid deformation and measurements were made on the above materials. A differential scanning calorimetry method was developed to characterize the melting behavior of stretched elastomers which were found to undergo stress-induced crystallization during stretching as deduced from the large but recoverable internal energy changes measured by deformation calorimetry during uniaxial extension and contraction. Wide angle x-ray diffraction and thermostatic measurements were also performed on the elastomers held in the extended state in order to characterize the amorphous-crystalline phase transition which occurs during deformation.

The motivation for this work was to evaluate the performance of the two polyurethane-urea elastomers which were found to function effectively as working substances in rubber heat engines. These elastomers could generate 1 Joule of work per gram of elastomer at about 3% of Carnot efficiency in experimental Sterling cycles.

Table of Contents

Dedication.....	iv
Acknowledgement.....	v
Abstract.....	vi
List of Tables.....	x
List of Figures.....	xi
Chapter	
I. Introduction.....	1
II. Theory.....	6
Thermodynamic Relations for Elastic Solids.....	6
Linear Thermoelastic Solid with Temperature Independent Properties.....	9
Linear Rubbery Solid With Temperature Dependent Properties.....	16
Additional Considerations.....	25
III. Experimental.....	28
Materials.....	28
Polyether Soft-segment Polyurethane-urea.....	28
Polyester Soft-segment Polyurethane-urea.....	29
Natural Rubber.....	31
Thermoplastic PBT/PTMO Elastomer.....	31
Low Density Polyethylene.....	32

Methods.....	33
Deformation Calorimetry.....	33
Background.....	33
Instrument Construction.....	40
Theory of Operation.....	44
Steady-State Gas Pressure.....	50
Transient Response.....	53
Calibrations.....	57
Testing Procedure.....	68
Differential Scanning Calorimetry of Stretched Samples.....	71
Wide Angle X-Ray Scattering.....	75
Thermostatic Measurements.....	76
Power Cycles of Polyurethane-urea Elastomers.....	78
IV. Results and Discussion.....	84
Deformation Calorimetry.....	84
Polyurethane-urea Elastomers and Natural Rubber.....	85
Thermoplastic Elastomer.....	119
Low Density Polyethylene.....	129
Differential Scanning Calorimetry.....	134
Wide Angle X-Ray Scattering Studies.....	149
Thermostatic Measurements and Stress-Strain Curves.....	162
Heat Engine Cycles of Polyurethane- urea Elastomers.....	175

V. Conclusions.....	191
Deformation Calorimetry as a Tool for Studying Polymer Deformation Processes.....	191
Internal Energy Changes and Stress-Induced Crystallization in Polyurethane-urea Elastomers and Natural Rubber.....	192
Thermomechanical Behavior of Polyurethane- urea Elastomers and Natural Rubber.....	194
Isothermal Mechanical Behavior.....	194
Isomechanical Thermal Behavior.....	200
Polyurethane-urea Elastomers as Working Substances in Rubber Heat Engines.....	202
Thermomechanical Behavior of PBT/PTMO Thermoplastic Elastomer.....	204
Thermomechanics of Polyethylene Drawing.....	205
References.....	207

List of Tables

1. Incremental Strain Deformation Calorimetry
Data for Natural Rubber 87
2. Incremental Strain Deformation Calorimetry
Data for Polyether Soft Segment
Polyurethane-urea Elastomer.....88
3. Deformation Calorimetry Data for Cyclic
Loading of Natural Rubber.....93
4. Deformation Calorimetry Data for Loading/
Unloading Cycles of Polyether Soft Segment
Elastomer at Three Test Temperatures.....97
5. Strain Rate Effect on the Heat and Work of
Deformation for Polyether Soft Segment
Elastomer.....98
6. Deformation Calorimetry Data for Loading/
Unloading Cycles of Polyester Soft Segment
Polyurethane-urea Elastomer.....101
7. Deformation Calorimetry Data for PBT/PTMO
Thermoplastic Elastomer.....120
8. Heat Engine Cycle Data for Polyether Soft
Segment Polyurethane-urea Elastomer.....176
9. Heat Engine Cycle Data for Polyester Soft
Segment Polyurethane-urea Elastomer.....177

List of Figures

1.	Heat, Work and Internal Energy versus Strain for Linear Thermoelastic Solid.....	13
2.	Heat, Work and Internal Energy versus Strain for Linear Rubbery Solid.....	22
3.	Deformation Calorimeter.....	41
4.	Calibration Data for Deformation Calorimeter.....	47
5.	Reconstruction of Square Wave Heating Input Using Equation 65.....	48
6.	Reconstruction of Ramp Heat Input Using Equation 64.....	49
7.	Calibration Curve for Deformation Calorimeter.....	59
8.	Pressure Response to Square Wave Heating Input.....	60
9.	Adiabatic and Isothermal Pressure Change of Air in Calorimeter.....	63
10.	Dynamic Pressure Response to Sinusoidal Heating Inputs.....	66
11.	Lissajou Figures for Sinusoidal Heat Flow versus Dynamic Pressure.....	67
12.	Graphical Procedure for Obtaining Heat and Work from Deformation Calorimeter Data.....	70
13.	DSC Sample Spool.....	72
14.	Comparison of Indium Melting Transition versus Heating Rate for Sample Spool and Standard Pan...	74
15.	Force versus Temperature Testing Apparatus.....	77
16.	Heat Engine Cycling Apparatus.....	79
17.	Strain and Temperature Programs Used in Heat Engine Cycles.....	81
18.	Idealized Heat Engine Cycle for Elastomer.....	82

19.	Internal Energy versus Extension Ratio for Natural Rubber.....	90
20.	Internal Energy versus Extension Ratio for Polyether Soft Segment Polyurethane-urea Elastomer.....	91
21.	Change of Internal Energy per Unit Extension versus Extension Ratio for Natural Rubber.....	95
22.	Pressure Data from Calorimeter for Polyester Soft Segment Polyurethane-urea Elastomer.....	102
23.	Mechanical Hysteresis versus Internal Energy Change for Elastomers.....	109
24.	Stress and Internal Energy versus Extension Ratio for Polyether Soft Segment Elastomer.....	112
25.	Stress and Internal Energy versus Extension Ratio for Polyester Soft Segment Elastomer.....	113
26.	Stress and Internal Energy versus Extension Ratio for Natural Rubber.....	114
27.	Internal Energy versus Stress for Polyether Soft Segment Elastomer.....	116
28.	Internal Energy versus Stress for Polyester Soft Segment Elastomer.....	117
29.	Internal Energy versus Stress for Natural Rubber.....	118
30.	Calculated and Measured Heat versus Strain for PBT/PTMO Thermoplastic Elastomer.....	121
31.	Heat, Work and Internal Energy versus Strain for PBT/PTMO Thermoplastic Elastomer.....	123
32.	Calorimeter Data for Thermoplastic Elastomer.....	125
33.	Standard Linear Viscoelastic Solid Model and Typical Stress-Strain Curve.....	126
34.	Force-Time Curve and Thermodynamic Processes for Drawing of Low Density Polyethylene.....	130
35.	Mechanical Power versus Heat Flow for Drawing of Low Density Polyethylene.....	132

36.	First Scan DSC Data for Polyether Soft Segment Elastomer at Various Extension Ratios.....	135
37.	First, Second and Third DSC Heating Scans for Polyether Soft Segment Elastomer at $\lambda=3$	137
38.	Internal Energy Change versus Extension Ratio for Polyether Soft Segment Elastomer: Comparison of Deformation and Scanning Calorimetry.....	138
39.	First DSC Heating Scans of Polyester Soft Segment Elastomer at Various Extension Ratios...	140
40.	Second DSC Heating Scans of Polyester Soft Segment Elastomer at Various Extension Ratios...	141
41.	Wide Angle X-Ray Equatorial Scans of Polyether Soft Segment Elastomer at Various Extension Ratios.....	151
42.	Wide Angle X-Ray Equatorial Scans of Polyester Soft Segment Elastomer at Various Extension Ratios.....	152
43.	Wide Angle X-Ray Equatorial Scans of Natural Rubber at Various Extension Ratios.....	153
44.	Wide Angle X-Ray Equatorial Scans of Extended Polyether Soft Segment Elastomer Before and After Heating to 400 K.....	154
45.	Crystallite Width versus Extension Ratio for Polyether, Polyester Soft Segment Elastomers and Natural Rubber.....	156
46.	Model for Stress-Induced Crystallization.....	161
47.	Stress versus Temperature Data for Polyether Soft Segment Elastomer at Various Extension Ratios.....	163
48.	Stress versus Temperature Data for Polyester Soft Segment Elastomer at Various Extension Ratios.....	164
49.	Stress versus Temperature Scans to Increasing Maximum Temperature for Polyether Soft Segment Elastomer.....	167

50.	Stress-Strain Loading Curves for Polyether Soft Segment Elastomer at Various Temperatures.....	171
51.	Stress-Strain Loading Curves for Polyester Soft Segment Elastomer at Various Temperatures.....	172
52.	Static Stress versus Extension Ratio for Natural Rubber.....	174
53.	Power Contour Map for Polyester Soft Segment Elastomer.....	179
54.	Power Cycles of Polyether Soft Segment Elastomer.....	180
55.	Power Cycles of Polyester Soft Segment Elastomer.....	183
56.	Calculated Stress-Strain Curve for Amorphous and Stress-Crystallizable Polyester Soft Segment Elastomer.....	185

C H A P T E R I

INTRODUCTION

Experimental measurements of stress and strain provide important information about the deformation process of solid materials, but it should be realized that this conjugate variable pair is only one of several characterizing a thermodynamic material. The first law of thermodynamics ensures that energy is conserved in all deformation processes, whether reversible or irreversible. Consequently, the mechanical response of any material reflects exactly that amount of energy appearing as heat and changes of internal energy. This would imply that molecular processes occurring during the deformation which are associated with a change of the internal energy should have an effect on the measured mechanical response.

Internal energy and entropy contributions to the reversible deformation behavior of solids can be derived from suitable constitutive equations. Alternatively, thermodynamic relationships can be employed to deduce internal energy and entropy contributions from equilibrium measurements of relevant macroscopic variables and temperature. These thermostatic measurements presuppose reversibility

through a dependence on the second law of thermodynamics. In many polymeric solids mechanical equilibrium is difficult to achieve due to weak intermolecular attractive forces, and the often pronounced effect of thermal history.

The constraint of reversibility is not imposed on direct measurements of the work and heat of deformation which always yield the change in internal energy by difference according to the first law of thermodynamics. Entropy changes are only obtainable from heat measurements under reversible conditions. Specially designed deformation calorimeters have been utilized to measure the heat and mechanical work of polymer deformation processes. These data have great value for specifying the energy balance to which mechanical models and constitutive equations must conform.

The majority of studies on elastomers using deformation calorimetry have been concerned with reexamining the statistical theory of rubber elasticity in terms of experimental data on internal energy and entropy changes. Stress-induced crystallinity has been cited as the major contribution to the decrease in internal energy observed at high elongations, although no detailed studies have been performed. The transfer of stress from entropic forces at low elongations to energetic forces at high elongations warrants a more detailed examination. This

becomes especially important in view of some investigations which indicate the predominant influence of stress-induced crystallization on the strength (1,2), craze resistance (3) and mechanical dissipation (4) in elastomers.

The possibility of utilizing stress-induced crystallization in an enthalpy cycle to enhance the performance of rubber heat engines employing elastomers as working substances was suggested by Wiegand and Snyder (5) as early as 1934. Mandelkern(6) performed a thermodynamic analysis of an equilibrium enthalpy cycle for a crystallizable polymer, and concluded that crystallization during stretching should increase the available work in a heat engine cycle relative to the same cycle employing an elastomer which was always in the amorphous state. A thermodynamic analysis of rubber heat engines has been given by Farris (7) using the ideal rubber equation of state which, analogous to the ideal gas law, assumes a single phase (amorphous) material in a pure entropy cycle.

The suggestion by Wiegand, Snyder and Mandelkern that crystallization during stretching should improve the performance of elastomers in rubber heat engines is in direct contrast to the often observed mechanical hysteresis in elastomers undergoing crystallization and melting during isothermal stretching and contracting, which would tend to reduce the available work in a heat engine cycle.

Flory (8) and Smith (9) have concluded that the simultaneous processes of crystallization during stretching is not conducive to the attainment of equilibrium.

In an attempt to resolve the apparent discrepancy concerning the role of stress-induced crystallization in rubber heat engines, and understand more fully the nature of this non-equilibrium process which has such far reaching commercial implications, calorimetric studies have been conducted of two polyurethane-urea elastomers and natural rubber. A novel deformation calorimeter has been developed for this purpose, which in conjunction with a differential scanning calorimetry method provides the means for establishing an energy balance for the deformation induced phase change in stretched elastomers and characterizing the melting behavior.

Experimental heat engine cycles utilizing the polyurethane-urea elastomers as working substances were also obtained and correlated with the calorimetric data to evaluate the performance and efficiency of these materials in rubber heat engines designed to convert low grade heat into useful work. Wide angle x-ray diffraction was used to confirm the presence of stress-induced crystallinity and estimate the size of the resulting crystallites. Thermo-static measurements were performed to characterize the thermal transitions at high elongations where the elastomers operate most effectively in the heat engine cycles.

The motivation for this work comes from previous studies which show that the polyurethane-urea elastomers are highly effective for converting heat into mechanical energy in pilot scale rubber heat engines.

Deformation calorimetry was also used to study the drawing of low density polyethylene and the deformation behavior of a segmented thermoplastic elastomer having a continuous hard segment phase, as opposed to the continuous soft-segment phase of the polyurethane-urea elastomers.

C H A P T E R I I

THEORY

Thermodynamic Relations for Elastic Solids

The first law of thermodynamics which describes the complete energy balance for any deformation process, whether reversible or irreversible, has the well known form:

$$dU = dq + dw + \sum_i \mu_i dn_i \quad (1)$$

where dU , dq and dw are the incremental internal energy change, heat and work per unit volume, and μ_i , n_i the chemical potential and number of moles of species i per unit volume, respectively.

The incremental work may be due to changes in any relevant extensive-intensive mechanical variable pair representing generalized forces and displacements. For homogeneous solid deformation, the work is

$$dw = \sigma_{ij} d\varepsilon_{ij} \quad (2)$$

where σ_{ij} , ε_{ij} are components of compatible stress-strain tensors. With Equation 2 the first law of

thermodynamics for solid deformation becomes

$$dU = dq + \sigma_{ij}d\epsilon_{ij} \quad (3)$$

The second law of thermodynamics gives the entropy balance, S , at constant temperature, T ,

$$dS \geq \frac{dq}{T} \quad (4)$$

where the inequality holds for spontaneous or irreversible processes and the equality for reversible processes.

The following derivations, including those for the linear thermoelastic solid, are essentially those given by Sneddon (10). For a reversible deformation process, the combined first and second laws give

$$dU = TdS + \sigma_{ij}d\epsilon_{ij} \quad (5)$$

The Helmholtz free energy, A , is

$$A = U - TS \quad (6)$$

which together with Equation 5 yields

$$dA = \sigma_{ij}d\epsilon_{ij} - SdT \quad (7)$$

From Equation 7 it follows that

$$\left(\frac{\partial A}{\partial \epsilon_{ij}} \right)_T = \sigma_{ij} \quad (8)$$

and

$$\left(\frac{\partial A}{\partial T}\right)_{\epsilon_{ij}} = -S \quad (9)$$

from which

$$\left(\frac{\partial \sigma_{ij}}{\partial T}\right)_{\epsilon_{pq}} = -\left(\frac{\partial S}{\partial \epsilon_{ij}}\right)_T \quad (10)$$

From Equations 5 and 10,

$$\left(\frac{\partial U}{\partial \epsilon_{ij}}\right)_T = \sigma_{ij} - T\left(\frac{\partial \sigma_{ij}}{\partial T}\right)_{\epsilon_{pq}} \quad (11)$$

Writing the total differential for the internal energy in terms of the strain and temperature,

$$dU = \left(\frac{\partial U}{\partial \epsilon_{ij}}\right)_T d\epsilon_{ij} + \left(\frac{\partial U}{\partial T}\right)_{\epsilon_{ij}} dT \quad (12)$$

and rearranging Equation 5 to read

$$dS = \frac{1}{T} dU - \frac{1}{T} \sigma_{ij} d\epsilon_{ij} \quad (13)$$

the incremental entropy change with Equation 12 in 13 is

$$dS = \frac{1}{T} \left[\left(\frac{\partial U}{\partial \epsilon_{ij}}\right)_T d\epsilon_{ij} + \left(\frac{\partial U}{\partial T}\right)_{\epsilon_{ij}} dT \right] - \frac{1}{T} \sigma_{ij} d\epsilon_{ij} \quad (14)$$

from which it follows that

$$T \left(\frac{\partial S}{\partial T} \right)_{\epsilon_{ij}} = \left(\frac{\partial U}{\partial T} \right)_{\epsilon_{ij}} = C_{\epsilon} \quad (15)$$

where subscripts ϵ_{ij} on all of the above partial differential equations imply that all strains are held constant. In Equation 15, C_{ϵ} is the heat capacity of the solid at constant strain. In the undeformed state, $C_{\epsilon} = C_V$.

The above equations provide the necessary relationships to deduce internal energy and entropy contributions to elastic deformation provided a suitable constitutive equation for the solid is known.

Linear Thermoelastic Solid with Temperature Independent Properties

Following the derivation of Sneddon, the constitutive equation relating the stress, strain and temperature of a linear thermoelastic solid is written

$$\sigma_{ij} = \frac{E_T}{(1+\nu)(1-2\nu)} \left[\nu \epsilon_{ij} + (1-2\nu)\epsilon_{ij} - (1+\nu)\alpha(T-T_0) \delta_{ij} \right] \quad (16)$$

where ϵ_{ij} are the components of the small strain tensor,

$$\epsilon_{ij} = \frac{1}{2} \left[\frac{\partial u_i}{\partial x_j} + \frac{\partial u_j}{\partial x_i} \right] \quad (17)$$

and E_T is the temperature independent, isothermal Young's modulus, and α the temperature independent linear thermal expansion coefficient. The dilatation, e , is $e = e_{ii} = \delta V/V$, and ν is Poisson's ratio. Equation 16 can be contracted showing that the mean normal pressure, p , is

$$P = -\frac{1}{3} \sigma_{kk} = \frac{-E_T}{3(1-2\nu)} \left[e - 3\alpha (T-T_0) \right] \quad (18)$$

from which

$$K_T = -\left(\frac{\partial P}{\partial e} \right)_T = \frac{E_T}{3(1-2\nu)} \quad (19)$$

is the isothermal bulk modulus for the solid whose constitutive equation is Equation 16.

From Equations 11 and 16, the change in internal energy with strain is-

$$\left(\frac{\partial U}{\partial \epsilon_{ij}} \right)_T = \frac{E_T}{(1+\nu)(1-2\nu)} \left[\nu e \delta_{ij} + (1+2\nu) \epsilon_{ij} + (1+\nu) \alpha T_0 \delta_{ij} \right] \quad (20)$$

Substituting Equations 15 and 20 into the total differential for the internal energy (Eqn.12) and integrating gives

$$U - U_0 = \frac{1}{2} \sigma_{ij} \epsilon_{ij} + \frac{E_T}{2(1-2\nu)} (T + T_0) + C_E (T - T_0) \quad (21)$$

where U_0 denotes the internal energy of the initial state, $\epsilon_{ij} = 0$, $T=T_0$. The stored strain energy per unit volume is $\frac{1}{2} \sigma_{ij} \epsilon_{ij}$. The last term $C_\epsilon (T-T_0)$, is the heat content, and the middle term-

$$\frac{E_T \alpha e (T + T_0)}{2(1 - 2\nu)}$$

results from the interaction of elastic deformation and thermal diffusion.

The entropy change is derived analogously. From Equations 10 and 16, the change in entropy with strain at constant temperature is

$$\left(\frac{\partial S}{\partial \epsilon_{ij}} \right)_T = \frac{E_T \alpha}{1-2\nu} \delta_{ij} \quad (22)$$

The total differential for the entropy in terms of the strain and temperature is

$$dS = \left(\frac{\partial S}{\partial \epsilon_{ij}} \right)_T d\epsilon_{ij} + \left(\frac{\partial S}{\partial T} \right)_{\epsilon_{ij}} dT \quad (23)$$

which together with Equations 15 and 22, and integration gives for the entropy change

$$S - S_0 = \frac{E_T \alpha}{1-2\nu} e + C_\epsilon \ln \frac{T}{T_0} \quad (24)$$

The second term in Equation 24 is the entropy change due to heat conduction alone, while the first term-

$$\frac{\alpha E_T}{1-2\nu} e$$

arises from coupling of the elastic and thermal processes. For a deformation process at constant temperature, $T=T_0$, it is seen that the entropy change is the result of volume dilatation.

If the coordinate axes are chosen such that the strains are in the principal directions, $e = \epsilon_1 + \epsilon_2 + \epsilon_3$, and $\nu = -\epsilon_2 / \epsilon_1$, so that for uniaxial deformation in the 1 direction at constant temperature, $T=T_0$,

$$\epsilon_1 = \frac{e}{1-2\nu} \quad \sigma_1 = E_T \epsilon_1$$

and the internal energy change for the isothermal uniaxial deformation at constant pressure becomes

$$U - U_0 = \frac{1}{2} E_T \epsilon_1^2 + T_0 E_T \alpha \epsilon_1 \quad (25)$$

which is quadratic in strain. The relationship between the heat, work and internal energy change for a linear thermoelastic solid in uniaxial deformation at constant temperature and pressure is shown in Figure 1. The two terms which contribute to the internal energy change

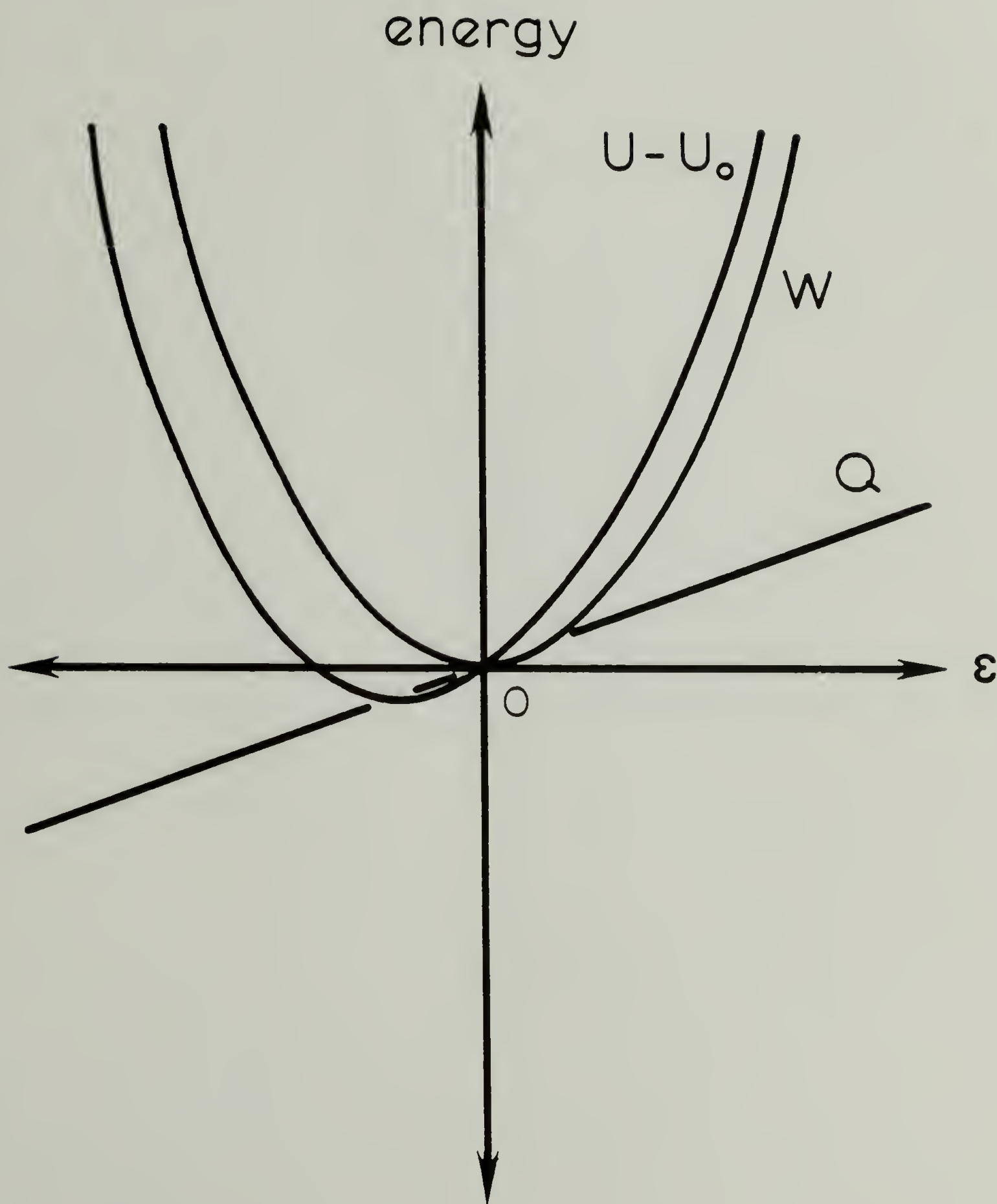


Figure 1. Heat, Q , Work, W , and Internal Energy, U , for Linear Thermoelastic Solid

depend on E_T , which represents essentially the harmonic character of the binding forces, and α which is associated with the anharmonicities (11-14).

From Equations 24 and 25 it is clear that the reversible heat of an isothermal tensile deformation process at constant pressure is

$$q = T_0(S-S_0) = T_0 E_T \alpha \epsilon_1 \quad (26)$$

This equation has been verified by deformation calorimetry of steel wires (15,16) and glassy and crystalline polymers (17,18).

In the absence of accurate values for the modulus and thermal expansion coefficient, the isothermal heat of reversible deformation can be deduced from an experimental determination of the stress-temperature coefficient at the temperature of interest, since according to Equations 4 and 10, at $T=T_0$,

$$dq = T_0 \left(\frac{\partial S}{\partial \epsilon_{ij}} \right)_{T_0} d\epsilon_{ij} = -T_0 \left(\frac{\partial \sigma_{ij}}{\partial T} \right)_{\epsilon_{pq}} d\epsilon_{ij} \quad (27)$$

Similarly, the internal energy contribution is obtained from Equation 11. These are general thermoelastic relations which are independent of the nature of the solid.

The above derivations showed that, in the final

analysis, volume changes determine the entropy contribution and influence the internal energy component of deformation for linear thermoelastic solids. In many cases, particularly in rubber elasticity, it is desired to separate the internal energy contributions arising from shape or length changes from those due to volume changes. Shape and volume changes can be considered separately by writing the stress and strain tensors in terms of their deviatoric (shape) and spherical (volumetric) components. Using this formulation, the stress components become

$$\sigma_{ij} = \sigma'_{ij} - p \delta_{ij}$$

where primes denote the deviatoric components and p is the mean normal pressure given by Equation 14. Similarly, the strain components become

$$\varepsilon_{ij} = \varepsilon'_{ij} - \frac{1}{3} e \delta_{ij}$$

Substituting for the stress and strain components in Equation 16, the constitutive equation for the linear thermoelastic solid in terms of the deviatoric stress and strain becomes simply-

$$\sigma'_{ij} = 2G \varepsilon'_{ij} \tag{28}$$

and

$$\left(\frac{\partial \sigma'_{ij}}{\partial T} \right)_{\varepsilon'_{ij}} = 0 \tag{29}$$

for a material having a temperature independent shear modulus, G . The internal energy change due only to shape changes at constant temperature then becomes

$$\left(\frac{\partial U}{\partial \varepsilon'_{ij}}\right)_T = \sigma'_{ij} - T \left(\frac{\partial \sigma'_{ij}}{\partial T}\right)_{\varepsilon'_{pq}} = \sigma'_{ij} \quad (30)$$

The ratio of the energetic component, $(\partial U/\partial \varepsilon'_{ij})$, to the deviatoric stress for the linear thermoelastic solid is

$$\frac{1}{\sigma_{ij}} \left(\frac{\partial U}{\partial \varepsilon'_{ij}}\right)_T = 1 \quad (31)$$

Consequently, in the absence of volume changes, the energetic component of the elastic stress is identical to the stress for a linear thermoelastic solid having temperature independent properties whose constitutive equation is given by Equation 16.

Linear Rubbery Solid with Temperature Dependent Properties

The previous relationships are expected to hold for a solid having temperature independent properties. Considerable effort has been expended to measure and derive relationships for the internal energy and entropy contributions to the deformation behavior of rubbery

solids, which are known to have a temperature dependent modulus. The constitutive equation most commonly used with the thermodynamic relations of the first section to derive internal energy and entropy expressions for rubbery solids is that obtained from the statistical theory of rubber elasticity. This is a single parameter equation in the temperature dependent shear modulus, $G = NkT$. Consequently, all of the temperature dependence (and none of the volume dependence) of the ideal rubbery solid is contained in the single mechanical constant, $G(T)$.

This type of formulation cannot account for dilatational effects caused by deformation which Gee (19) and Flory (20) have suggested are the primary source of the internal energy contribution to rubber deformation. Internal energy changes resulting from volume changes cannot be calculated from the one parameter ideal rubber equation of state as was previously done for the two (independent) parameter linear thermoelastic solid. However, some simple assumptions can be made to deduce the relationship between two of the thermoelastic constants for rubber which are necessary to make internal energy and entropy changes calculable.

As a starting point we assume that at infinitesimal strains rubber behaves like a typical linear thermoelastic solid. This is consistent with the positive thermal expansion coefficient of rubber in the isotropic state and

at very small strains. From Equation 12, the uniaxial stress-strain-temperature equation for a linear solid is, with $\sigma_{11} = \sigma$, $\sigma_{22} = \sigma_{33} = 0$, and $\epsilon_{11} = \epsilon$,

$$\sigma = E \left[\epsilon - \alpha(T - T_0) \right] \quad (32)$$

Experiments show that the stress-temperature slope for rubber is linear (i.e. independent of temperature) over a wide range of temperature, but that it is a function of strain, going from negative to positive with increasing strain. While the modulus is known to be a linear function of temperature, the thermal expansion coefficient must be inversely proportional to temperature since the product of the two is independent of temperature. Assuming both a temperature dependent modulus and thermal expansion coefficient in Equation 32, differentiating the stress with respect to temperature at constant strain gives

$$\left(\frac{\partial \sigma}{\partial T} \right)_{\epsilon} = \left(\frac{\partial E}{\partial T} \right)_{\epsilon} \epsilon - E\alpha - (T - T_0) \left(\frac{\partial}{\partial T} \right) (E\alpha) \quad (33)$$

but since $(\partial \sigma / \partial T)_{\epsilon} \neq f(T)$, the third term in Equation 33 must be zero. As a further consequence of the temperature independent slope-

$$\left(\frac{\partial E}{\partial T}\right)_{\epsilon} \neq f(T) \quad (34)$$

$$E\alpha \neq f(T) \quad (35)$$

Knowing that $E(T) = 2(1+\nu)G(T) = E_0 T/T_0$ (which satisfies Equation 34) the only possible choice for $\alpha(T)$ which satisfies Equations 33 and 35 is- $\alpha(T) = \alpha_0 T_0 / T$. Using these relationships for $\alpha(T)$ and $E(T)$ the stress-temperature slope at constant strain from Equations 32 or 33 is

$$\left(\frac{\partial \sigma}{\partial T}\right)_{\epsilon} = \frac{E_0}{T_0} \epsilon - \alpha_0 E_0 \quad (36)$$

which is independent of temperature as required, and is a linear function of strain, being negative at small strains and positive at large strains, as is observed experimentally.

At the thermoelastic inversion, the stress-temperature slope of rubber is zero. Setting the left hand side of equation 36 to zero, it is found that the thermoelastic inversion occurs when $\epsilon = \alpha_0 T_0$. For natural rubber with $\alpha_0 = 2.2 \times 10^{-4}/K$ and $T_0 = 300K$, $\epsilon_{inv} = .07$, which is close to experimental values for this rubber. From Equation 36 and the relationship between the

shear and tensile moduli, it follows that Poissons ratio is also independent of temperature.

Using $E(T)$, and $\alpha(T)$ given above in the constitutive equation for the linear thermoelastic solid, leads to interesting results for the internal energy and entropy changes in a material such as rubber which has temperature dependent properties. Proceeding as previously for the linear thermoelastic solid, the following relationships are obtained with $E(T)$ and $\alpha(T)$ substituted for the corresponding temperature independent quantities in Equation 16

$$\left(\frac{\partial U}{\partial \epsilon_{ij}}\right)_T = E_0 T_0 \alpha_0 \delta_{ij} \quad (37)$$

$$\left(\frac{\partial S}{\partial \epsilon_{ij}}\right)_T = -\left(\frac{\partial \sigma_{ij}}{\partial T}\right)_{\epsilon_{pq}} = \frac{-\sigma_{ij}}{T} + \frac{E_T \alpha_0 T_0}{(1-2\nu) T} \delta_{ij} \quad (38)$$

which upon substitution into the respective total differentials, using the previously derived temperature dependence, and integrating gives for the internal energy and entropy change of rubber

$$U - U_0 = \frac{E_0 T_0 \alpha_0}{1-2\nu} e + C_E (T - T_0) \quad (39)$$

$$S - S_0 = -\frac{1}{T} \left[\frac{1}{2} \sigma_{ij} \epsilon_{ij} - \frac{E_0 T_0 \alpha_0}{1-2\nu} e \right] + C_E \ln \frac{T}{T_0} \quad (40)$$

At constant volume, and temperature $T=T_0$,

$$U - U_0 = 0 \quad (41)$$

$$S - S_0 = -\frac{1}{T} \left(\frac{1}{2} \sigma_{ij} \epsilon_{ij} \right) \quad (42)$$

For comparison with experiment, the uniaxial form of Equations 40 and 41 are, at constant pressure and temperature, $T=T_0$,

$$U - U_0 = E_0 T_0 \alpha_0 \epsilon_1 \quad (43)$$

$$T_0(S - S_0) = Q = -\frac{1}{2} E_0 \epsilon_1^2 + E_0 \alpha_0 T_0 \epsilon_1 \quad (44)$$

$$W = A - A_0 = (U - U_0) - T_0(S - S_0) = \frac{1}{2} E_0 \epsilon_1^2 \quad (45)$$

The heat, work and internal energy for rubber at small strains are shown schematically in Figure 2. The form of these functions has been confirmed several times for natural rubber by Muller (21), Godovskii (22) and Killian (14), using deformation calorimetry. In particular the heat goes through an inversion at $\epsilon_1 = 2 \alpha_0 T_0$, while the internal energy is found to be a linear function of strain at constant temperature and pressure, this being a result of the linear relationship between strain and dilitation at small strains.

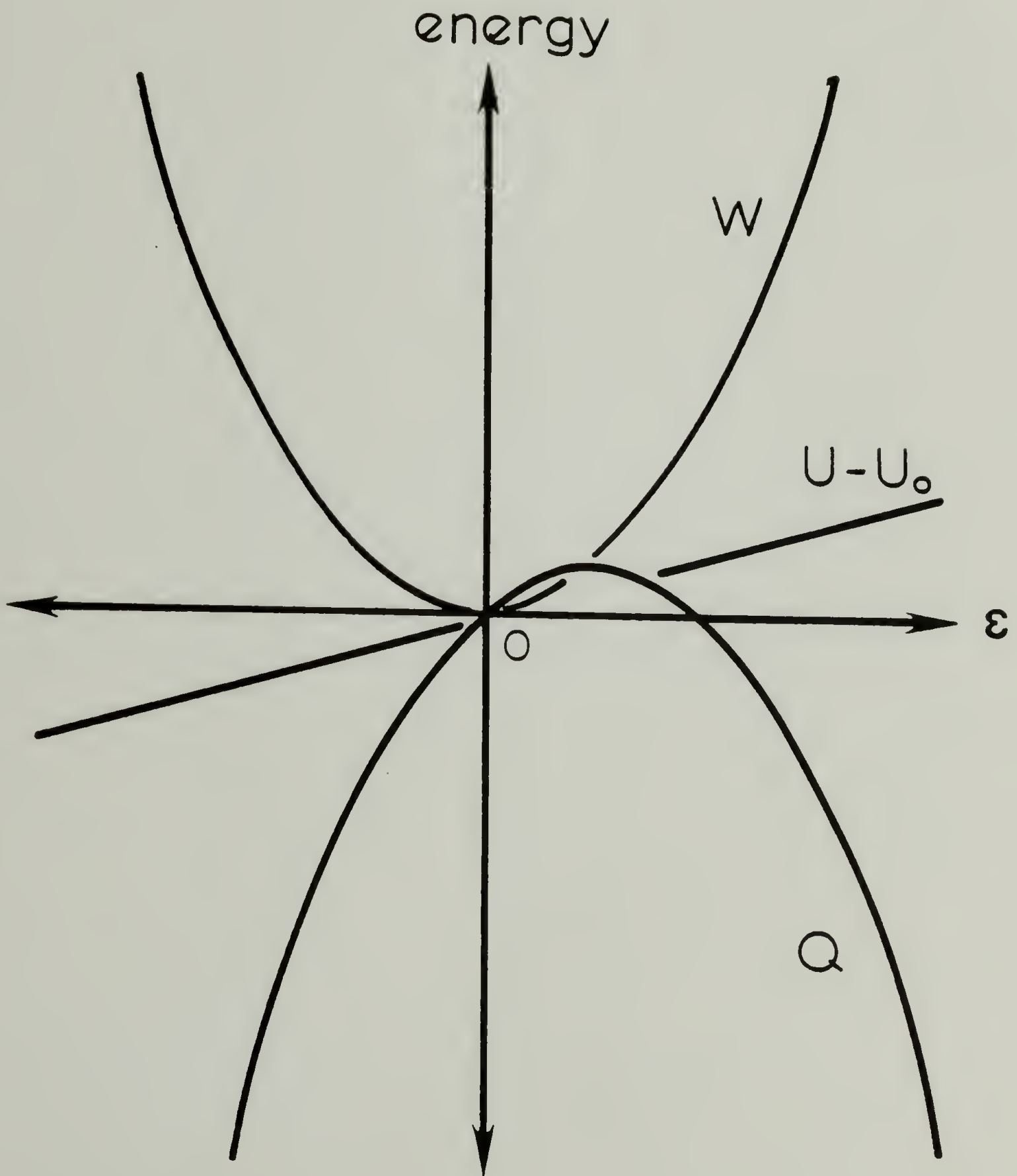


Figure 2. Heat, Q , Work, W , and Internal Energy, U , for Linear Rubbery Solid

Experiments by Gee, Stern and Treloar (23) show a quantitative relationship between measured dilatation and that calculated from Equation 39 using internal energy changes obtained from stress-temperature data of natural rubber at constant pressure. Gee (19) obtained Equation 39 in differential form, $(\partial U / \partial e)_T$, by assuming the relationship between internal energy and volume for a material under hydrostatic pressure to hold when the volume change is due to a tensile stress. Thermostatic measurements in shear by Meyer and van der Wyk (24) showed no thermoelastic inversion and no energetic component to the stress, since shear strain involves no volume changes.

Volume and shape contributions to the internal energy and entropy changes during deformation can be separated by considering the principal stress difference, $\sigma_{11} - \sigma_{22}$, which removes the volume dependent terms for a uniaxial experiment as is normally done in rubber elasticity formulations. In this way the uniaxial stress becomes, with $E(T)$ and $\alpha(T)$ in Equation 16,

$$\begin{aligned} \sigma = \sigma_{11} - \sigma_{22} &= \frac{E_0 T/T_0}{(1-\nu)} (\epsilon_{11} - \epsilon_{22}) \\ &= 2G_0 T/T_0 (\epsilon_{11} - \epsilon_{22}) \end{aligned} \quad (46)$$

but since $\epsilon_{22} = (e - \epsilon_{11})/2$,

$$\begin{aligned}\sigma &= 3G_0 T/T_0 (\epsilon_{11} - e/3) \\ &= 3G_0 T/T_0 \epsilon'_{11}\end{aligned}\quad (47)$$

and the stress-temperature coefficient is

$$\left(\frac{\partial\sigma}{\partial T}\right)_{\epsilon'_{11}} = \frac{3G_0 \epsilon'_{11}}{T_0} = \frac{\sigma}{T}\quad (48)$$

from which the internal energy change with strain at constant temperature is

$$\left(\frac{\partial U}{\partial \epsilon'_{11}}\right)_T = \left(\frac{\partial \sigma}{\partial T}\right)_{\epsilon'_{11}} - \frac{\sigma}{T} = 0\quad (49)$$

The energetic component of the stress arising solely from shape or length changes at small strain and constant pressure in a ratio with the stress is

$$\frac{1}{\sigma} \left(\frac{\partial U}{\partial \epsilon'_{11}}\right)_T = \frac{1}{\sigma} \left(\frac{\partial U}{\partial \epsilon_{11}}\right)_{T,V} = 0\quad (50)$$

in agreement with the definition of an ideal rubber exhibiting no volume changes during deformation.

The previous equations show that the internal energy change in rubber is related to the dilatational behavior, while the stored strain energy resides in the entropy change, in contrast to hard elastic solids but in complete agreement with statistical and molecular theories of

rubber elasticity. Consequently, the temperature dependent modulus and thermal expansion coefficient of rubber reverses the role of internal energy and entropy contributions to deformation at small strains. Quoting from Gee's 1946 paper, "We conclude therefore that for small extensions, the observed expansion is produced by the hydrostatic component of the tensile force. It consists of an increase in the average intermolecular spacing, and is accompanied by the equivalent increases in both internal energy and entropy."

Additional Considerations

The previous results show that the internal energy and entropy changes for reversible homogeneous deformation are calculable from suitable thermoelastic equations of state. For inhomogeneous deformation processes during which structural changes take place in the solid the above relations cannot be expected to hold, and experimental determination of the heat and work are required to obtain the energy balance.

Typical phenomenon leading to inhomogeneous deformation in polymers include voiding, drawing and crystallization induced by stretching. In such cases new surface area can be formed, so that the work becomes

$$dW = \sigma_{ij} d\epsilon_{ij} + \frac{1}{V} \gamma dA \quad (51)$$

where γ is the interfacial or surface free energy and dA the incremental change in surface area within the solid. In addition, heats due to irreversible processes such as crystallization and viscous dissipation must be considered.

The energy balance for irreversible or dissipative processes in homogeneous solids can be formulated by defining a function, Θ , (25) analogous to the enthalpy, H , of pure PV systems, such that

$$\Theta = U - \sigma_{ij} \epsilon_{ij} \quad (52)$$

and

$$d\Theta = dq - \epsilon_{ij} d\sigma_{ij} \quad (53)$$

At constant stress,

$$(d\Theta)_{\sigma_{ij}} = dq \quad (54)$$

whereas at constant Θ , the isothermal heat flow is

$$\left(\frac{dq}{dt}\right)_{T,\Theta} = \epsilon_{ij} \left(\frac{d\sigma_{ij}}{dt}\right)_{T,\Theta} \quad (55)$$

Equation 55 shows that at constant ϵ_{ij} , the heat flow is negative (exothermic) for stress relaxation, as has been verified calorimetrically by Muller (26) for glassy polycarbonate.

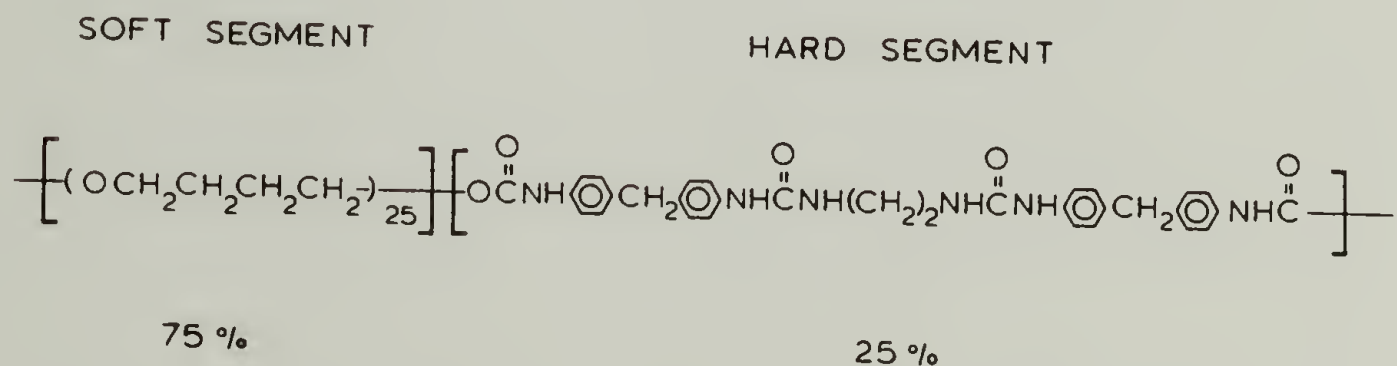
C H A P T E R I I I

EXPERIMENTAL

Materials

Polyether Soft-segment Polyurethane-urea Elastomer

A polyether soft-segment polyurethane-urea block copolymer was obtained from the Dupont Company in the form of a coalesced multifilament yarn dry-spun from the polymerization solvent, dimethylacetate. The chemical structure is shown below.



This polymer has approximately 75% w/w soft-segment of 1800 molecular weight poly(tetramethylene-oxide). The hard segment is 25% w/w of the polymer being composed of methylene-bis-diisocyanate(MDI) and ethylenediamine. The poly(tetramethylene-oxide) (PTMO) soft-segments exhibit only low amounts of crystallinity in the pure state and have an equilibrium melting point for extended chain crystals of 323K (27,28). The heat of fusion for the 100%

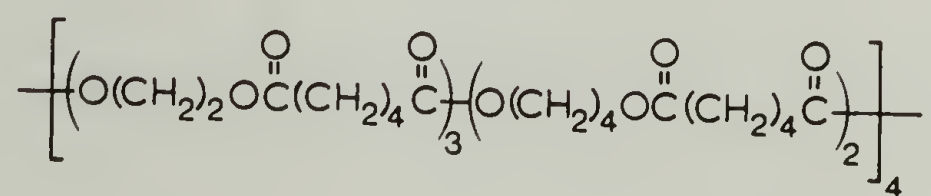
crystalline material is 200 J/g (29). The small strain tensile modulus (E) of this material is measured to be 4.7 MPa and the linear thermal expansion coefficient is $3.1 \times 10^{-4}/K$ (30). Strain at break is approximately 500% and the density given by Dupont is 1.2 g/cc. Molecular weight between crosslinks, determined from the shear modulus ($G=E/3$) and the statistical theory of rubber elasticity is 1860 g/mole, which agrees fairly well with the soft-segment prepolymer molecular weight, indicating that the hard segments are almost quantitatively associated into domains to form a system of physical crosslinks.

Polyester Soft-segment Polyurethane-urea Elastomer

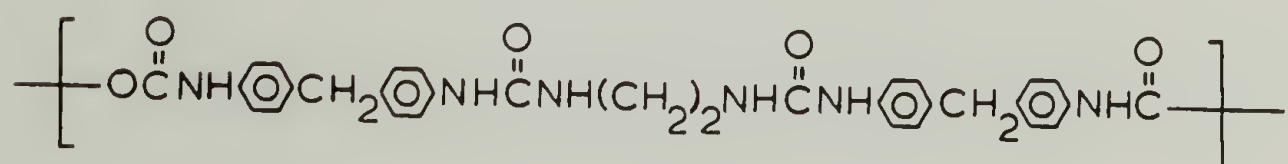
A mixed polyester soft-segment polyurethane-urea linear block copolymer elastomer was also obtained from Dupont as a coalesced multifilament yarn manufactured under the same conditions as the PTMO soft-segment material. The chemistry, properties and manufacture of both of these polyurethane-urea elastomers has been reported (31,32). The polyester soft-segment material is composed of a 3500 molecular weight mixed polyester sequence containing adipic acid/ ethylene glycol/ butane diol in a mole ratio of 5:3:2. This random structure was used to suppress crystallinity in the soft segments and improve low temperature elastomeric properties. These rubbery

sequences are terminated with MDI and chain extended with ethylene diamine as in the PTMO elastomer. The chemical structure is shown below, with soft-segments comprising 85%, and hard segments 15%, of the weight of the polymer.

SOFT SEGMENT, 85 %



HARD SEGMENT, 15%



The small strain tensile modulus of this material is 2.46 MPa, the strain at break approximately 600% and the density and thermal expansion coefficient are reported to be the same as for the PTMO soft-segment elastomer. The molecular weight between crosslinks, again determined from the shear modulus and statistical theory is found to be 3564 g/mole, which agrees with the reported prepolymer molecular weight of 3500. The heat of fusion of the predominant adipic acid/ethylene glycol sequences is reported to be 122 J/g at the equilibrium melting temperature of 338K (28).

Natural Rubber

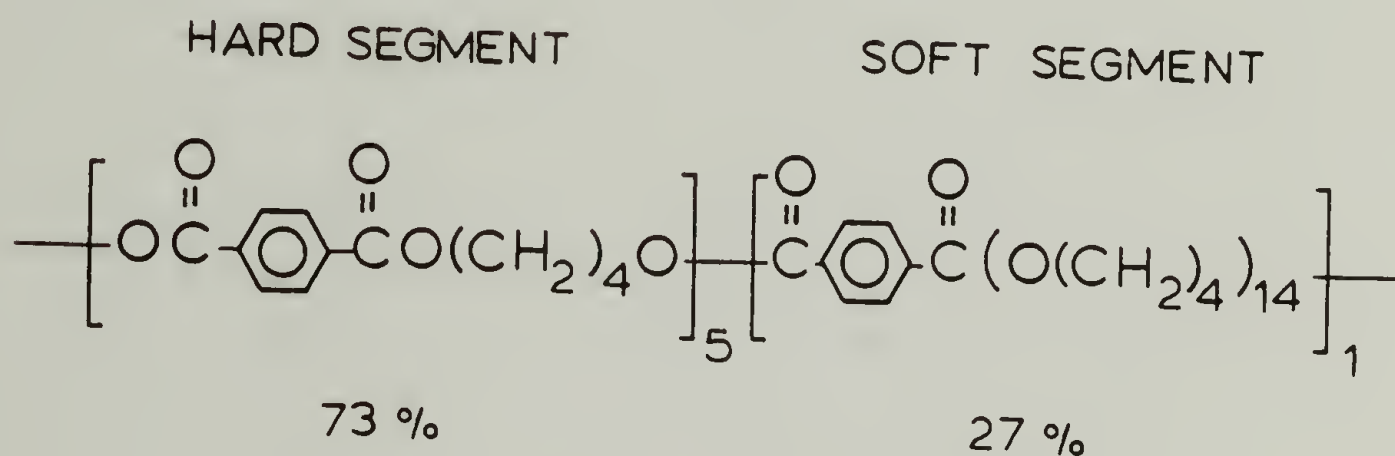
Natural rubber (predominantly cis-polyisoprene) was obtained as vulcanized cut thread having no filler. The small strain tensile modulus of the natural rubber is .592 MPa, the strain at break about 900% and the density of the uncrystallized polymer is reported to be .91 g/cc (33). The heat of fusion is 64 J/g at the equilibrium melting temperature of 300K (34).

Thermoplastic Elastomer (Hytrel[®])

A high hard-segment content block copolymer marketed by Dupont under the tradename Hytrel[®], was also studied. This material is a true thermoplastic elastomer, in contrast to the polyurethane-ureas which degrade before the hard segments melt. Hytrel[®] was obtained as a 1410 denier (g/9000 M) monofilament which had been drawn and heat set in the extended state during manufacture. The small strain tensile modulus is 274 MPa and the density is reported to be 1.3 g/cc. The breaking strain of this fiber is near 20%, showing orders of magnitude lower extensibility than the polyurethane-ureas of natural rubber due to the continuous heat-set hard-segment phase.

The chemical composition of Hytrel[®] is shown below to consist of poly(butylene-terephthalate) (PBT) hard seg-

ments and 1000 MW PTMO soft-segments. Hard segment content was determined from differential scanning calorimetry melting temperature (35) and proton NMR (36) to be 73% , both techniques agreeing to within 2%. These weight fractions are based on the designations shown below, which is somewhat different than that used for the polyurethane-ureas, but is standard practice in the literature for this polymer.



Low Density Polyethylene

Low density polyethylene (.920 g/cc) was also obtained from DuPont. This material is marketed under the tradename Alathon Resin 20, and had a DSC crystallinity of 60% in the melt pressed films used for deformation calorimetry studies.

Methods

Deformation Calorimetry

Background The theory and practice of measuring quantities of heat is generally termed calorimetry. Numerous experimental techniques have been utilized to determine heats of phase transitions (melting, vaporization) mixing and specific heats. A lesser known application of calorimetry, especially relevant to the study of polymeric solids, is the determination of the heats associated with deformation. These heats are extremely small and endothermic for hard elastic solids—about .01 and .002 cal/g for polystyrene and steel, respectively for uniaxial deformation to 1/10 of the breaking strain. For rubbery solids, the heat is on the order of the work but opposite in sign (exothermic), being typically $-.04$ cal/g at 1/10 of the breaking strain. Consequently, very high sensitivities are required in an instrument designed to measure the thermal effects accompanying the deformation of milligram quantities of solid.

The earliest measurements of the heat of solid deformation date back at least to 1805, when John Gough (37) reported a series of qualitative experiments on the heating and cooling of rubber during stretching and contrac-

ting. Fifty years later J.P. Joule (38,39) published comprehensive studies of the temperature changes in wood and rubber using thermocouples. In 1915 Compton and Webster (40) made precise measurements of the temperature changes during elastic straining of metal wires. In these experiments the wire acted as one arm of a sensitive Wheatstone bridge, whose resistance change with temperature was used to measure heating and cooling produced by deformation.

In 1927, W. Swietoslowski designed a microcalorimeter specifically for studying processes where the heats and rates of heat production were small (41). Among numerous studies was the measurement of the heat produced by a piece of lead deforming plastically under its own weight over a period of 25 days. Heat flow rates of about .1 mcal/sec were reported. Elastic heats of tensile deformation for various steel alloys were reported in 1935 by Esser, Cornelius and Banck (42) using a flow calorimeter first described by Callender and Barnes (43). Taylor and Quinney (44,45) studied thermal effects in relation to mechanical energy storage in metals using temperature measurements and temperature scanning calorimetry.

The commercial introduction of synthetic polymers inspired several techniques for studying the often complicated thermal effects of these materials during deformation. Foremost in the literature of deformation calorime-

try of polymers is F.H. Muller, who together with A. Engelter introduced in 1958 a new method for measuring heat flow during solid deformation (46). This technique, which forms the physical basis of the method to be described in this section, combines the sensitivity of gas thermometry with the principle of hot-wire methods for measuring thermal conductivity of gases first described by Schleirermacher (47).

Briefly, the technique consists of sensing the pressure change of a gas at constant volume due to heating of a sample being deformed along the centerline of a sealed cylinder. The heat flow during the deformation process in the sample cylinder was equated to the measured electrical heat generated in an identical reference cylinder which is required to maintain the differential pressure between the two cylinders at zero. In this respect the calorimeter functions as a null or compensating device, as opposed to a direct measuring system. One disadvantage of this measurement principle is that endothermal (cooling) processes are relatively difficult to measure. A second problem with this technique is that a strict proportionality between the gas pressure and the heat flow is required at all times during the process to be measured. This is a fairly good approximation for very short lag times between the gas pressure and heat flow.

Virtually identical instruments to the Muller-Engelter device were constructed by Morbitzer et.al. (48) and Foster and Benner (49). The latter authors extended Muller's calculations for the transient gas pressure response to heating using the one-dimensional conduction solution of Carslaw and Jaeger (50) for the radial temperature distribution in a gas having an arbitrary heat flux on the inner surface and a specified temperature on the outer surface. The result, though significantly more complicated mathematically, afforded only minor improvement over the quasi-static single exponential solution obtained originally by Muller and Engelter, which was found to fit the transient response to within a few percent.

In addition to gas calorimeters, commercial Calvet microcalorimeters have been adapted to study the thermal effects of stretching natural rubber (5). A detailed description of the theory, construction and calibration of the original instrument has been given by Calvet and Pratt (52). The Tian equation which describes the relationship between the heat flow in the calorimeter dq/dt , and the temperature difference, ΔT , between the outer surface of the sample cell and the constant temperature reservoir, is

$$\dot{q} = \frac{dq}{dt} = K \left[\Delta T + \tau \frac{d\Delta T}{dt} \right] \quad (56)$$

where K and τ are the experimentally determined thermal and time constants of the calorimeter. In this device thermopiles are used to sense the temperature difference instead of gas pressure, which has the advantage of being independent of volume changes in the sample caused by deformation, but the drawback of very long (30 sec) lag times before steady-state is achieved due to the large thermal capacity of the metal cylinder walls and thermocouples.

The total heat of the process which has occurred in the calorimeter up to time t , is given by the integral of Equation 56 ,

$$Q(t) = \int_0^t \dot{q}(\xi) d\xi = K_0 \int_0^t \Delta T(\xi) d\xi + K \tau \Delta T(t) \quad (57)$$

$$Q(\infty) = Q = K_0 \int_0^{\infty} \Delta T(t) dt \quad (58)$$

where it is seen that the total heat is proportional to the area under the temperature-time curve after baseline has been reestablished and the temperature difference becomes zero. Equation 56 is simply the inverted single exponential or quasistatic solution referred to previously in the discussion of gas calorimeters. More accurate solutions can be obtained by considering the temperature response to consist of n exponential terms (53).

The use of Laplace transforms for solving such problems in microcalorimetry has been discussed (54).

The Tian-Calvet principle and construction design was utilized by Godovskii (55), Andrianova (56) and more recently Hohne and Killian (57) in building microcalorimeters specifically for the simultaneous measurement of thermal and mechanical effects during solid polymer deformation. The governing equations are those given above. Godovskii made many measurements in the so-called ballistic mode, whereby loading of the elastic solid takes place in about one second- much less than the 30 sec time constant of the calorimeter. Under these conditions an acute temperature spike is observed, the height of which is proportional to the heat flow. This is seen by inverting equation 56 and expanding the exponential term in a power series of t/τ . Neglecting higher order terms since $t \ll \tau$, the temperature spike, ΔT is related to the heat flow dq/dt by-

$$\Delta T \approx \frac{\dot{q} t}{K\tau} \quad (59)$$

and the heat of the process is $q = \dot{q} t = K \tau \Delta T$. Although this method affords considerable improvement in sensitivity, the deformation process would not even approach isothermal conditions as would be required for application of the second law of thermodynamics. The detection limit of

the Godovskii device is reported to be .1 mcal in the ballistic mode.

A flow calorimeter for conducting thermomechanical studies of polymer deformation was described by Duvdevani, Biesenberger and Gogos (58) utilizing the principles of Barnes and Callendar. Duvdevani et.al. are the only authors to use deformation calorimetry for the study of thermal effects during periodic deformation of a viscoelastic material (59).

Thermal effects during the necking of polymers were reported by Maher, Hayward and Hay (60). Heat generated in the specimen neck were calculated from temperature measurements using an infra-red camera. With this technique direct heat measurements cannot be made and the heat loss to the surroundings must be taken into account. Equations were derived for heat generation with convective heat loss to the surroundings which were later used by Warner (61) to estimate heat generation from the drawing of poly(ethylene-terephthalate).

The above methods for measuring heat generation during solid deformation are always accompanied by simultaneous measurements of the mechanical work. In this way an energy balance is obtained for the deformation process as required by the first law of thermodynamics. The following section describes a new calorimeter for studying the thermodynamics of solid deformation,

combining the design features, high sensitivity and fast response time of the Muller/Engelter device with the direct measurement principle of the Tian-Calvet microcalorimeter. A primary objective in building the calorimeter was to to make real-time measurements of quasi-isothermal heat flow during the stretching of elastomers which, in conjunction with mechanical measurements, would yield continuous data for internal energy changes during deformation. This would facilitate the study of stress-induced crystallization as it occurs during the deformation process, and allow for a truly dynamic thermodynamic analysis of the actual deformation processes of elastomers.

Instrument Construction An instrument has been built based on the original construction design of the Muller/Engelter device which directly measures the heat evolved or absorbed by materials undergoing deformation. Simultaneous measurement of the work of deformation yields the internal energy change in the material according to the first law of thermodynamics.

Figure 3 shows a schematic diagram of the deformation calorimeter which consists of two hollow cylindrical chambers which can be sealed and are in thermal contact with a constant temperature bath at any temperature T_0 . In one

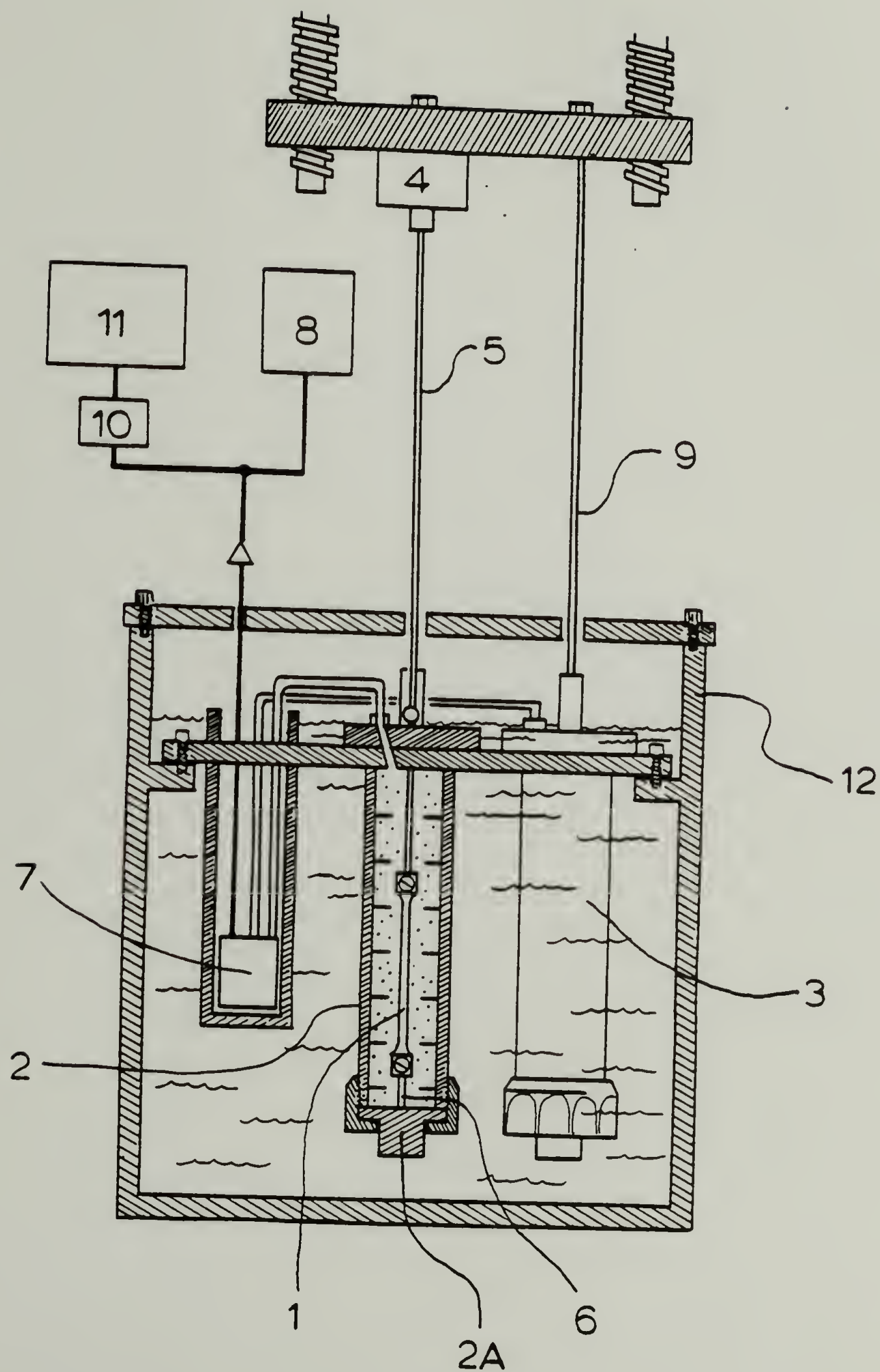


Figure 3. Deformation Calorimeter; 1) Sample, 2) Sample Cylinder
 3) Reference Cylinder, 4) Load Cell, 5) Invar Pullwire, 6) Bottom
 Clamp, 7) Pressure Transducer, 8, 11) Recorders, 9) Invar Pullwire
 10) Amplifier, 12) Constant Temperature Bath

of the cylinders a sample is attached to the bottom and deformed via a pullwire which exits the top of the cylinder through a frictionless mercury seal. The other cylinder is identical but contains a small return spring instead of a sample to facilitate reentry of the pullwire during retraction.

The two cylinders are separated by a pressure transducer which produces a voltage signal proportional to the difference in the gas pressure between the two cylinders. This signal is recorded versus time on one channel of an electronic recorder. The pullwire which is attached to the sample is suspended from a force transducer mounted on a movable crosshead. The force transducer produces a voltage signal which is proportional to the force exerted by the sample during the deformation process. This signal is recorded simultaneously with the gas pressure signal on a second channel of the electronic recorder. The reference cylinder pullwire is attached directly to the crosshead.

Measurements are made by simultaneously displacing the pullwires from both cylinders so as to cause no pressure difference between the cylinders due to a volume change in the gas.

The cylinders are 20 cm in length and made of stainless steel, having inner diameter 1.905 cm and outer diameter 3.175 cm. Both cylinders are fixed to a circular

stainless steel plate which is mounted in a thermoregulated liquid bath, filled typically with water or a water/ethylene glycol mixture (antifreeze). The sample cylinder is positioned in the center of the bath.

Teflon coated .025 cm diameter Invar wires are used for the pullwires because of the low thermal expansion coefficient of the Invar iron/nickel alloy, which yields negligible thermal effects on deformation. Spurious thermal effects arising from deformation of the spring in the reference cylinder are likewise avoided since opposing tensile and compressive effects effectively cancel in torsion.

The pressure sensing system consists of a Celesco P7D variable reluctance pressure transducer having a maximum range of $\pm .1$ PSI differential pressure. A Celesco CD25 transducer indicator supplies a ± 10 V DC analog signal at maximum pressure to one channel of a Bascom-Turner 4120T two channel electronic recorder. Pressure (voltage) versus time data is stored digitally on disk. Because the pressure sensing system was typically operating at 1-5% of full scale, a 1 sec RC filter was used to eliminate unwanted 60 Hz noise from the pressure signal. A maximum pressure response of 10^{-4} PSI (.69 Pa) FSD at 10 mV is determined by the lowest input range of the recorder. Baseline drift measured over a three hour period was found to be ± 17 mV/hr.

Due to convection effects at heating rates greater than about 3 mcal/sec, thin flexible polyester baffles were positioned horizontally inside the sample cylinder at 3 cm intervals. This effectively eliminated vertical stratification of the gas and ensured that pressure response was independent of the axial position of the sample or heating element

The mechanical system consisted of a specially designed stretching device having a twin screw-driven crosshead with gear transmission capable of ten preset linear velocities from .027-27 cm/min. An Interface 5 Kg loadcell attached to the movable crosshead measured the force on the sample, and the amplified analog signal was fed to the second channel of the Bascom-Turner recorder.

Theory of Operation Preliminary studies showed that the differential gas (air) pressure was related to the heat flow, dQ/dt , through the linear hereditary integral equation:

$$\Delta P(t) = \int_0^t K(t-\xi) \frac{\partial Q}{\partial \xi} d\xi \quad (60)$$

which can be inverted using Laplace transforms to give

$$Q = C \int_0^{\infty} P(t) dt \quad (61)$$

where

$$C = \left[\int_0^{\infty} K(t) dt \right]^{-1} \quad (62)$$

is a constant which was found to be independent of the heat source position and properties using the construction design previously described. In addition, the transient response of the gas was found to be well described by a single exponential kernel function

$$K(t) = \frac{1}{C\tau} e^{-t/\tau} \quad (63)$$

in which the time constant τ , was about 7 sec. Using this kernel function, Equation 60 can be inverted to give

$$Q(t) = C \int_0^t \Delta P(\xi) d\xi + C\tau \Delta P(t) \quad (64)$$

which is the Tian-Calvet equation with gas pressure replacing temperature. However, specific knowledge about the form of the kernel function is not required to obtain values of heat from pressure data. As shown by Equation 61 all that is required is to obtain a numerical value for the integral of the kernel function at infinite time by constructing a calibration curve of electrically generated heat Q , versus the area under the pressure-time curve once baseline has been reestablished following the heat pulse. Alternatively, the steady-state pressure for a constant

heat flow, $(dQ/dt)_0$ can be used to evaluate the kernel function, as this will be independent of the transient response.

The heat flow $\dot{Q}(t)$, in terms of the measured gas pressure is given by the time derivative of Equation 64 ,

$$\dot{Q}(t) = C \Delta P(t) + C\tau \frac{d\Delta P(t)}{dt} \quad (65)$$

Equations 61 , 64 , and 65 are the operating equations for the deformation calorimeter from which the total heat Q , the dynamic heat $Q(t)$, and the heat flow $\dot{Q}(t)$ are estimated in terms of the measured gas pressure. The graphical procedure for obtaining the total heat, Q , of a process using Equation 61 is shown in Figure 4, for an actual heat pulse of 3 millicalories. The way in which the original heat flow, $\dot{Q}(t)$, is recreated using Equation 64 and the measured gas pressure is shown schematically in Figure 5 for a square wave heating function. The operations are performed on the electronic recorder by digitally adding the reduced pressure derivative, $\tau dP(t)/dt$ at time t , to the original pressure $P(t)$ and multiplying by the calibration constant, C .

The heat $Q(t)$, evolved (or absorbed) up to time t , is recreated from the original pressure data as shown schematically in Figure 6 for the same square wave heating function described in Figure 5 . The heat evolved up to

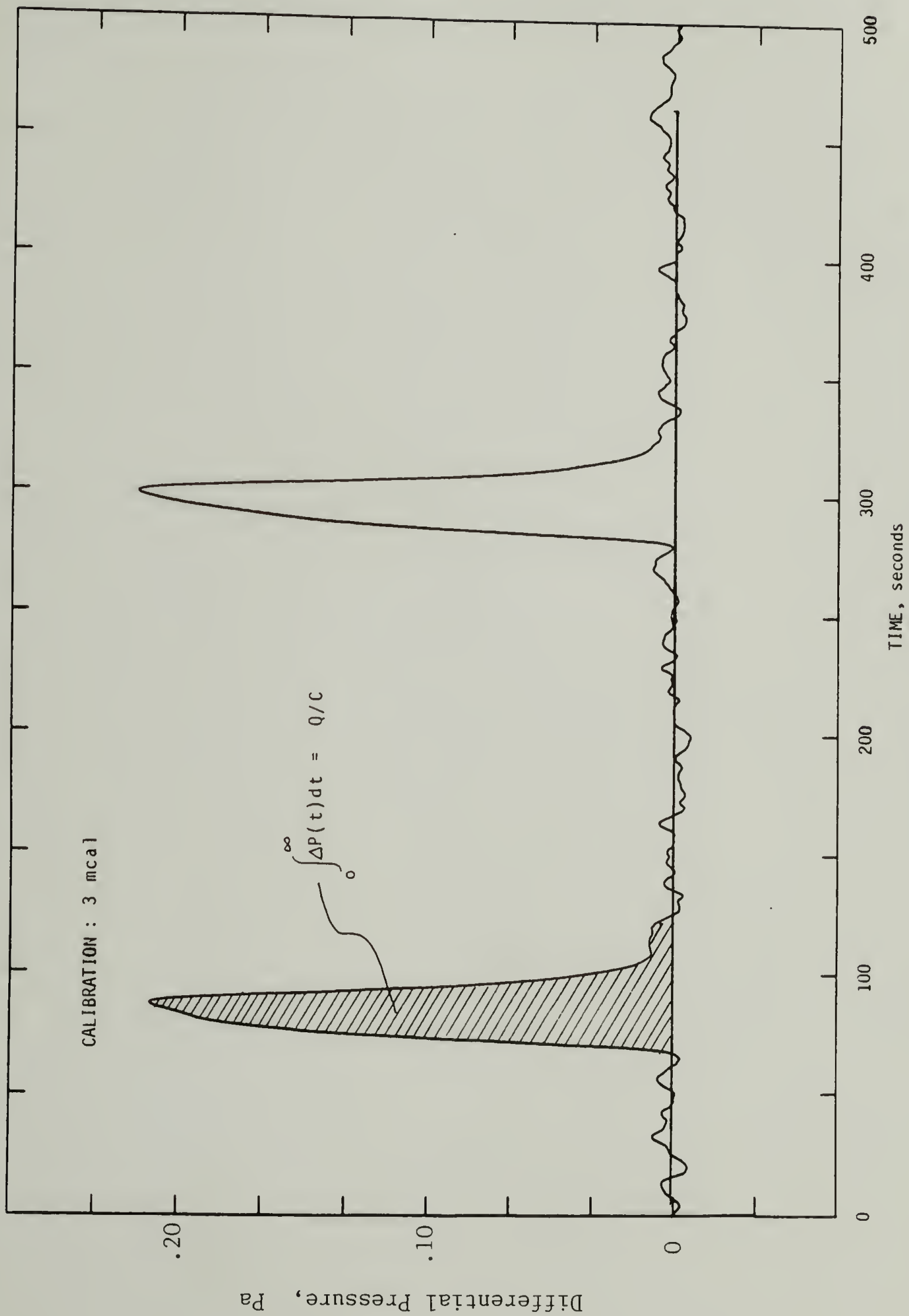


Figure. 4 Calibration Data for Deformation Calorimeter

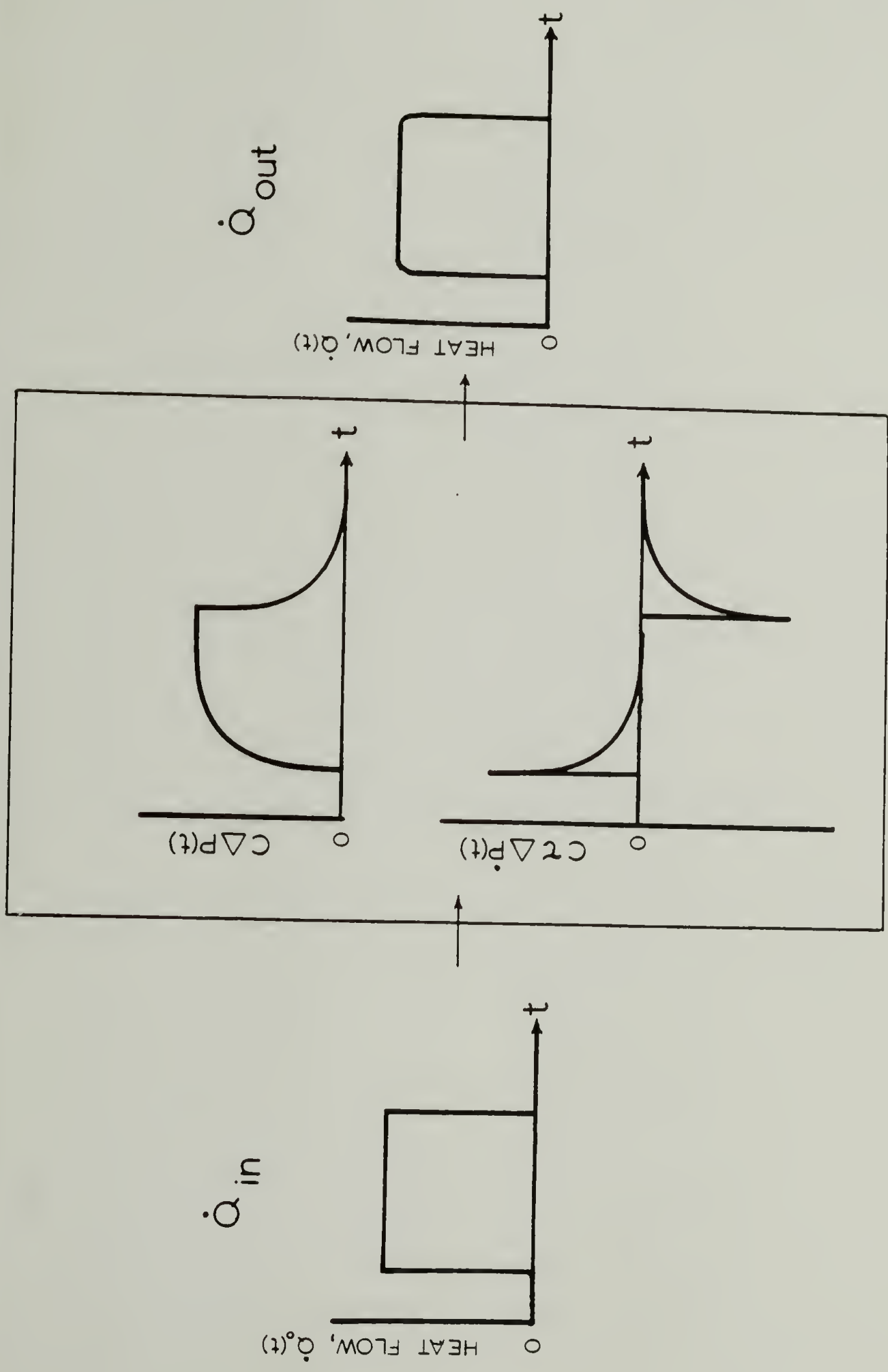


Figure 5. Reconstruction of Square Wave Heating Input Using Equation 65

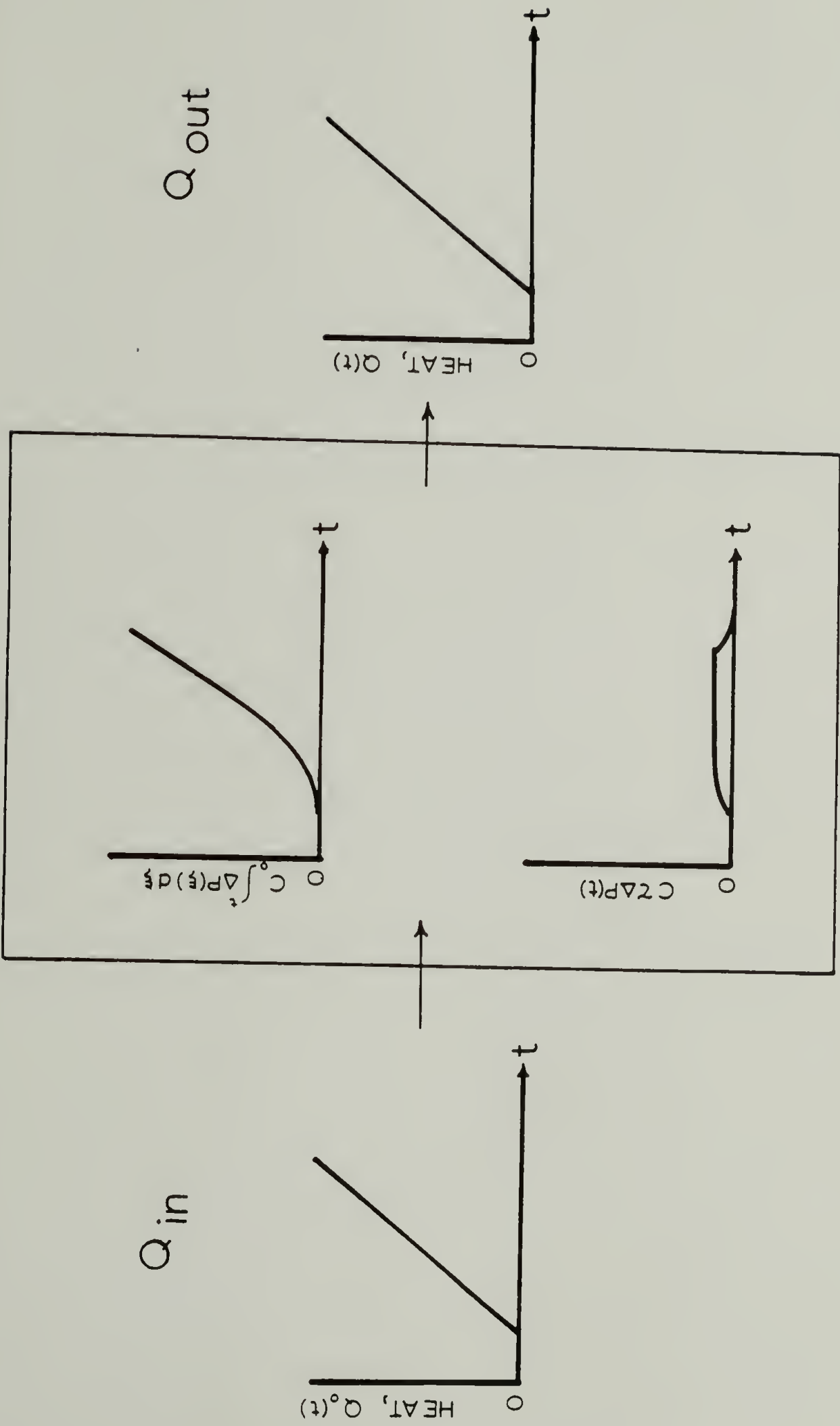


Figure 6. Reconstruction of Ramp Heat Input Using Equation 64

time t , will be simply the integral of the square wave heating function $(dQ/dt)_0$, or a ramp beginning at $t=0$. The pressure integral $\int_0^t \Delta P(\xi) d\xi$, is digitally added to the reduced pressure $\tau\Delta P(t)$ and multiplied by the calorimeter constant C , to recreate the ramp function. These procedures for obtaining the dynamic heat and heat flow are independent of the form of the heating input, and are expected to faithfully recreate the heating history in the deformation calorimeter for any actual deformation process.

In this section a quantitative analysis of the observed behavior will be attempted to aid in understanding the factors which effect the operation of the micro-calorimeter.

Steady-state Gas Pressure

The steady-state gas pressure in the sealed sample cylinder of inner radius R , having a localized heat source of radius r , along the centerline is calculated assuming radial heat conduction only through the gas and no end effects. Since gas pressure is uniform over the volume of the cylinder it necessarily represents the volume average of the temperature gradient between r and R .

The governing equation for steady-state heat conduction is

$$\nabla^2 T = 0 \quad (66)$$

For radial conduction only the temperature difference is-

$$\Delta T = T(r) - T(R) = \frac{\dot{q} \ln R/r}{2\pi k l} \quad (67)$$

where $\dot{q} = dq/dt$ is the heat flow from a generation source of length, l at steady-state through the gas of thermal conductivity k . The volume average temperature is then

$$\langle \Delta T \rangle = \frac{1}{V} \int_V \Delta T dV \quad (68)$$

Using the temperature difference of Equation 67, with $V = \pi (R^2 L - r^2 l)$, $dV = -2\pi r l dr$, and defining a new variable, $x = r/R$, Equation 68 becomes

$$\langle \Delta T \rangle = -\frac{\dot{q} R^2}{k V} \int_x^1 x \ln x dx \quad (69)$$

which is integrated to give

$$\langle \Delta T \rangle = \frac{\dot{q}}{4\pi k L} \left[1 + \frac{x^2 \ln x^2}{1 - x^2} \right] \quad (70)$$

The gas pressure then, assuming an ideal gas, is

$$\Delta P(\infty) = \frac{P_0}{T_0} \langle \Delta T \rangle = \frac{\dot{q} P_0}{4\pi k L T_0} \left[1 + \frac{x^2 \ln x^2}{1 - x^2} \right] \quad (71)$$

which is the equation originally derived by Muller and Engelter and later by Foster and Benner using slightly different, although equivalent reasoning. It is seen that in the limit as $r \rightarrow R$, Eqn. 70 becomes Eqn. 67 as it must. The effect of sample length is included in \dot{q} , while the effect of the sample radius is contained in the bracketed term, which is essentially unity for $x < .1$. A linear dependence of steady-state gas pressure on heat generation is predicted which is nearly independent of sample dimensions provided the sample radius does not exceed 10% of the cylinder radius. This is in agreement with experiment.

The proportionality constant C , between heat flow and steady-state gas pressure from Equation 71 is

$$C = \frac{\dot{q}}{\Delta P(\infty)} = \frac{4\pi k L T_0}{P_0} \quad (72)$$

which is estimated to have a value of 2.0×10^{-4} watt/Pa using standard properties for air at atmospheric pressure and room temperature (62). Experiments by Gregory and

Archer (63) yield a slightly higher value of .0342 w/M-K for the apparent thermal conductivity of air in 2.3 cm diameter vertical cylinders using hot-wire methods. Using this value for the thermal conductivity of air the predicted constant C, becomes 2.60×10^{-4} W/Pa which is within 3% of the measured value of 2.66×10^{-4} W/Pa as will be shown in the calibration section.

Transient Pressure Response

The transient pressure response of an ideal gas contained in an enclosure and subjected to internal heat generation from a localized source can be simply calculated if both the heat source and the gas can be treated separately using a lumped analysis. This amounts to assuming quasi-static behavior whereby the rate of heat transfer is proportional to the instantaneous value of the temperature gradient. Dring and Gebhart (64) have studied the transient heating of thin vertical wires in air and found agreement to within 7% of the single exponential quasi-static solution, suggesting that the lumped formulation should hold, at least for the heat source or sample. For the heat source, which may be a solid undergoing deformation or a resistance heating element, the energy balance is written

$$\rho_s V_s C_s \frac{dT_s}{dt} = \dot{q} - h A (T_s - T_g) \quad (73)$$

where the rate of increase of internal energy of the source is equated to the difference between the rate of distributed internal heat generation and the rate at which heat is conducted away from the surface into the adjacent gas at temperature T_g . The energy balance for the gas is written

$$\rho_g V_g C_g \frac{dT_g}{dt} = hA (T_s - T_g) - K_g(T_s - T_o) \quad (74)$$

where the rate of increase of internal energy of the gas equals the rate of heat addition from the source minus the rate of heat transfer to the enclosure wall maintained at temperature T_o .

Equations 73 and 74 constitute a pair of simultaneous linear ordinary differential equations having initial conditions:

$$\begin{aligned} T_g(0) &= T_s(0) = T_o \\ \dot{Q}(0) &= 0 \end{aligned} \quad (75)$$

$$\frac{dT_g(0)}{dt} = \frac{dT_s(0)}{dt} = 0$$

The solution procedure is to obtain T_s , dT_s /dt from Equation 74 and substitute these results into 73 to obtain the governing differential equation for the gas temperature. Defining

$$\theta = T_g - T_o , \quad \tau_s = \frac{\rho_s V_s C_s}{h A} , \quad \tau_g = \frac{\rho_g V_g C_g}{K_g}$$

the result is

$$\frac{d^2\theta}{dt^2} + C_1 \frac{d\theta}{dt} + C_2\theta = C_3 \dot{q} \quad (76)$$

where

$$C_1 = \frac{hA \tau_s + K_g (\tau_s + \tau_g)}{K_g \tau_g \tau_s}$$

$$C_2 = 1/ \tau_s \tau_g$$

$$C_3 = 1/ K_g \tau_s \tau_g$$

Taking Laplace transforms of Equation 76 subject to the initial conditions (Eqn.75), inverting and evaluating coefficients the heat at any time t , is just

$$Q(t) = K_{g_0} \int_0^t \theta(\xi) d\xi + \left[K_g (\tau_s + \tau_g) + K_s \tau_s \right] \theta(t) \quad (77)$$

$$+ K_g \tau_s \tau_g \frac{d\theta}{dt}$$

If the time lag between the temperature of the source and the heat generation is small compared to the time constant of the gas (i.e. $\tau_s \ll \tau_g$) then

$$Q(t) = K_g \int_0^t \theta(\xi) d\xi + K_g \tau_g \theta(t) \quad (78)$$

and by the usual assumption of an ideal gas we obtain Equation 64

$$Q(t) = C \int_0^t \Delta P(\xi) d\xi + C\tau \Delta P(t)$$

where C is the proportionality constant given by Equation 72, and τ the time constant of the gas, given by

$$\tau = \frac{Q}{\dot{Q}} = \frac{(\rho VC)_g \Delta T}{\left(\frac{2\pi kL \Delta T}{\ln R/r} \right)} = \frac{\rho C_v R^2 \ln R/r}{2k} \quad (79)$$

The important result is that the constant C is independent of the source (sample) properties and depends only on the rate of heat transfer through the gas, regardless of the approximation $\tau_s = 0$. This is essential for interpreting pressure data to obtain heat measurements. The steady-state calculation showed that C is also virtually independent of sample dimensions.

The transient equation for the gas pressure at any time t , during an arbitrary heat generation process is obtained by solving Equation 76 . The ideal gas result is found to be Equation 60 given previously, with a two exponential kernel function resulting from the two time constants, i.e.

$$K(t) = \frac{1}{C(\tau_2 - \tau_1)} \left[e^{-t/\tau_2} - e^{-t/\tau_1} \right] \quad (80)$$

where

$$\tau_1 = \frac{2}{C_1 - \sqrt{C_1^2 - 4C_2}}$$

$$\tau_2 = \frac{2}{C_1 + \sqrt{C_1^2 - 4C_2}}$$

$$C = \frac{4\pi kLT_0}{P_0}$$

Calibrations Calibration of the calorimeter was performed at atmospheric pressure and 293K by electrical resistance heating of .2546 mm diameter Nichrome wires having a linear resistance of 6.84 ohm/foot. Heating elements of various lengths of straight wire and 1/8 inch diameter coils were located along the sample cylinder axis at different vertical positions. A regulated power supply

with timing circuits was used to produce square wave heat pulses of 20.2, 40.7, 61.3 and 81.6 sec duration. The instantaneous heating rate, or thermal power, was calculated as $dq/dt = i^2 R$, where i is the measured current and R the resistance of the heating element in the calorimeter.

The calibration constant C , was evaluated according to Equation 61 from the reciprocal slope of the pressure-time integral versus the total heat input, $q = (dq/dt) \times \Delta t$ for a square wave pulse of duration, Δt . The calibration curve is shown in Figure 7, which contains data from short and long heating wires as well as different length heating coils. It is seen that all the data fall on the same curve, confirming the weak dependence of pressure response on source (sample) dimensions. The working value of $C = 2.66 \times 10^{-4}$ W/Pa was determined from all of the data using a weighted linear regression forced through the origin.

The same value for C was obtained by measuring the steady-state pressure at constant heating rate, as required by the linear relationship between gas pressure and heat flow implied by Equations 60-65. Original pressure-time data for a square wave heating input are shown in Figure 8 along with calculated points for a single exponential kernel function with a time constant of 7.1 sec. The fit is seen to be very good for the single exponential approximation, affirming the validity of the simplified dynamic

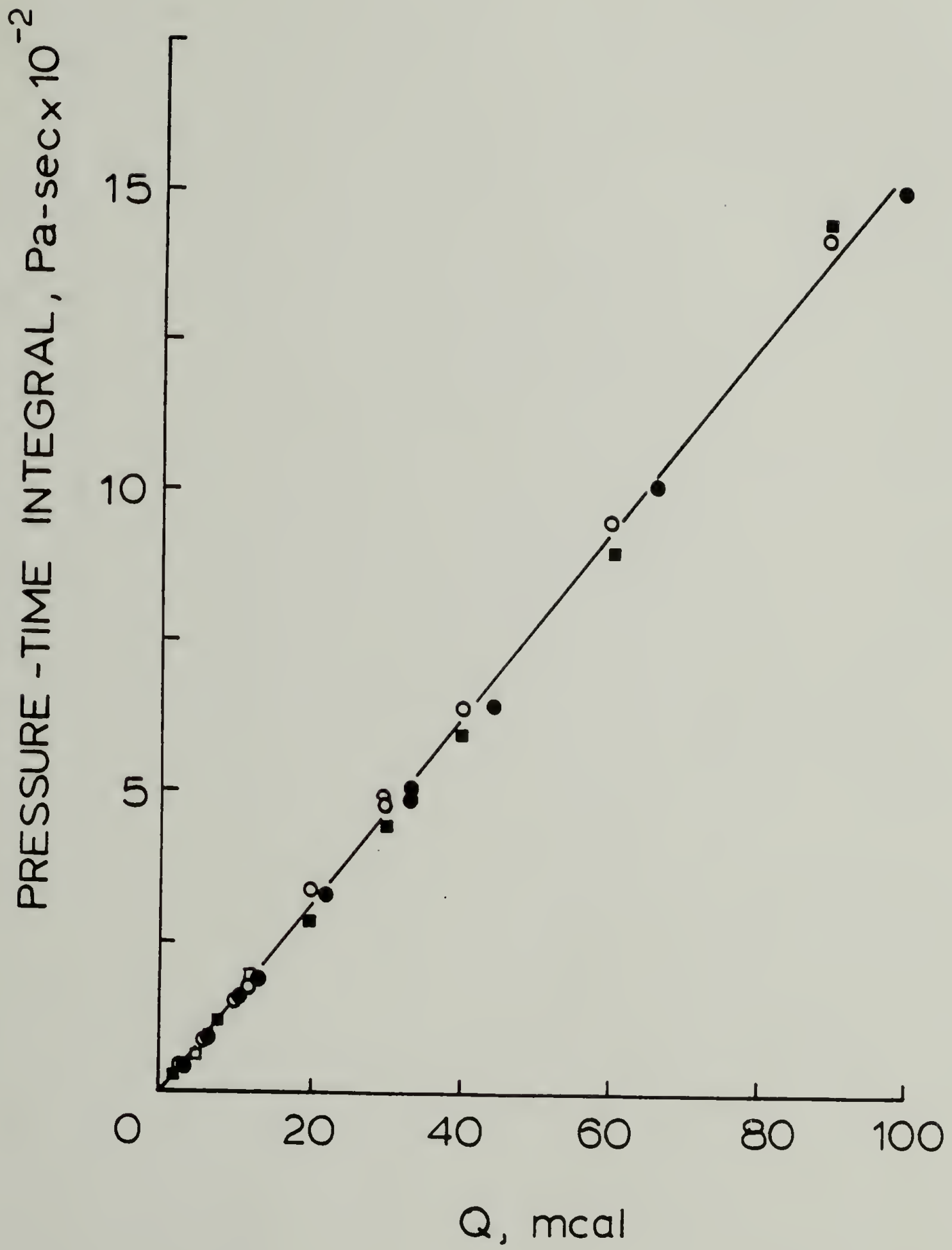


Figure 7. Calibration Curve for Deformation Calorimeter

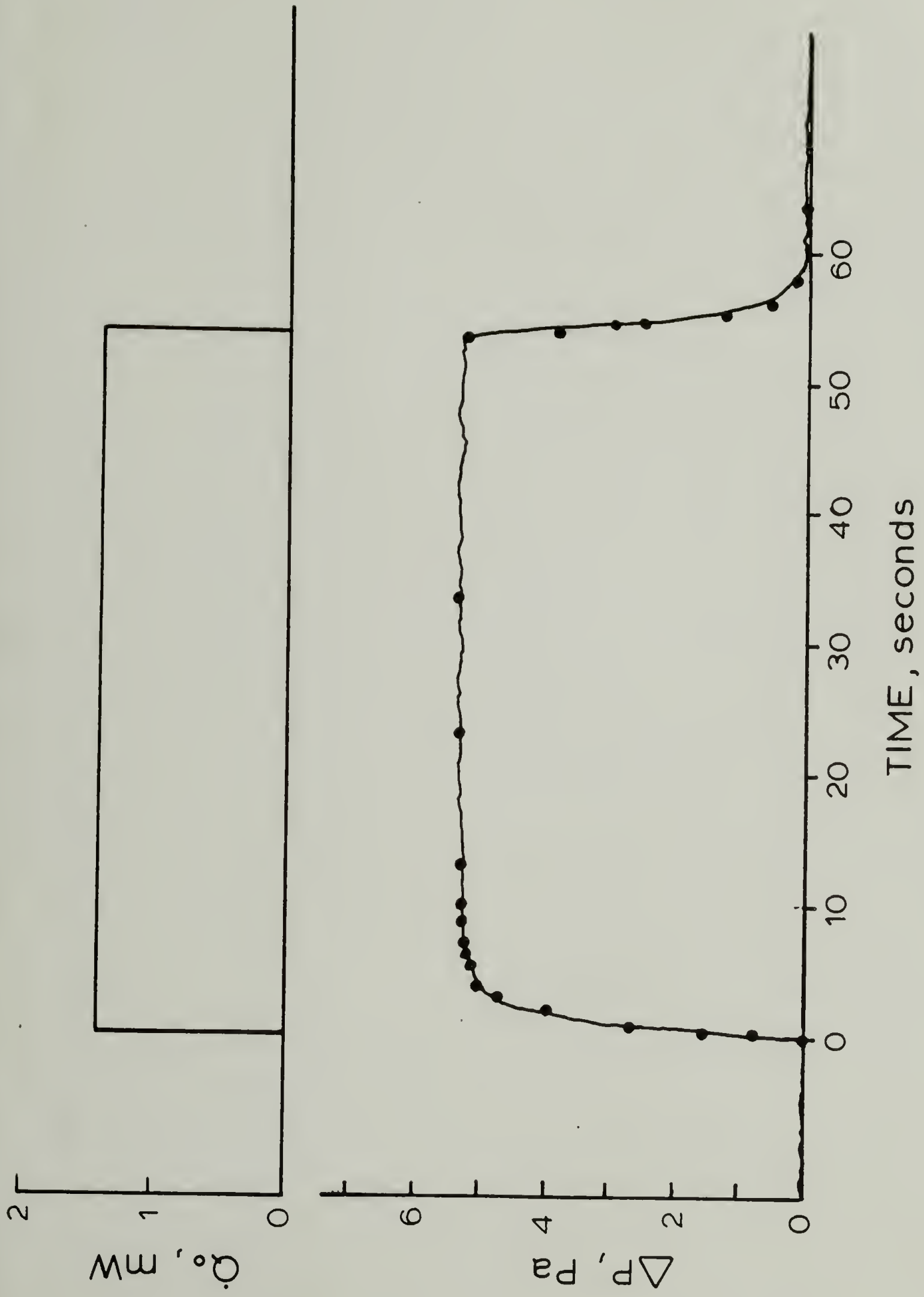


Figure 8. Pressure Response to Square Wave Heating Input. Points Calculated Using $\tau=7.1$ Sec.

equation for estimating heat flow directly from the instantaneous pressure curve. The time constant of 7.1 sec is in good agreement with the calculated value of about 7 sec using Equation 79 and the wire diameter. Since sample dimensions were always in the range $r/R=.03-.05$, a value of 6.8 sec was chosen for the working time constant, which for experiments longer than 10τ amounts to less than 1% error between the extremes using Equation 64 .

A heat flow detection limit of 20 microcalories/sec (84 microwatts) was determined from the electrically generated heat flow required to produce a pressure (voltage) deflection equal to twice the signal-to-noise ratio. The minimum detectable heat under quasi-isothermal conditions is about .1 mcal (.42 mJ) .

The pressure dynamics for homogeneous distributed internal heat generation in the gas were tested by compressing the air in the sample cylinder adiabatically using a double spring arrangement on the pullwire. In this way the temperature of the gas is made uniform throughout the cylinder. For an isentropic process, the pressure and volume are related by $P V^\gamma = k$, so that

$$\left(\frac{dP}{dV}\right)_s = \frac{-k\gamma}{V^{\gamma+1}} \quad (81)$$

whereas for isothermal compression of an ideal gas

$$\left(\frac{dP}{dV}\right)_T = -\frac{P}{V} \quad (82)$$

consequently,

$$\frac{(dP)_S}{(dP)_T} = \gamma = \frac{C_p}{C_v} \quad (83)$$

or the ratio of the adiabatic to the isothermal pressure change is equal to the heat capacity ratio of the gas. Figure 9 shows the pressure-time curves for adiabatic compression and expansion of the air in the sample cylinder. The adiabatic/isothermal pressure ratio is about 1.5, which is near the value of 1.4 for air. It is seen from this data that thermal equilibration of the gas is established in less than one second, which is significantly less than the overall time constant of about 7 sec for localized heat generation along the centerline. Since the temperature is uniform throughout, $T(r)=T(R)=\langle T \rangle$ so that dq/dt is given by Equation 71, and the time constant for homogeneous distributed generation becomes

$$\tau = \frac{Q}{\dot{Q}} = \frac{\rho C_v R^2}{4k} \approx .7 \text{ seconds} \quad (84)$$

which is closer to the measured value.

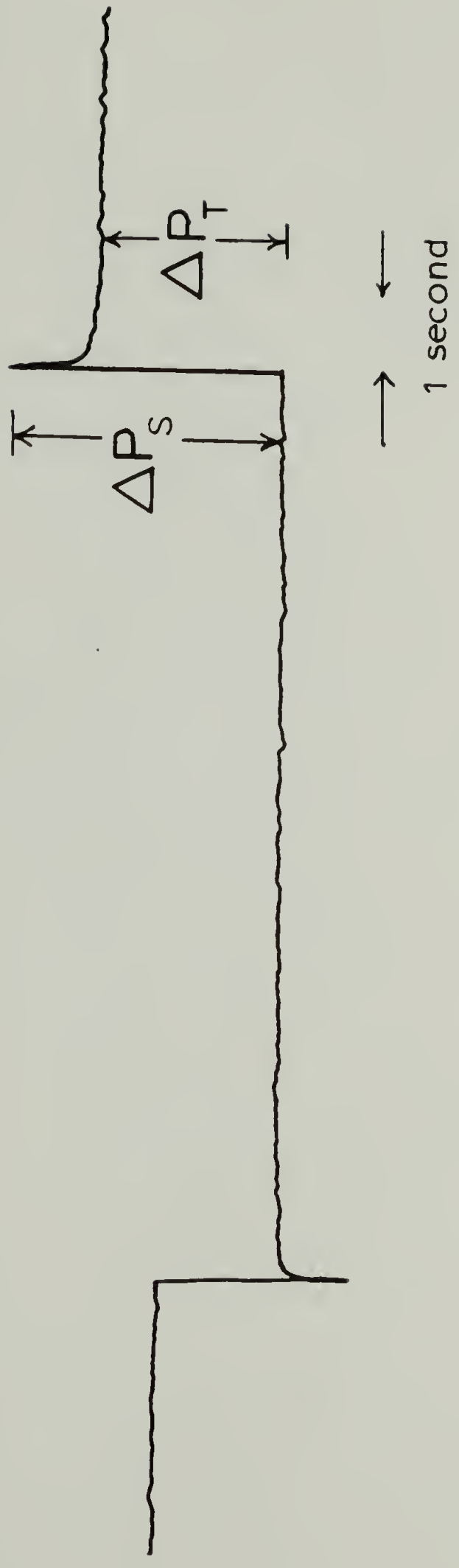


Figure 9. Aiabatic (ΔP_S) and Isothermal (ΔP_T) Pressure Change of Air in Calorimeter

In order to test the derived relationship between the gas pressure and heating history for something other than a step change , a sinusoidal heating program was used. A function generator with current amplification provided over three decades of frequency. For a sinusoidal current, $i = i_0 \sin \omega t$ and the instantaneous thermal power is

$$\dot{Q}(t) = i^2 R = i_0^2 R \sin^2 \omega t = \dot{Q}_0 \sin^2 \omega t \quad (85)$$

Substituting this heating history into Equation 60 with the two exponential kernel function of Equation 80 and solving yields a general solution which is the sum of periodic and transient terms. For long times the steady-state periodic solution is

$$\Delta P(t) = \frac{\dot{Q}_0}{2C(\tau_2 - \tau_1)} \left[\frac{4\omega^2 \tau_2^3 + 2\tau_2 \sin^2(\omega t - \delta)}{1 + 4\omega^2 \tau_2^2} - \frac{4\omega^2 \tau_1^3 + 2\tau_1 \sin^2(\omega t - \phi)}{1 + 4\omega^2 \tau_1^2} \right] \quad (86)$$

where

$$\tan \delta = 2\omega \tau_2, \quad \tan \phi = 2\omega \tau_1,$$

$$\text{and } \tan(\delta + \phi) = \frac{2\omega(\tau_2 + \tau_1)}{1 - 4\omega^2 \tau_1 \tau_2}$$

The two exponential kernel function therefor admits negative phase angles at high frequencies. The low frequency limit of Equation 86 is

$$\lim_{\omega \rightarrow 0} \Delta P(t) = \dot{Q}_0 \sin^2 \omega t \quad (87)$$

while at high frequencies

$$\lim_{\omega \rightarrow \infty} \Delta P(t) = \frac{1}{2} \frac{\dot{Q}_0}{C} = \frac{1}{2} \Delta P(\infty) \quad (88)$$

The predicted behavior is confirmed in Figure 10 which shows the transient and steady-state dynamic pressure response to sinusoidal heating frequencies of .004, .04 and .4 Hz. At high frequencies the pressure converges to exactly one half of the equilibrium value for $\dot{Q}_0 = 4.2 \text{mW}$. Lissajou figures for heating rate versus instantaneous pressure are shown in Figure 11 for all of the sinusoidal frequencies tested. Negative phase angles at high frequencies reflect the thermal inertia (second time constant) of the heating element, while at low frequency a time constant of about 7 sec corresponds to the value for air.

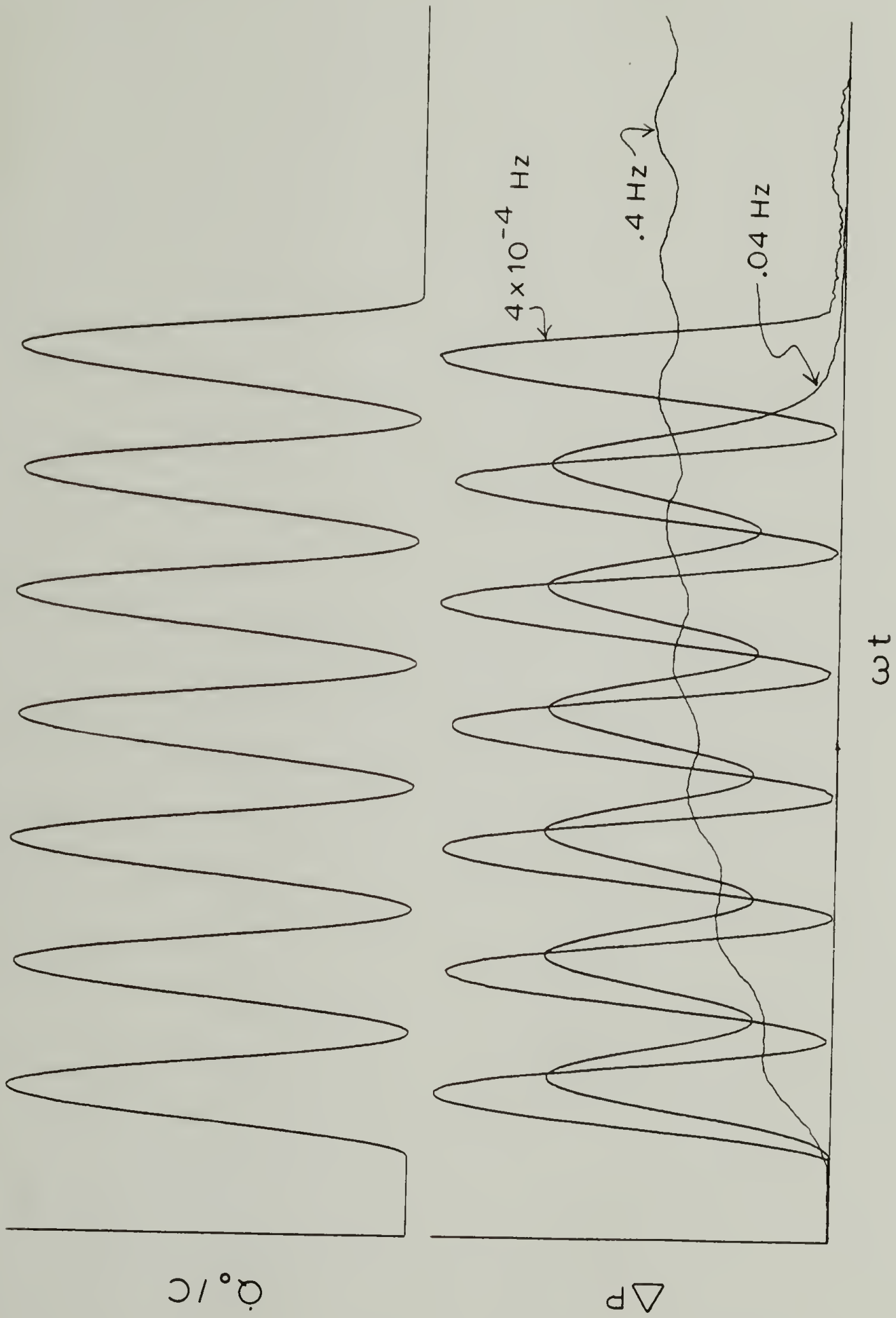


Figure 10. Dynamic Pressure Response to Sinusoidal Heating Inputs of .0004, .04 and .4 Hz

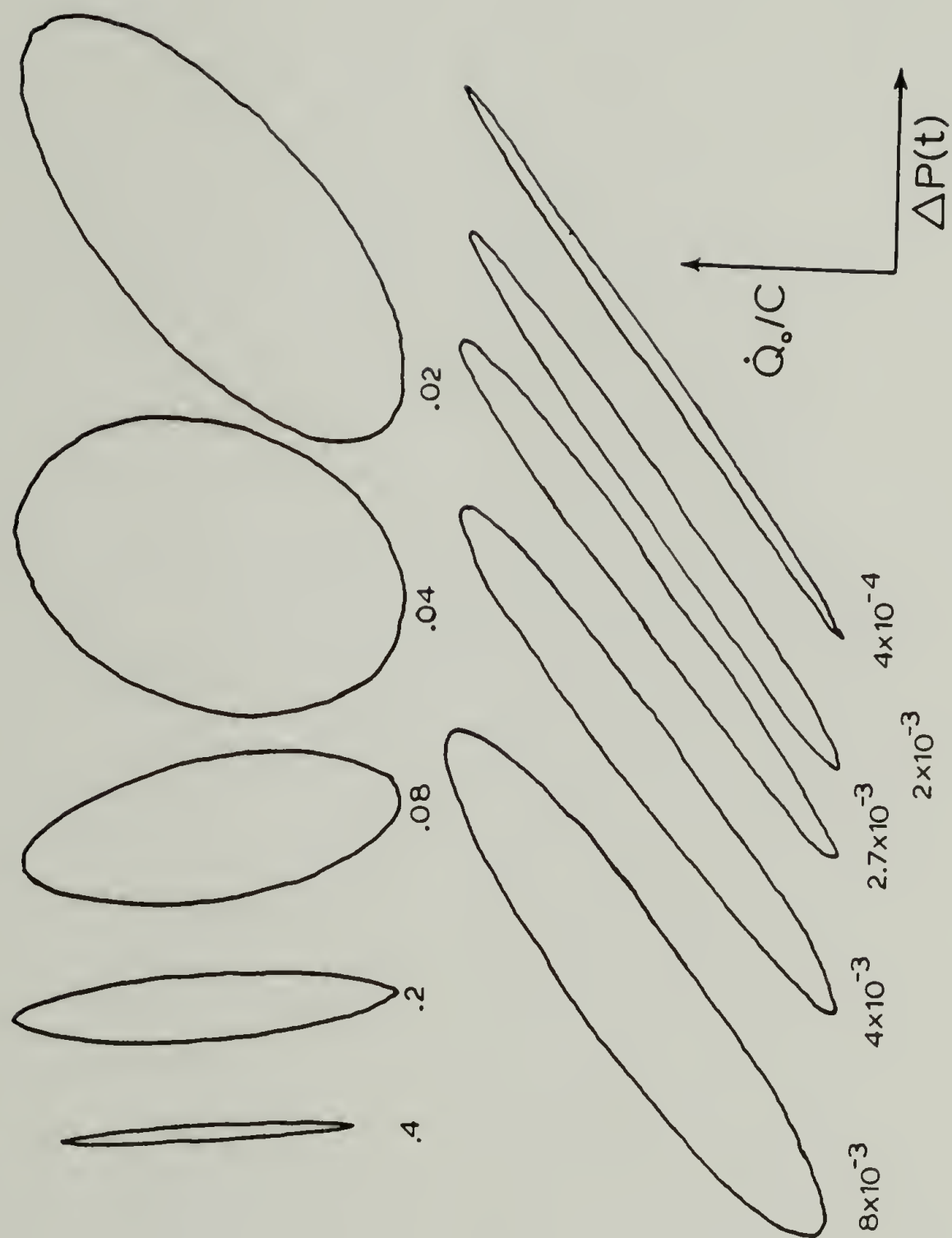


Figure 11. Lissajou Figures for Sinusoidal Heat Flow versus Dynamic Pressure at Indicated Frequencies (Hz)

Testing Procedure Polyurethane-urea elastomer samples tested were always in the form of loops made by tying together the ends of .05 x .1 x 6 cm strips cut from solvent cast films or as-spun fibers. Films of the polyurethane-ureas were cast from 10%w/w DMF solution, dried under vacuum at 100 C for 24 hours and held in a dessicator until testing. Loops of natural rubber were made from the as-received cut thread having .054 x .12 cm crossection and length 5-6 cm. The PBT/PTMO thermoplastic elastomer was also tested in the form of a loop made from the as-spun monofilament.

The knots were secured with a drop of cyanoacrylate adhesive (Super Glue) to prevent slipping during loading and unloading of the specimen. This testing geometry offers several advantages including uniform strain in the sample and minimum contact between the sample and wire hooks which are used to suspend it in the calorimeter, thus minimizing heat transfer to the pullwires. Sample weight and gauge length were determined after the experiment by carefully removing the knot with a razor knife. Sample weights were always in the range 10-50 mg.

Loops were suspended between hooks in the calorimeter and preworked to the highest strain level of the test until reversible length changes were observed. This usually required only one or two cycles, and was accompanied by a certain amount of thermally reversible extension

set, which, depending on the strain level could be as much as 10-12% for the polyurethane-ureas, but only a few percent for natural rubber. The extension set of the polyurethane-ureas could be almost wholly erased in less than a minute by heating the sample to 150 C. Polyethylene was tested in the form of small dogbones punched from compression molded .2 mm thick films having a cross-sectional area of .56 mm². Samples were connected to the wire hooks using small tabs attached to the end of the specimen.

The majority of heat measurements were made by digitally integrating the pressure-time curve after a deformation process and multiplying the value of the integral by the calorimeter calibration constant in the corresponding units. These values were divided by the sample weight and reported in units of Joules/gram sample. The graphical procedure for obtaining the reported values of heat and work is demonstrated in Figure 12 for a typical large strain loading/relaxation/unloading cycle of the polyether soft-segment elastomer between extension ratios ($\lambda = L/L_0$) of $\lambda = 1-3.93$ at a strain rate of 14.5%/minute.

The dynamic heat was calculated for some large strain deformation cycles of the elastomers using Equation 64 with $\tau = 6.8$ sec and the value of C obtained from the calibration curve. This was accomplished by writing a

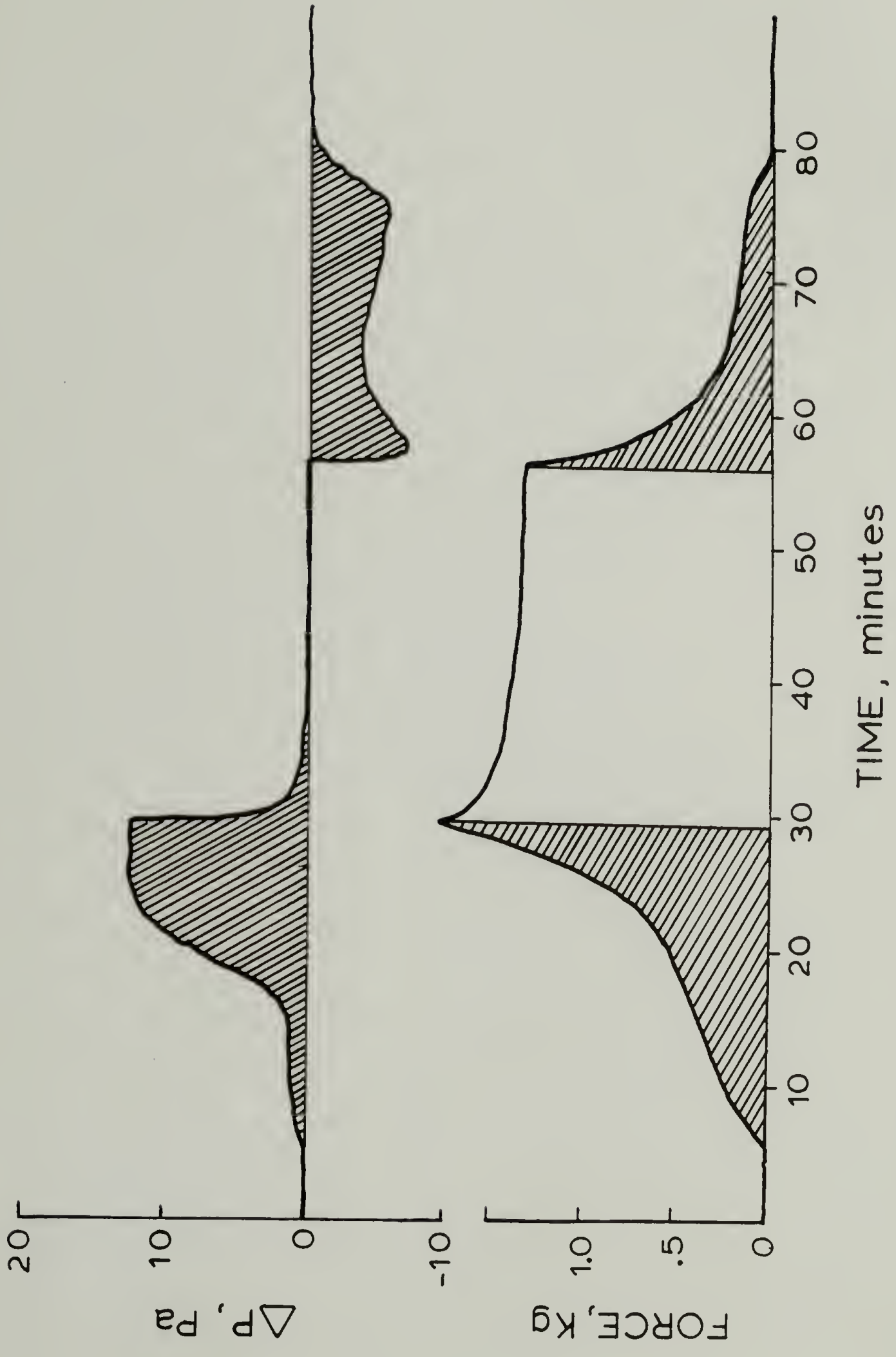


Figure 12. Graphical Procedure for Obtaining Heat (Q) and Work (W) from Deformation Calorimeter Data

small program in the Bascom-Turner recorder to operate on the stored pressure-time data. The instantaneous heat flow was calculated during the drawing of the polyethylene using Equation 65 and the same thermal and time constants.

Mechanical work was determined for the deformation process by digitally integrating the force-time data and multiplying by the loadcell calibration constant and the strain rate. Values are reported in Joules/gram after dividing by the sample weight. Since pressure-volume work resulting from sample dilatation against atmospheric pressure was several orders of magnitude less than the stress-strain work of deformation, no significant error is involved in neglecting this term.

Internal energy was obtained directly from the difference between the heat and mechanical work according to the first law of thermodynamics.

Differential Scanning Calorimetry of Stretched Samples

In order to characterize the melting behavior of stress-induced crystallinity a method was needed to hold the elastomer samples in the strained state during the differential scanning calorimetry (DSC) experiment. Holders for stretched fiber samples were machined from brass to the geometry shown in Figure 13 . Spool weights

averaged $530 \text{ mg} \pm 1\%$. Brass was chosen due to its high thermal diffusivity, high melting point and low expansion coefficient. The dimensions are such that the spools fit snugly inside the sample and reference compartments of a Perkin-Elmer DSC-2 differential scanning calorimeter with platinum compartment covers in place. The center hole is 0-80 threaded to facilitate automatic windup at low linear velocity using a motor-driven windup apparatus.

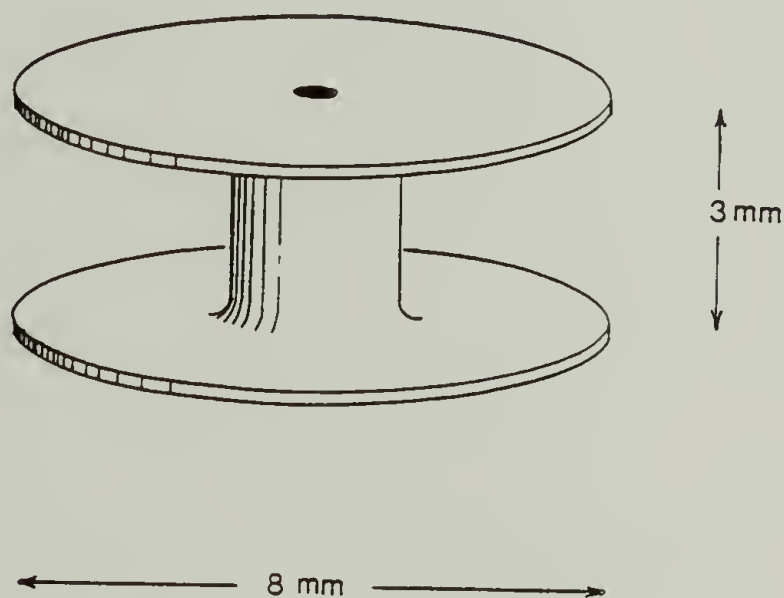


Figure 13. DSC Sample Spool

Sample preparation is relatively simple. The spool is first threaded onto the motor-driven shaft and a 25-50 mg fiber sample is secured to the spool at one end. The remaining end hangs freely and is dead weight loaded to obtain the desired elongation. After creep is complete, the equilibrium strain is measured from fiducial marks on the fiber, and the sample is then wound onto the spool

with the weight in place. When the entire fiber has been wound onto the spool, the weight is removed and the ends tied together to prevent contraction of the sample during the DSC experiment. Maintaining the sample in the elongated state is critical, as no stress-induced crystallinity melting peak is observed if the sample is allowed to contract during the scan (65,66). The spool containing the sample is then placed opposite a reference spool in the DSC-2, and the experiment is conducted in the normal manner.

To optimize DSC operating conditions it was necessary to determine the heat transfer characteristics of the sample + spool system. To this end a small piece of indium metal calibration standard ($T_m^0 = 429.78 \text{ K}$) was inserted under the upper lip of the spool and held in place by a fiber sample under low tension. This locates the indium at maximum distance from the sample chamber heating surface. This configuration was scanned at 5-mcal/sec sensitivity in the vicinity of the indium transition to determine the temperature lag of the transition due to thermal gradients in the spool.

Observed transition temperatures versus heating rate for indium are plotted in Figure 14 for comparison of the spool and standard aluminum DSC pans furnished by Perkin-Elmer. It is seen that both environments show linearity over the entire range of heating rates, although excessive

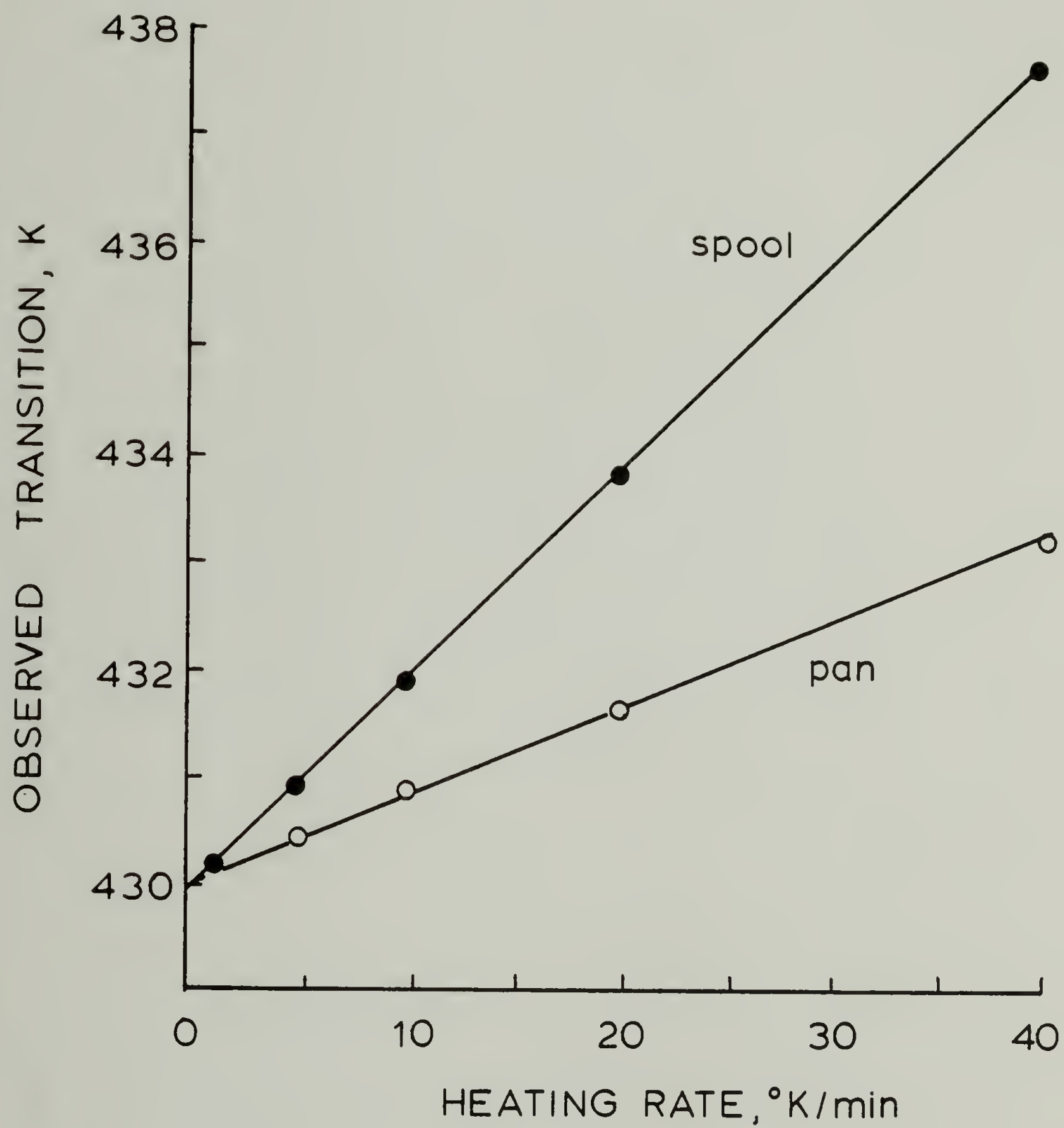


Figure 14. Comparison of Observed Melting Transition Versus Heating Rate for Indium in DSC Sample Spool and Standard Pan

peak broadening was observed for the spool at heating rates greater than 20 K/ min. Consequently, heating rates of 10 K/min were used for all experiments.

Wide-Angle X-Ray Diffraction Studies

Wide-angle x-ray diffraction (WAXD) equatorial scans were performed on stretched films of the polyurethane-urea elastomers and fiber bundles of natural rubber using a stretching device similar to that described by Alexander (67). Strain was measured from the displacement of fiducial marks on the samples. A Siemens D-500 X-ray diffractometer using 1.54 \AA $\text{CuK}\alpha$ radiation was employed for all the studies. Equatorial intensity scans were performed at $1^\circ/\text{min}$ from 4° to 40° 2θ at room temperature. Integral breadth or peak width at 1/2 maximum intensity was measured to estimate oriented crystallite dimensions, a , perpendicular to the stretching according to the Scherrer (68) equation-

$$\delta\beta = \frac{K \lambda}{a \cos \theta} \quad (89)$$

where $\delta\beta$ is the half-height peak width in radians at scattering angle, θ and K is a constant assumed to be

unity. Corrections for lattice strain and lattice paracrystalline distortion proposed by Hosemann and Bagchi (69) were not performed due to the absence of higher order reflections. Consequently, the calculated values for crystallite lateral size represent a lower bound estimate.

Thermostatic Measurements

The retractive force of fiber samples held at fixed length during heating and cooling at 5 K/min was measured using the device shown in Figure 15. During experiments the sample is suspended between an upper hook and a lower hook connected directly to a Tyco, Toyo or Interface load-cell which produces a voltage signal proportional to the force on the sample. The position of the upper hook connected to the stretching rod is adjusted to fix the length (strain) of the sample during heating and cooling scans. Heating of the sample is accomplished by increasing the voltage to a 1000 watt tubular glass furnace surrounding the sample. Cooling is achieved by simply allowing the furnace and sample to return to room temperature, sub-ambient temperatures being obtained by flowing gasified liquid nitrogen through the sample chamber at a controlled rate.

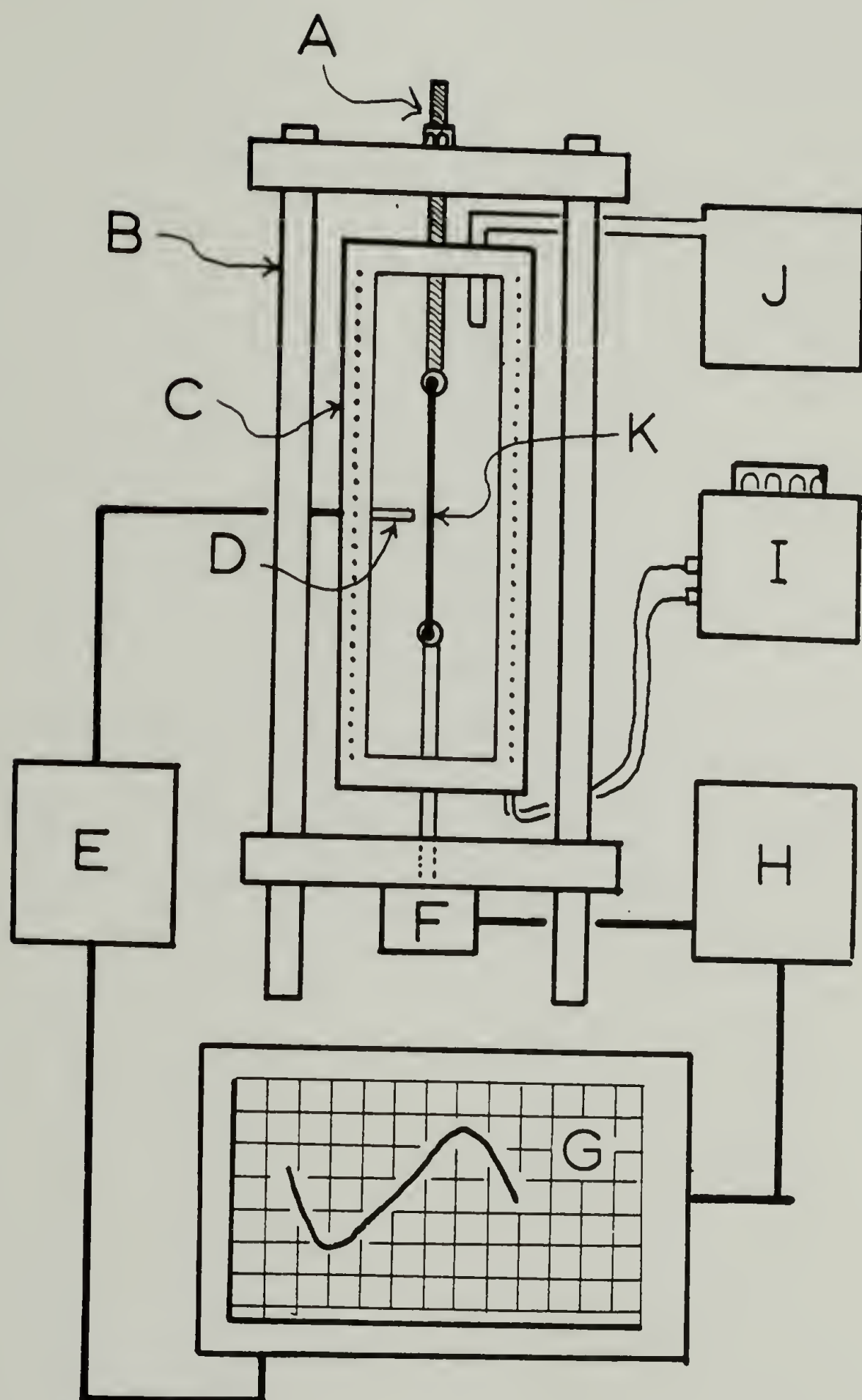


Figure 15

Force versus Temperature Apparatus; A) Stretching Rod, B) Load Frame, C) Environmental Chamber, D) Temperature Probe, E) Temperature Readout, F) Load Cell, G) Recorder, H) Load Cell Control, I) Variac, J) Liquid Nitrogen Reservoir, K) Sample

Sample temperature was measured during the heating and cooling scans by an Omega platinum resistance probe placed within the fiber bundle at a mid-height vertical position. Sample force and temperature signals were fed directly to a Houston-Instruments X-Y recorder to produce a direct graphical recording of the force-temperature curve.

Power Cycles of Polyurethane-urea Elastomers

Experimental thermodynamic cycles were obtained for the polyurethane-urea elastomers using an Instron Servo-Hydraulic Tensile Tester fitted with a specially designed quick-response environmental chamber. The experimental apparatus is shown schematically in Figure 16. A ramp strain program was used to cyclically deform the elastomers between a minimum (λ_{\min}) and maximum (λ_{\max}) extension ratio ($\lambda = L/L_0$) in a fixed amount of time. As a consequence of the fixed time interval (10 sec), strain rates for extension and contraction varied from 20 to 60 % sec⁻¹. Previous experiments showed that the mechanical response of these materials is insensitive to variations of four decades of strain rate.

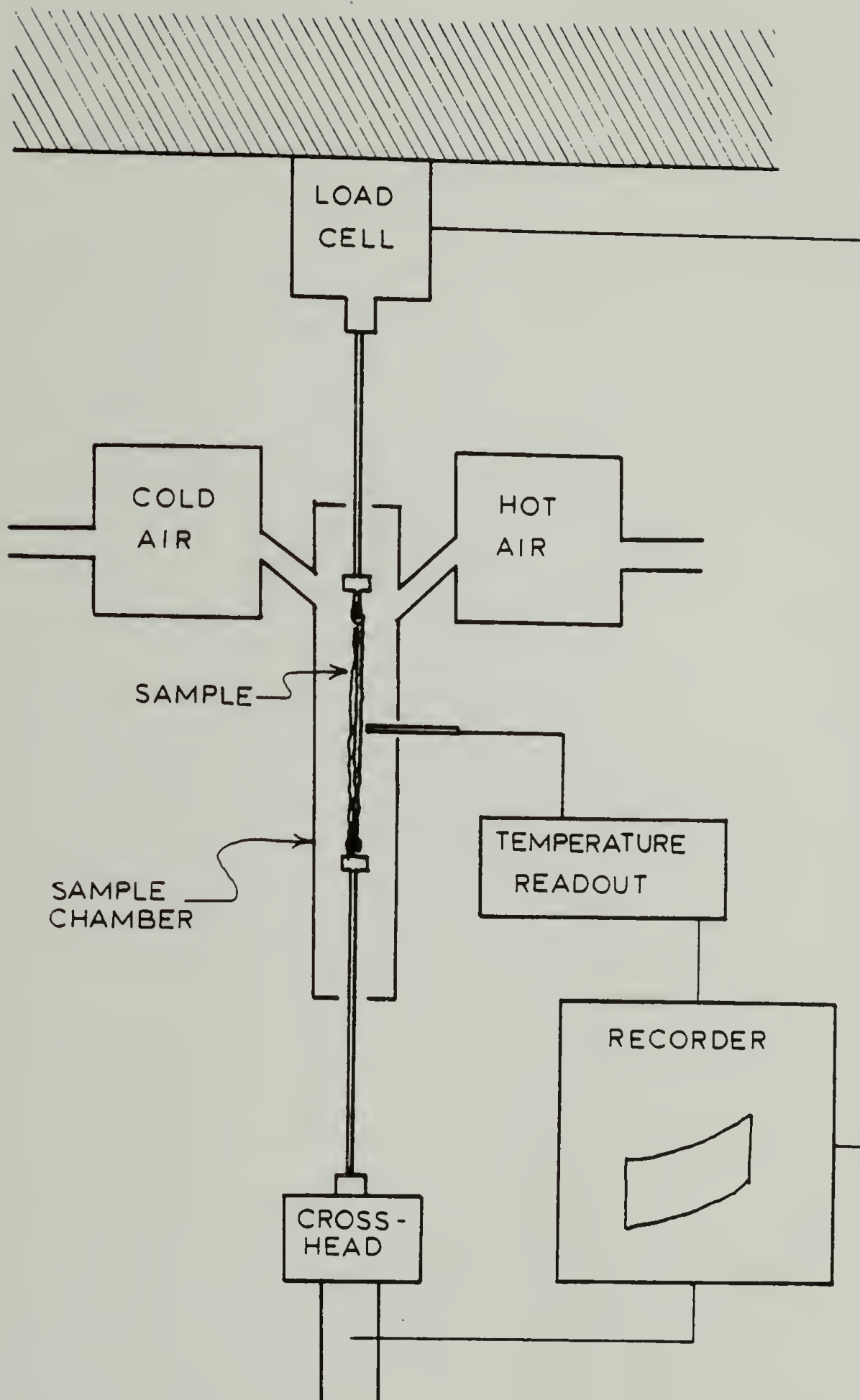


Figure 16. Heat Engine Cycling Apparatus

The sample temperature was cycled between a low ($T_{10} = 283 \text{ K}$) and various high temperatures ($T_{hi} = 313, 333, 353, 373$ and 393 K) by alternately forcing cold and hot dry air through the sample chamber at a flow rate of 1.5 L/sec . This produced a heating and cooling rate in the sample of 200 K/min . Heating of incoming air was accomplished by using an in-line 1500 watt resistance heater. Cold air was supplied through copper tubing heat exchange coils immersed in liquid nitrogen. Sample temperature was measured at the fiber surface using an Omega RTD platinum resistance probe whose thermal response was matched to that of the fiber. The cyclic strain and temperature program used to impart the thermodynamic cycle to the elastomer fibers is illustrated schematically in Figure 17.

The purpose of this strain-temperature program is to cycle the elastomer through the idealized (Sterling) cycle shown in Figure 18. The individual thermodynamic processes are:

1-2: The elastomer is deformed isothermally at T_{10} from λ_{\min} to λ_{\max} releasing heat Q_{12} to the low temperature reservoir. Work is done on the elastomer during this step.

2-3: The temperature is raised from T_{10} to T_{hi} at λ_{\max} adding heat Q_{23} to the elastomer. Since elastomers possess positive force-temperature coefficients in the

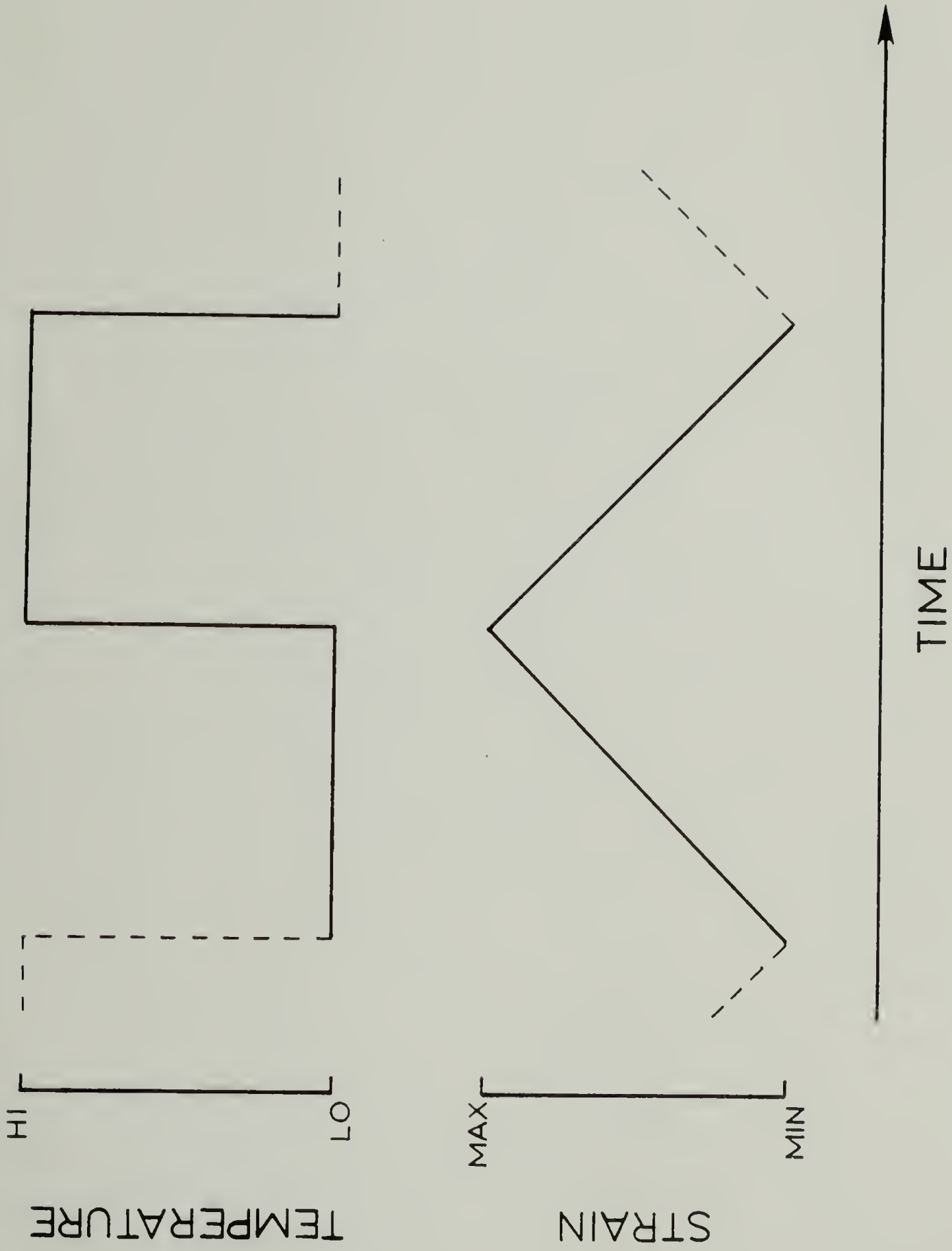


Figure 17. Strain and Temperature Programs Used in Heat Engine Cycles

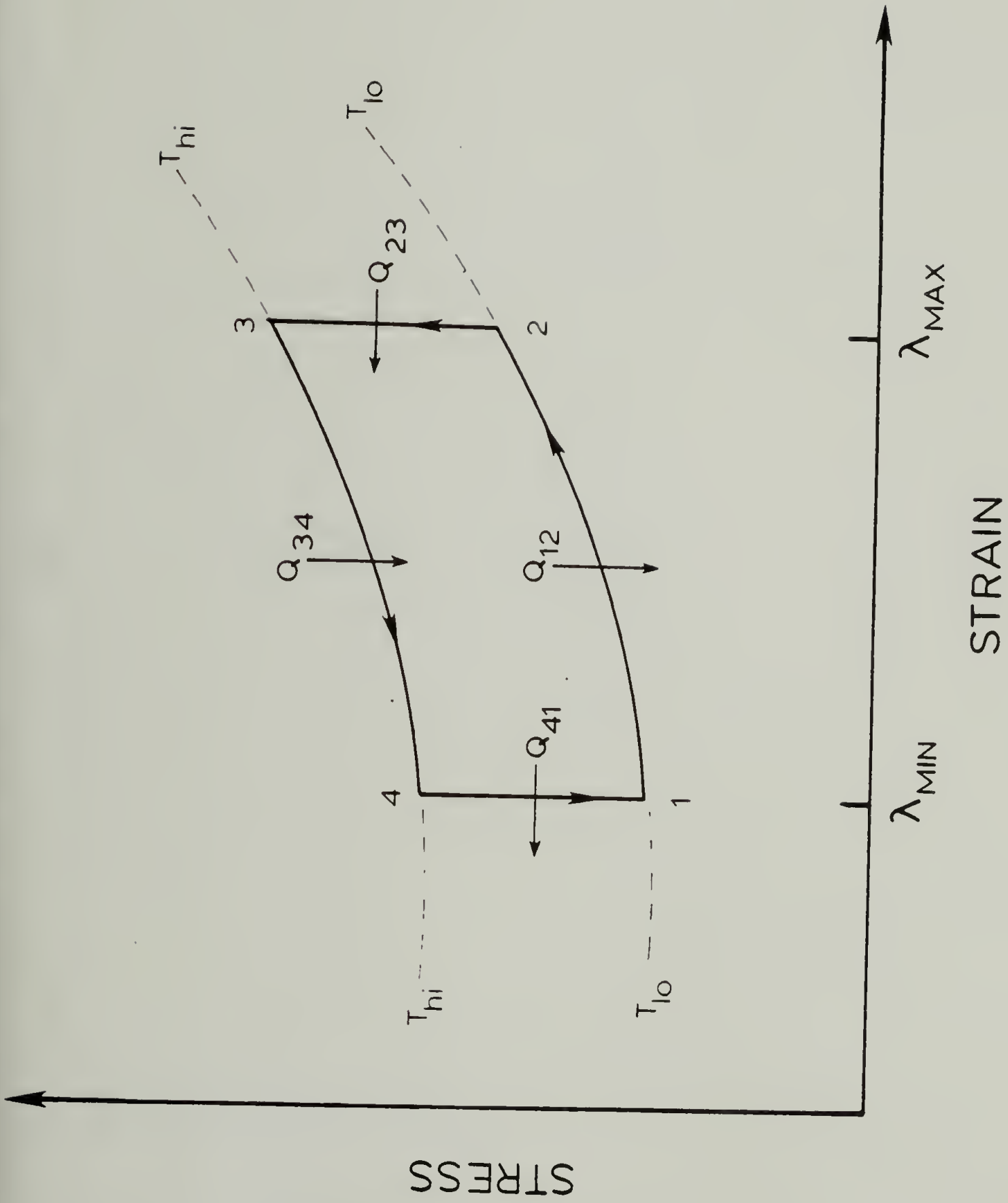


Figure 18. Idealized Heat Engine (Sterling) Cycle

extended state the force is expected to increase at constant strain. No work is done during this step.

3-4: The elastomer is allowed to contract isothermally at T_{hi} from λ_{max} to λ_{min} , doing work in the process. An amount of heat, Q_{34} , is absorbed from the high temperature reservoir.

4-1: The temperature is lowered from T_{hi} to T_{lo} at λ_{min} , extracting an amount of heat Q_{41} from the sample. The force decreases at constant length due to cooling but no work is done. The elastomer has now returned to the initial state, completing the cycle.

A direct graphical recording of the actual experimental cycle, as idealized in Figure 18, was obtained by measuring the force versus displacement on a Hewlett-Packard x-y-y recorder. The work performed on or by the elastomer during a complete cycle is obtained as the area bounded by the closed curve 1-2-3-4-1 of Fig. 18. Sample temperature was simultaneously measured on the third channel.

Separate fiber samples of approximately 70 mg were used for each strain perturbation after suitable equilibration at the maximum strain and temperature of the cycle. Power cycles were performed until reproducible traces were obtained for those conditions of the cycle. This usually required several preconditioning cycles.

C H A P T E R I V

RESULTS AND DISCUSSION

Deformation Calorimetry

Isothermal deformations were performed in the calorimeter to measure the heat, work and by difference the internal energy change accompanying a deformation process. The principle focus of these studies was to characterize the stress-induced crystallization of the polyether and polyester soft-segment polyurethane-urea elastomers as it occurs during room temperature stretching and contracting, and subsequently relate this to the thermomechanical behavior of these materials in heat engine cycles. Natural rubber was also studied by deformation calorimetry since the thermoelastic behavior of this polymer is well documented, providing a broad data base for comparison purposes. Moreover, since natural rubber is a single component chemically crosslinked elastomer, it should be free of the possibility of thermal effects arising from deformation-induced phase mixing or changes in hydrogen bonding- both of which could be operable during polyurethane-urea deformations. The fact that natural rubber is also very nearly an ideal rubber, (i.e., $q=w$) suggests its use for checking the

calibration of the deformation calorimeter.

The segmented thermoplastic elastomer (Hytrel)[®] having a continuous hard segment phase was studied for comparison with the more highly extensible polyurethane-ureas in which the soft-segment phase is continuous. It was expected that these two different phase structures would yield entirely different mechanisms of mechanical energy storage.

Anticipating the deformation of elastomers possessing a significant degree of crystallinity (induced by stretching), necking of polyethylene was studied to characterize the thermodynamic behavior of an inherently crystalline material subjected to a disruptive mechanical process, as would describe stress-crystallized elastomers at ultimate elongations.

Polyurethane-urea Elastomers and Natural Rubber

Incremental strain deformation experiments at 292 K were conducted on previously worked samples of the PTMO soft-segment polyurethane-urea and natural rubber at strain rates of 14 and 26%/min, respectively. Incremental strain experiments consisted of monotonically increasing the strain of the elastomer in small deformation steps with time allowed between steps for thermal and mechanical equilibration of the sample. The heat of each deformation

step (ΔQ) was determined from the area under the pressure-time curve for that step multiplied by the calorimeter constant, C . The work for each deformation step (ΔW) was similarly determined from the area under the force-time curve for the particular step multiplied by a suitable constant containing the strain rate and force calibration. The internal energy change per step (ΔU), was obtained directly from the difference between the heat and work for the step.

After incremental loading to the maximum strain of the experiment, the samples were allowed to relax for about 15 minutes before the incremental unloading sequence was begun through the same strain states used for the loading sequence.

The results of these experiments are shown in Tables 1 and 2 for natural rubber and the polyether soft-segment elastomer, respectively. Since the same sequence of strain was used for loading and unloading, the incremental heat, work and internal energy for a particular value of strain can be compared directly.

It is immediately apparent from this data is that the values for loading and unloading are significantly different, although the internal energy change for the complete cycle is approximately zero. The step-loading curve is characterized by a negligible internal energy component until a critical extension ratio of about 2.5 and 6 for

TABLE 1

Incremental Strain Deformation Calorimetry Data for Natural Rubber

EXTENSION RATIO		LOADING			UNLOADING		
MIN	MAX	ΔQ	ΔW	ΔU	ΔQ	ΔW	ΔU
1.0	1.6	-.09	.07	-.02	.03	-.01	.02
1.6	2.1	-.13	.20	.07	.11	-.07	.04
2.1	2.6	-.23	.31	.08	.10	-.11	-.01
2.6	3.0	-.27	.37	.10	.22	-.28	-.06
3.0	3.5	-.30	.40	.10	.20	-.31	-.11
3.5	4.0	-.42	.38	-.04	.52	-.34	.18
4.0	4.5	-.37	.52	.15	.88	-.40	.48
4.5	5.0	-.42	.58	.16	1.09	-.41	.68
5.0	5.5	-.50	.57	.07	1.09	-.41	.68
5.5	6.0	-.68	.64	-.04	1.16	-.44	.72
6.0	6.4	-1.73	.71	-1.02	1.34	-.50	.84
6.4	6.9	-2.52	.73	-1.79	1.29	-.50	.79
6.9	7.4	-2.96	.79	-2.17	1.37	-.64	.73
Totals:		-10.62	6.27	-4.35	9.40	-4.42	4.98

All values in Joules/gram of elastomer, $T = 292 \text{ K}$

TABLE 2

Incremental Strain Deformation Calorimetry Data for
Polyether Soft Segment Polyurethane-urea Elastomer

EXTENSION RATIO		LOADING			UNLOADING		
MIN	MAX	ΔQ	ΔW	ΔU	ΔQ	ΔW	ΔU
1.00	1.18	-.11	.11	.00	.00	-.01	-.01
1.18	1.30	-.10	.12	.02	.00	-.03	-.03
1.30	1.37	-.10	.10	.00	.15	-.03	.12
1.37	1.42	-.08	.07	-.01	.13	-.03	.10
1.42	1.54	-.25	.21	-.04	.71	-.12	.59
1.54	1.63	-.23	.23	.00	.66	-.09	.57
1.63	1.74	-.32	.25	-.07	.86	-.12	.74
1.74	1.85	-.36	.25	-.11	1.03	-.13	.90
1.85	1.95	-.43	.25	-.18	.96	-.13	.83
1.95	2.00	-.45	.22	-.23	.79	-.11	.68
2.00	2.14	-.45	.28	-.27	1.21	-.13	1.08
2.14	2.23	-.57	.28	-.29	.78	-.14	.64
2.23	2.31	-.58	.25	-.33	.53	-.12	.41
2.31	2.39	-.80	.26	-.54	.66	-.13	.53
2.39	2.49	-1.24	.38	-.86	.83	-.18	.65
2.49	2.58	-1.27	.33	-.94	.61	-.18	.43
2.58	2.66	-1.05	.27	-.78	.36	-.16	.20
2.66	2.75	-1.68	.35	-1.33	.61	-.22	.39
2.75	2.83	-1.27	.36	-.91	.55	-.23	.32
2.83	2.92	-1.76	.45	-1.31	.44	-.30	.14
2.92	3.00	-1.21	.39	-.82	.54	-.29	.25
3.00	3.08	-1.18	.44	-.74	.57	-.40	.17
Totals:		-15.5	5.9	-9.6	13.0	-3.3	9.7

All values in Joules/gram elastomer, $T = 292 \text{ K}$

the PTMO soft-segment elastomer and natural rubber respectively, at which points the internal energy decreases sharply indicating that crystallization had begun.

The raw data showed consistently negative (exothermic) heat flow for every deformation step during loading. In contrast, the raw unloading data showed an initial endotherm (melting) followed by a more protracted exotherm, possibly due to recrystallization. The combination of the two processes during unloading delays the complete melting of stress-induced crystallinity to much lower extension ratios than that required to initiate crystallization during loading. Consequently, the internal energy (as an estimate of crystallinity) is not a unique function of strain once crystallization has commenced during loading, even for the quasi-static process of loading and unloading in small strain increments. The cumulative internal energy versus extension ratio, obtained by summing the incremental values in Tables 1 and 2, are shown in Figures 19 and 20 for natural rubber and the PTMO soft-segment elastomer respectively.

In addition to the small strain step-loading and step-unloading experiments, the polyurethane-urea elastomers and natural rubber were subjected to continuous loading-unloading cycles with intermediate relaxation. In this way the elastomers were deformed between two states of strain in a single process. These cyclic

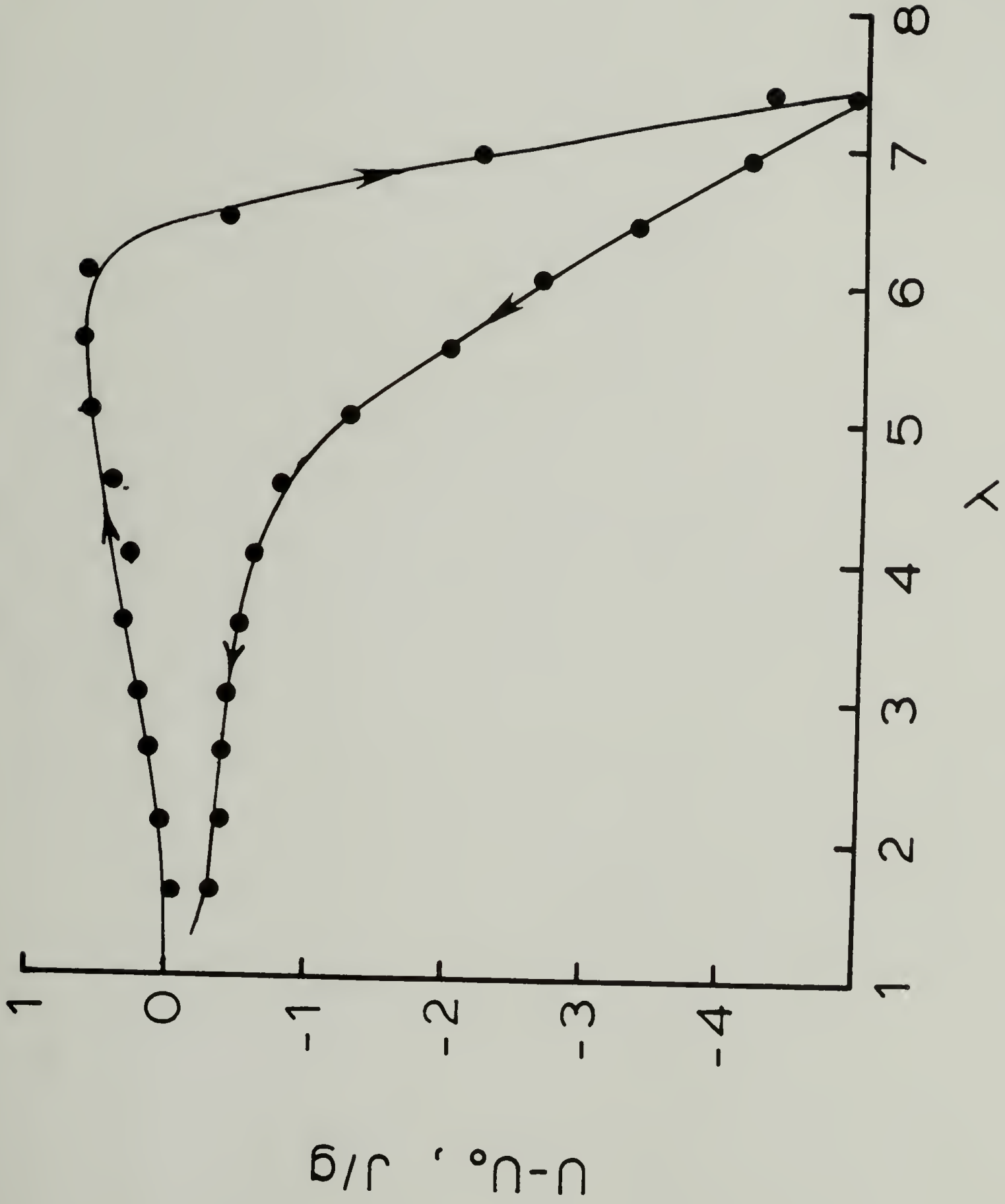


Figure 19. Cumulative Internal Energy Change versus Extension Ratio for Incremental Loading and Unloading of Natural Rubber

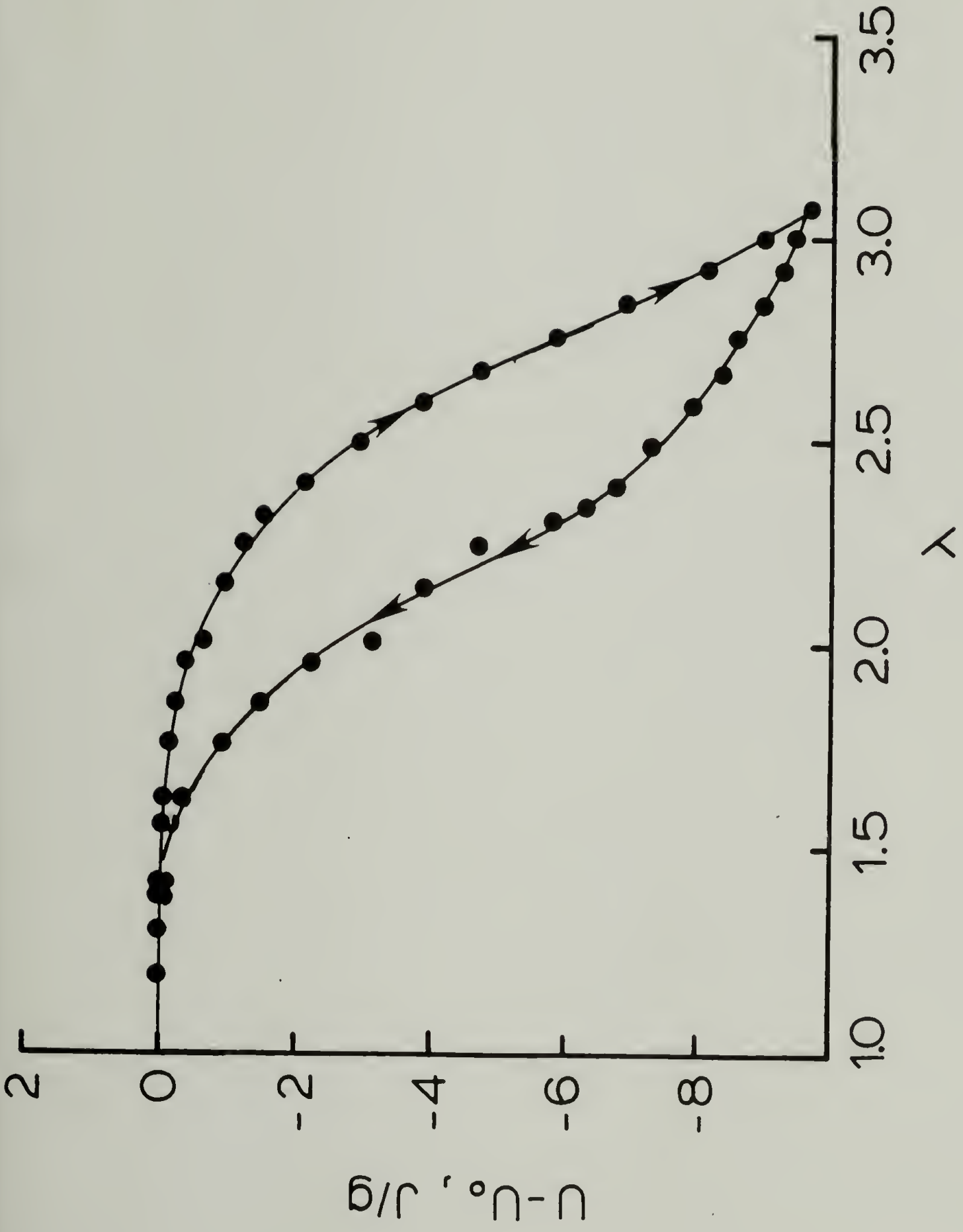


Figure 20. Cumulative Internal Energy Change versus Extension Ratio for Incremental Loading and Unloading of Polyether Soft Segment Polyurethane-urea Elastomer

loading/relaxation/unloading cycles were performed at constant temperature and various strain perturbations, including small strain perturbations on top of large static strains where the polyurethane-ureas were found to operate most effectively in heat engine cycles.

Data obtained in this way for natural rubber are shown in Table 3 . It is seen that the internal energy changes during room temperature deformation of preworked samples are recoverable over the entire range of strain and strain perturbation. At extension ratios less than 5-6, the internal changes are small or zero, but at higher extension ratios consistently large but recoverable internal energy changes are observed, indicating that crystallization and melting occur to yield no net internal energy change for the particular strain interval. The maximum internal energy change of 11.5 J/g obtained in large strain deformation cycles between extension ratios of 1-8.9 corresponds to about 18% crystallinity using 64 J/g for the heat of fusion of natural rubber. This is in good agreement with X-ray scattering estimates of stress-induced crystallinity by other workers (70-72). At the higher test temperature of 333 K, only 3.6 J/g is obtained for the internal energy change over the same strain interval, corresponding to only 5.6% crystallinity. It is not surprising that the amount of stress-induced crystallinity decreases at higher test temperatures, but

TABLE 3

Deformation Calorimetry Data for Cyclic Loading
of Natural Rubber

EXTENSION RATIO		LOADING			UNLOADING		
MIN	MAX	ΔQ	ΔW	ΔU	ΔQ	ΔW	ΔU
T = 292 K							
1.0	2.0	-.6	.5	-.1	.6	-.5	.1
2.0	3.0	-.6	.6	.0	.5	-.5	.0
3.0	4.0	-.7	.8	.1	.7	-.7	.0
4.0	5.0	-1.0	.9	-.1	1.0	-.9	.1
5.0	6.0	-1.3	1.3	.0	1.2	-1.3	-.1
6.0	7.0	-2.4	1.3	-1.1	2.4	-1.3	1.1
1.0	3.0	-.9	.8	-.1	.8	-.7	.1
1.0	4.0	-1.8	1.6	-.2	1.6	-1.5	.1
1.0	5.0	-2.6	2.5	-.1	2.4	-2.4	.0
1.0	6.0	-4.0	3.8	-.2	3.9	-3.5	.4
1.0	7.0	-7.0	5.3	-1.7	6.4	-4.4	2.0
1.0	7.4	-11.5	6.1	-5.4	10.5	-4.7	5.8
1.0	8.9	-20.2	8.7	-11.5	18.6	-6.5	12.1
8.2	8.8	-3.2	2.6	-.6			
8.8	9.1	-2.1	2.0	-.1			
9.1	9.4	-2.0	2.3	.3			
9.4	9.7	-1.9	2.4	.5			
9.7	9.9	1.6	2.9	1.3			
T = 333 K							
1.0	8.9	-12.7	9.1	-3.6	11.9	-8.1	3.8

All values in Joules/gram elastomer

the fact that any crystallinity can exist at 333 K, which is about 30 K above the equilibrium melting point suggests a different morphological state than that obtained by thermally-induced crystallization. Sietz, Goritz and Muller(73,74) have shown that the end of melting for crystallization induced by stretching is about 345 K for natural rubber, which would account for a certain amount of crystallinity being stable at the test temperature of 333 K.

The incremental change of internal energy with extension for natural rubber undergoes a sign inversion from negative to positive at extension ratios approaching break. This is seen more clearly in Figure 21, where the variation in internal energy per unit extension, $(\delta U/\delta \lambda)_{T,P}$ is plotted versus extension ratio for room temperature loading of the natural rubber up to break. Above an extension ratio of 7.5, $(\delta U/\delta \lambda)_{T,P}$ becomes less negative with increasing strain and eventually becomes positive as the breaking extension ratio of 10 is approached. Wiegand and Snyder (5) published an identical curve for natural rubber in 1934 based on thermostatic measurements of $(\Delta U/\Delta L)_{T,P}$ from force-temperature slopes using Equation 11, which holds only for reversible processes. The dramatic increase in internal energy at ultimate extension is characteristic of hard or energy elastic solids, but may in fact be due to distortional energy or the breaking

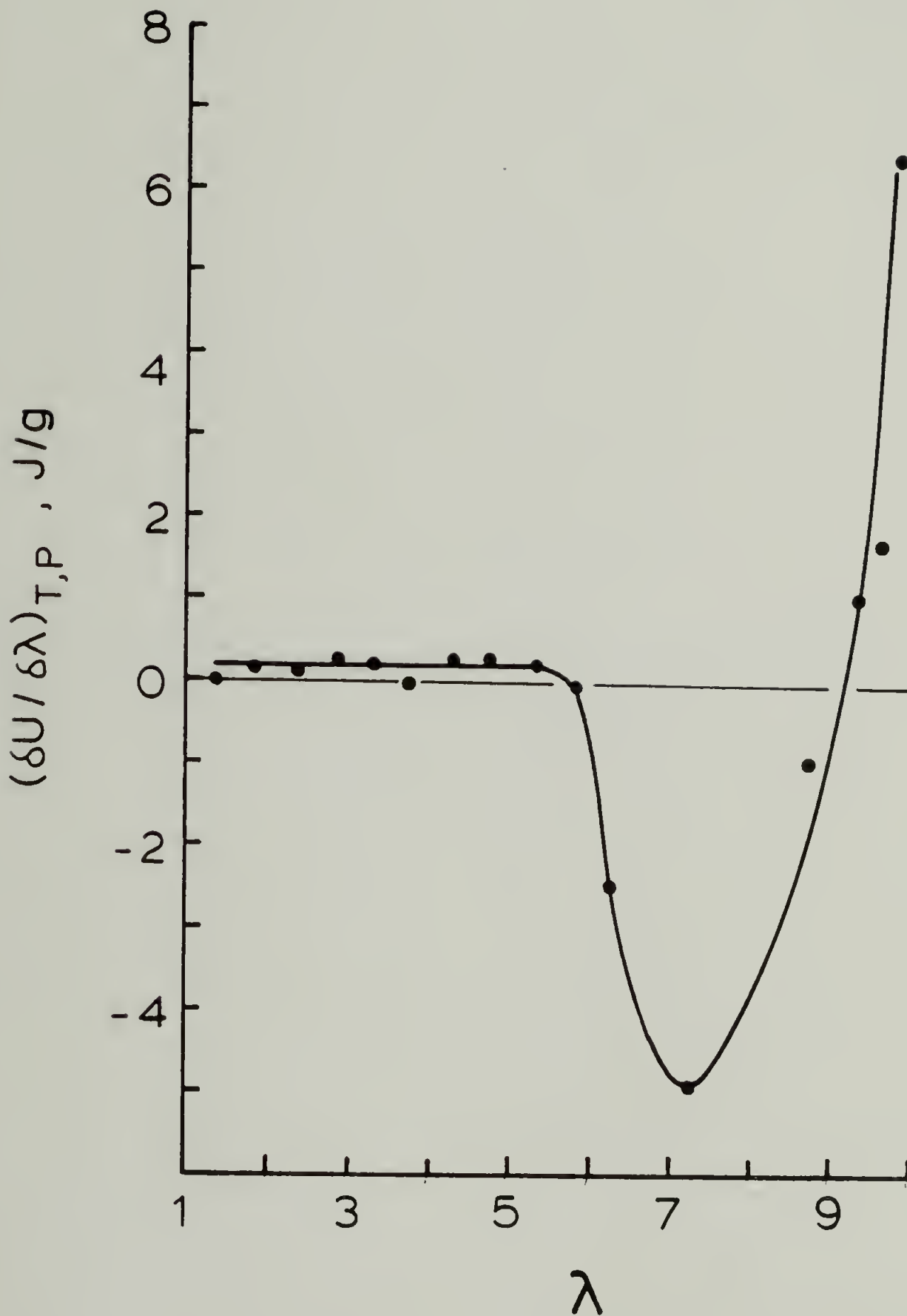


Figure 21. Change of Internal Energy per unit Extension versus Extension Ratio for Incremental Loading of Natural Rubber

apart of crystallites at high stress levels (stress-induced decrystallization). Some evidence for this comes from the deformation calorimetry data for polyethylene which is presented in a later section. In general it appears that mechanical energy storage in natural rubber is characterized by a variety of entropy and energy elastic mechanisms at room temperature.

Deformation calorimetry data obtained at three different test temperatures- 292, 313 and 333 K are shown in Table 4 for the polyether soft-segment elastomer. In general the data shows that the internal energy changes between any two states of strain are reversible in preworked samples, implying that the PTMO soft-segments crystallize and melt on loading and unloading at constant temperature. Increasing the test temperature from 292 to 333 K results in a decrease in stress-induced crystallinity for a given strain interval.

A study was conducted to determine the strain- rate dependence of the heat, work and internal energy change in the polyether soft-segment elastomer during room temperature large strain deformation cycles. The elastomer was cycled between the unstretched state and an extension ratio of 3.9 at 292 K . The data, which spans three decades of strain rate from 3.5 to 350 %/min, is shown in Table 5 . No significant difference in the internal energy change can be seen with deformation rate,

Table 4

Deformation Calorimetry Data for Loading/Unloading Cycles
of Polyether Soft Segment Polyurethane-urea Elastomer
at Three Test Temperatures

EXTENSION RATIO		LOADING			UNLOADING		
		ΔQ	ΔW	ΔU	ΔQ	ΔW	ΔU
		T = 292 K					
MIN	MAX						
1.0	2.0	-2.3	1.8	-.5	2.2	-1.7	.5
2.0	2.5	-2.6	1.1	-1.5	2.6	-1.1	1.5
2.5	3.0	-5.3	1.9	-3.4	4.8	-1.5	3.3
2.8	3.0	-2.4	1.0	-1.4	2.4	-1.0	1.4
2.9	3.0	-.9	.4	-.5	.9	-.4	.5
1.0	3.0	-17.2	5.9	-11.3	15.1	-3.5	11.6
		T = 313 K					
1.0	1.7	-1.3	.8	-.5	1.1	-.7	.4
1.0	3.8	-38.1	13.4	-24.7	35.9	-9.1	26.0
3.2	3.8	-14.4	5.9	-8.5	12.4	-4.4	8.0
1.0	4.3	-38.6	14.3	-24.3	-35.1	-9.4	25.7
		T = 333 K					
1.0	4.3	-26.3	12.2	-14.1	23.9	-8.7	15.2

All values in Joules/gram elastomer

Table 5

Strain Rate Effect on the Heat and Work of Deformation
Between $\lambda = 1-3.9$ for Polyether Soft Segment Elastomer

STRAIN RATE (%/MIN)	LOADING			UNLOADING		
	ΔQ	ΔW	ΔU	ΔQ	ΔW	ΔU
3.5	-37	11	-26	33	-5	28
6.9	-39	13	-26	35	-7	28
13.9	-39	11	-28	32	-5	27
34.9	-41	11	-30	36	-6	30
53.8	-41	13	-28	37	-6	31
139	-41	11	-30	36	-6	31
346	-42	13	-29	38	-8	30

All values in Joules/gram elastomer, $T = 292 \text{ K}$

although the work and heat appear to increase slightly in a parallel manner with increasing strain rate perhaps due to viscoelastic effects. The average value of the internal energy change at the extension ratio of 3.9 is about 29 J/g, which corresponds to 19% crystallinity based on the weight of the polymer using 200 J/g as the heat of fusion for the pure PTMO soft segments. Assuming the internal energy changes are solely due to stress-induced crystallization and melting, no apparent strain-rate dependence is observed for this phase transition over the range tested. This is not surprising considering that Mitchell and Meier(75) have shown, at least for natural rubber, that the half-time for crystallization during stretching is about 50 milliseconds, which is orders of magnitude less than the duration of the fastest experiment.

In contrast to this are the data which have been reported for the kinetics of crystallization of oriented networks (76,77) on cooling from the melt. Typical half-times for oriented crystallization under these conditions are on the order of minutes or hours- several orders of magnitude slower than crystallization during stretching. Goritz, Muller and Sietz (65) from their studies of the melting behavior of deformation induced crystallinity in natural rubber attribute the difference to two completely different mechanisms of crystallization: one occurring during deformation, or stress-induced crystal-

lization (SIC); the other brought about mainly by cooling, or thermally-induced crystallization (TIC). This nomenclature will be used in subsequent discussions.

Isothermal deformation calorimetry data was also obtained at 292 K for the mixed polyester soft-segment polyurethane-urea elastomer at a variety of strains and strain perturbations. This data is shown in Table 6 . The data are qualitatively equivalent to the PTMO soft-segment elastomer in that internal energy changes for preworked samples are recoverable and become more negative at higher strain. Consistently negative values of internal energy change are observed even at low extension ratios, which is in contrast to the positive values for natural rubber and zero order values for the PTMO elastomer. It is also seen that the magnitude of the internal energy changes are less than the PTMO elastomer, and that crystallization commences at a higher extension ratio, undoubtedly due to the more random soft-segment chemistry.

The magnitude of the heat flow accompanying soft-segment stress-induced crystallization and melting relative to rubber elastic heats of entropic origin, are shown clearly in Figure 22 for the polyester soft-segment elastomer. The two curves are baseline corrected pressure data from the calorimeter for loading/relaxation/unloading cycles between extension ratios of 1-2 and 1-2.4 at a strain rate of 24%/minute. It is seen that increasing the

Table 6

Deformation Calorimetry Data for Loading/Unloading Cycles
of Polyester Soft Segment Polyurethane-urea Elastomer

EXTENSION RATIO		LOADING			UNLOADING		
MIN	MAX	ΔQ	ΔW	ΔU	ΔQ	ΔW	ΔU
1.0	2.0	- .7	.6	- .1	.6	- .5	.1
2.0	2.9	-2.3	1.9	- .4	2.0	-1.6	.4
2.9	4.0	-4.9	3.1	-1.8	4.4	-2.5	1.9
4.0	4.9	-6.0	3.8	-2.2	4.9	-3.1	1.8
4.9	5.8	-4.0	2.1	-1.9	3.4	-1.7	1.7
5.8	6.2	-3.0	2.7	- .3	2.5	-1.9	.6
1.0	1.5	- .2	.2	0	.2	- .2	0
1.0	2.4	-1.8	1.2	- .6	1.6	-1.0	.6
1.0	2.9	-3.1	2.0	- .9	2.5	-1.5	1.0
1.0	3.4	-5.7	2.7	-3.0	4.7	-1.8	2.9
1.0	4.0	-9.0	3.6	-5.4	8.3	-2.3	5.0
1.0	4.4	-11.8	4.9	-6.9	10.1	-2.8	7.3
1.0	4.9	-17.0	6.1	-11.1	13.8	-3.4	10.4
1.0	5.3	-20.5	8.1	-12.4	16.6	-3.9	12.7
1.0	5.8	-25.0	10.1	-14.9	20.1	-4.8	15.3

All values in Joules/gram elastomer, T = 292 K

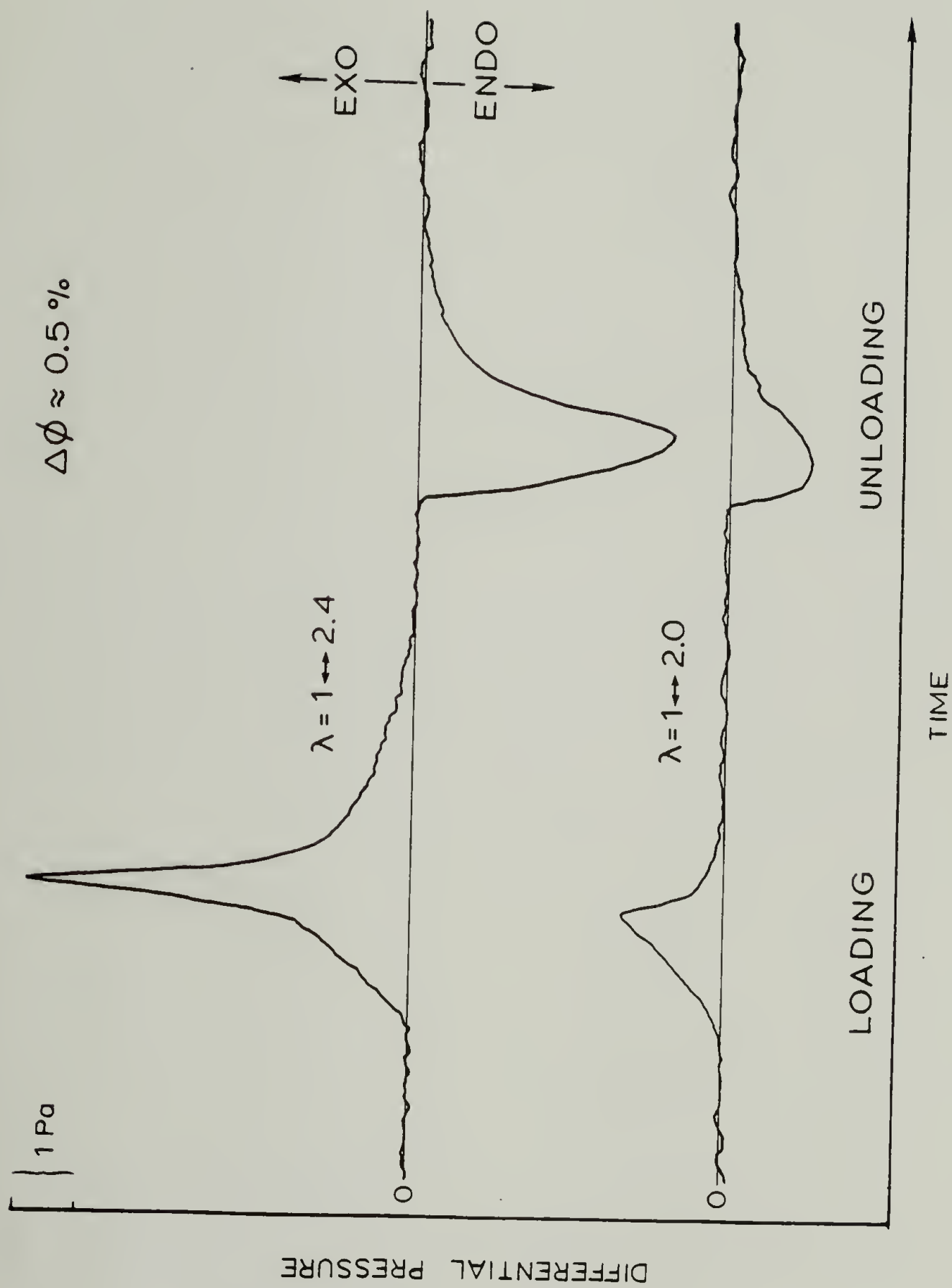


Figure 22. Pressure Data from Calorimeter for Loading/Relaxation/Unloading Cycle of Polyester Soft Segment Polyurethane-urea Elastomer Illustrating Magnitude of Thermal Effect due to Crystallization

maximum extension of the cycle from 2.0 to 2.4 results in a thermal effect 5 times greater. The reduced data, which is contained in Table 6, shows that the magnitude of the internal energy changes are .1 and .6 J/g for the 2.0 and 2.4 maximum extension ratios, respectively. This corresponds to a change of only about 0.5% crystallinity in the polymer based on the heat of fusion of 122 J/g for the adipic acid/ethylene glycol sequences in the mixed polyester soft-segments.

The thermoelasticity of segmented polyurethane block copolymers (Estane, Sanprene and MDI/BDO + oligobutadiene) was studied by Godovskii and Bessonova (78) using deformation calorimetry, who found positive values of $(dU/dW)_{T,V}$ for extension ratios less than 1.5, but negative values above this strain where crystallization was assumed to be absent. This was in contrast to the positive values of $(dU/dW)_{T,V}$ expected from the soft blocks alone. Negative internal energy contributions at moderate strains were attributed to restructuring of hard blocks, wherein hydrogen bonding was thought to be increased by deformation.

These observations suggest that the decrease of internal energy with deformation in the polyurethane-ureas of the present study may have an origin other than crystallization of the soft segments. An examination of the relative magnitudes of the contributions which could arise from hydrogen bonding and soft-segment

crystallization in the polyether and polyester soft-segment elastomers shows that a maximum of about -15 J/g could be expected for 100% hydrogen bonding induced by deformation where none existed previously. This is about $1/10$ of the heat for complete crystallization of the polyether and polyester soft-segments, being -150 J/g and -104 J/g respectively. Consequently, hydrogen bonding contributions to the internal energy change with deformation are small compared to crystallization effects, but cannot be completely neglected, especially at small strains.

In support of non-crystalline contributions to the observed internal energy changes, evidence exists for increased domain mixing at high extension ratios for initially demixed polyurethanes of MDI/BDO + mixed polyester soft-segment (79). The actual process of mixing, however would be an endothermic process on the order of $1-5 \text{ J/g}$ for the present systems, which would contribute to an apparent increase in internal energy in contrast to the decrease typically observed.

Small-angle x-ray studies by Bonart and Muller (80) on polyurethane-urea elastomers of comparable hard segment content and both PTMO and polyester soft-segments show diffuse interphase zones with isolated hard-segments in the soft-segment matrix and soft-segments included in the hard-segment domains. This picture of the quiescent mor-

phology provides a plausible route to increased hydrogen bonding during deformation, as isolated hard-segments are brought into register with more well developed blocky structures. Indeed, Kong and Wilkes (79) report demixing with deformation for initially phase separated systems obtained by quench cooling from the melt. This could account for the consistently negative values of the internal energy change during stretching of the polyester soft-segment elastomer, which is expected to be less phase separated than the PTMO elastomer based on solubility parameter calculations.

Crystallization of a small amount of highly stretched soft-segment chains cannot be ruled out as an additional and perhaps dominant source of the decrease in internal energy even at small strains. Since a distribution of soft-segment lengths is unavoidable in the commercial materials studied, it can be imagined that a certain small percentage of these could be sufficiently extended to nucleate crystallization even at small strain. Morbitzer and Bonart (81) have suggested such a model to explain soft-segment stress-induced crystallization at extension ratios less than 2 in polyurethane elastomers.

These authors used deformation calorimetry to study stress-crystallizable polyurethane-ureas having MDI/hydrazine hard segments and various soft segments including PTMO, polycaprolactone and a mixed polyester of

unspecified chemical composition. The results, reported as dQ/dW during room temperature step-loading, showed a high tendency to stress-crystallize at low elongation ($\lambda = 2$) for the homopolyester, less crystallization beginning at higher elongation ($\lambda = 3$) for PTMO and almost no crystallization induced by stretching the mixed polyester. Mechanical data showed an upswing in the stress-strain curve during loading coincident with the maximum in dQ/dW (first derivative of crystallinity versus strain). In addition, a one-to-one correspondence was found between the amount of crystallinity obtained by stretching and the amount of thermally reversible extension set, which suggests an unusual stability for crystallites formed during stretching since these could persist in the stress free state at room temperature. This phenomenon has long been known in the natural rubber industry. Indeed Bekkedahl notes that "a strip of stretched [natural] rubber with its ends nailed to a board will actually rise to form an arc from crystallization" (82). These same effects were observed, to a lesser extent, in first deformation cycles of the present study. However, since this data was not reproducible it was not considered to be representative of the steady-state thermomechanical behavior over the particular strain interval in question.

In later studies, Morbitzer and Hespe (83) investigated the room temperature stress-induced crystallization

behavior of polyurethane-ureas having soft-segments of high (2000) molecular weight polycaprolactone and low (830) molecular weight polycaprolactone chain extended with MDI/hydrazine. Deformation calorimetry results indicated that the crystallizability of the soft segments decreased dramatically with increasing chain extension. Also observed was a maximum tendency to crystallize at intermediate strains, on the order of $1/2$ the maximum elongation. These authors found the usual linear relationship between strain and soft-segment crystallinity during loading. Unloading data was either not reported or not obtained in the experiments.

The only authors to report deformation calorimetry data for a complete stress-strain cycle into the stress-crystallization region are DeCandia, Romano, Russo and Vittoria (84), who studied the behavior of natural rubber at large deformation using a Tian-Calvet calorimeter in conjunction with birefringence measurements. These authors found significant hysteresis in the stress-strain curve, internal energy and birefringence data. In particular, the incremental-loading, -unloading experiments showed that the orientation was higher at a particular strain during the unloading sequence than during the loading sequence. Similarly, negative values of internal energy persisted to lower strain as was observed in the step-strain experiments of the present study. The con-

clusion was that the crystallinity developed during stretching did not melt during contraction within the timescale of the experiment, suggesting a kinetic origin for the observed hysteresis.

Earlier studies by Treloar (85) on the uniaxial stress-strain-birefringence behavior of natural rubber at room temperature showed the same relationship between mechanical hysteresis and birefringences hysteresis, with higher birefringence and lower stress on unloading than on loading. Both photoelastic and mechanical hysteresis could be eliminated by swelling the rubber or raising the test temperature. Ko and Blatz (86) published a static loading-unloading curve for natural rubber up to an extension ratio of 6 in which one hour was allowed for mechanical equilibrium at each level of strain during loading and subsequent retraction. Even under these conditions, the mechanical hysteresis amounted to about 20% of the work of unloading.

The correlation between stress-induced crystallinity and mechanical hysteresis is clearly shown in Figure 23 , where is plotted the cyclic integral for the work (i.e. the work of loading minus the work of unloading) versus the internal energy change between the two states of deformation. Data for natural rubber and both of the polyurethane-urea elastomers at all strain perturbations and test temperatures are included in the plot, which

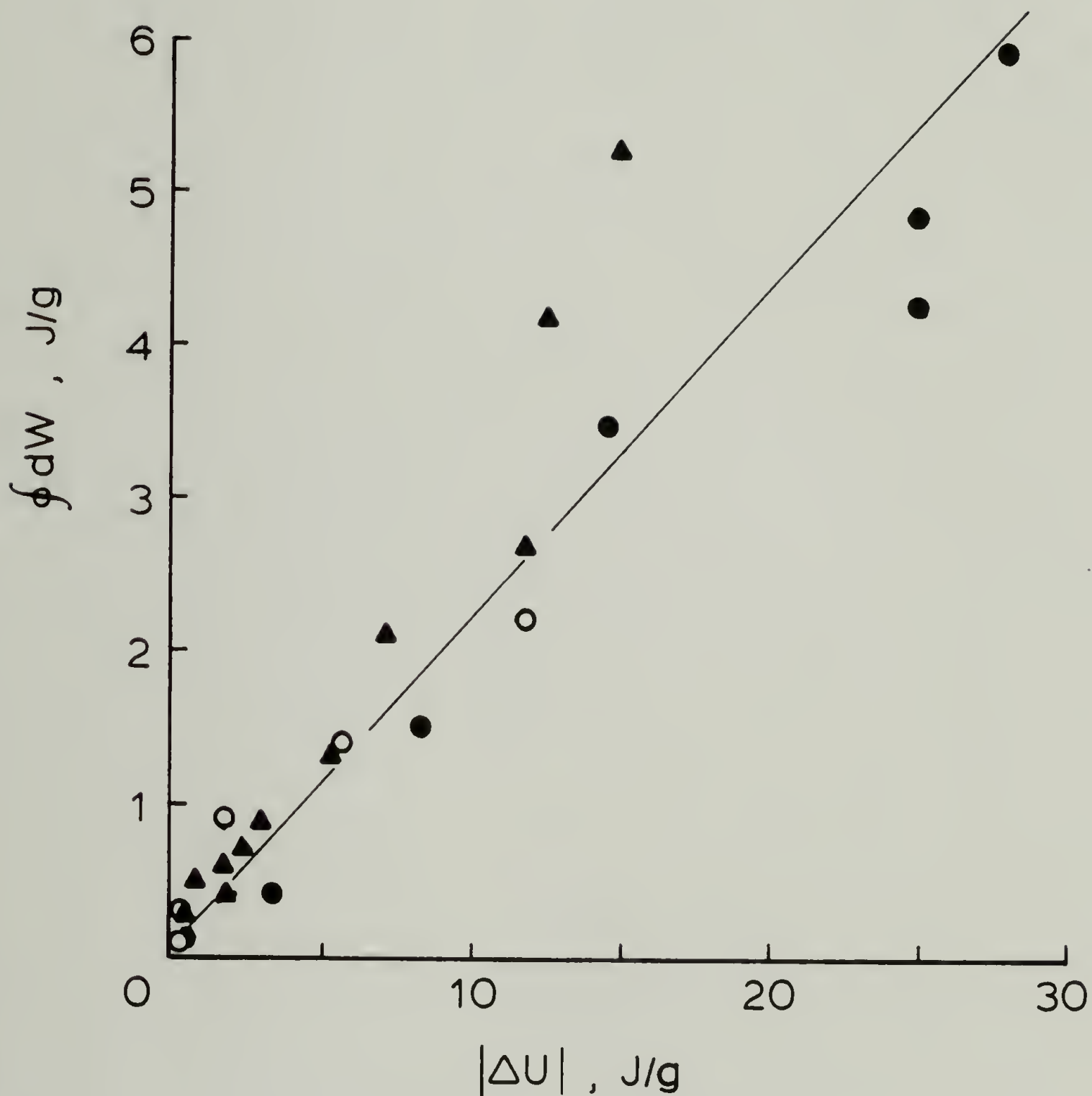


Figure 23. Mechanical Hysteresis versus Magnitude of Internal Energy Change Between Deformation States for Polyether Soft Segment Elastomer (solid circles), Polyester Soft Segment Elastomer (triangles) and Natural Rubber (open circles)

shows that approximately 1/5 of the internal energy change due to crystallization is lost to the surroundings and is unrecoverable as useful work. Since the mechanical hysteresis is equal to the heat lost during the isothermal cycle, by the second law of thermodynamics:

$$TdS \geq dq = TdS_{rev} + TdS_{irr}$$

or

$$\oint dq = 0 + T \Delta S_{irr}$$

Consequently, the spontaneous process of crystallization and melting during isothermal stretching and contraction is irreversible and results in an entropy gain by the surroundings equal to about 1/5 of the heat of crystallization divided by the test temperature. Lindenmeyer (87,88) has pointed out that polymer crystallization is an intrinsically irreversible process, since no matter how slowly the crystallization process is carried out, the resulting crystals always melt at a temperature higher than that at which they formed. As will be shown in the DSC studies, this is certainly the case for stress-induced crystallization.

The conclusion which can be drawn from the above observations and the deformation calorimetry data in the present study is that once crystallization during stretching has commenced the process is irreversible and

the stress-strain curve is permanently altered due to the high mechanical stability of the crystallites which resist dissolution during unloading, or to residual orientation which persists to lower strain- the two phenomenon being somewhat interdependent.

In order to characterize the internal energy hysteresis during room temperature stress-strain cycles of the elastomers in the present study, the dynamic heat was calculated for a large strain cycle of each of the polyurethane-ureas and natural rubber using Equation 64 of the Experimental section. Continuous curves of the heat $Q(t)$, generated or absorbed up to time, t , during the loading and unloading process were digitally added to the work, $W(t)$ to obtain the internal energy change, $\Delta U(t)$. At constant crosshead speed, the sample strain is simply related to time, so that the internal energy change can be plotted directly versus extension ratio. Internal energy change, $U-U_0$, is plotted versus extension ratio in Figures 24, 25, and 26, for the PTMO soft-segment elastomer, mixed polyester soft-segment elastomer and natural rubber, respectively. The stress-strain curves are also plotted. It is seen that the internal energy change is on the order of zero until a critical extension ratio is reached, at which point a precipitous drop occurs as crystallization commences during stretching. The quasi-linear dependence of internal energy (crystallinity) on

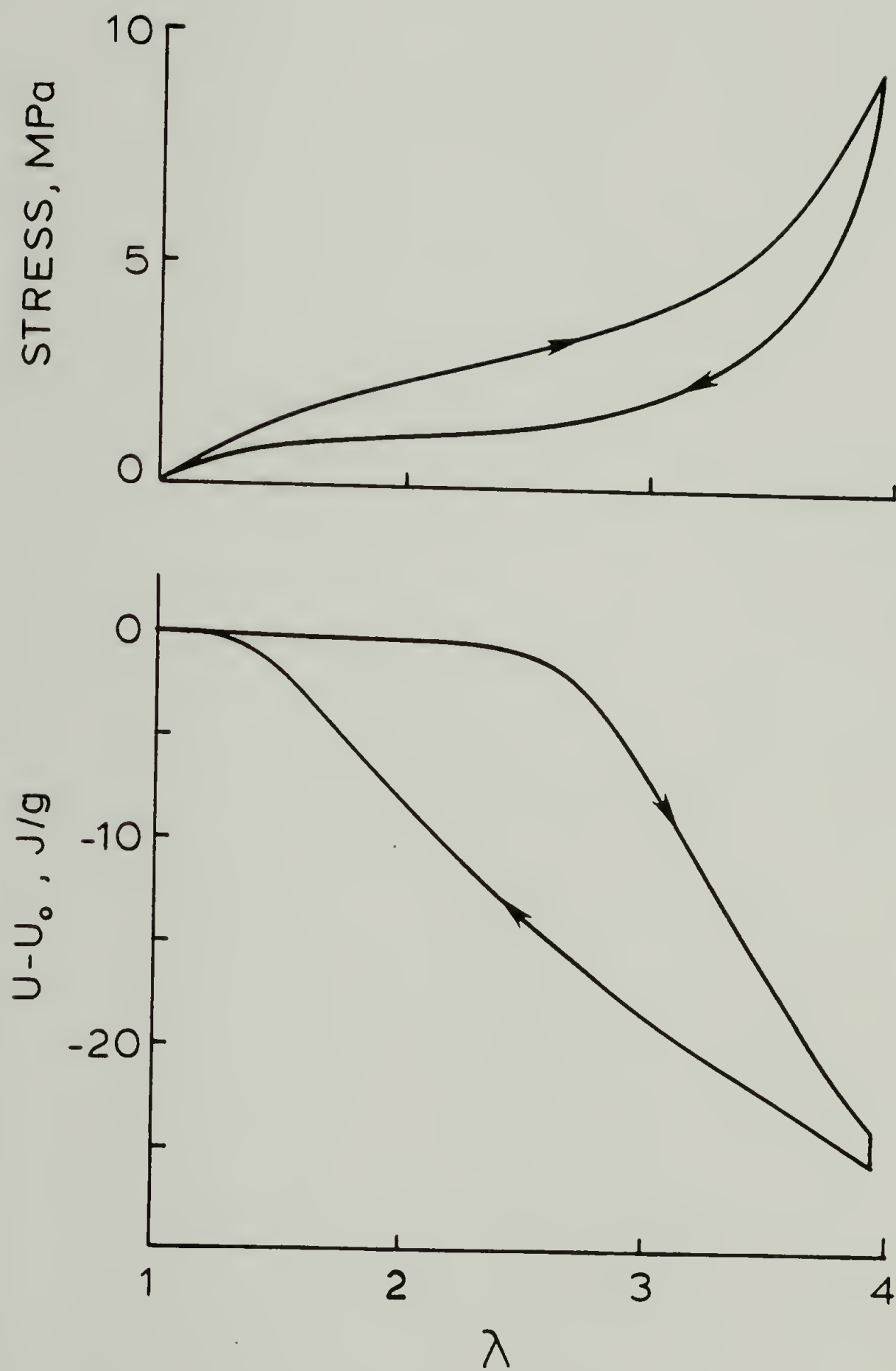


Figure 24. Stress and Internal Energy versus Extension Ratio for Polyether Soft Segment Elastomer

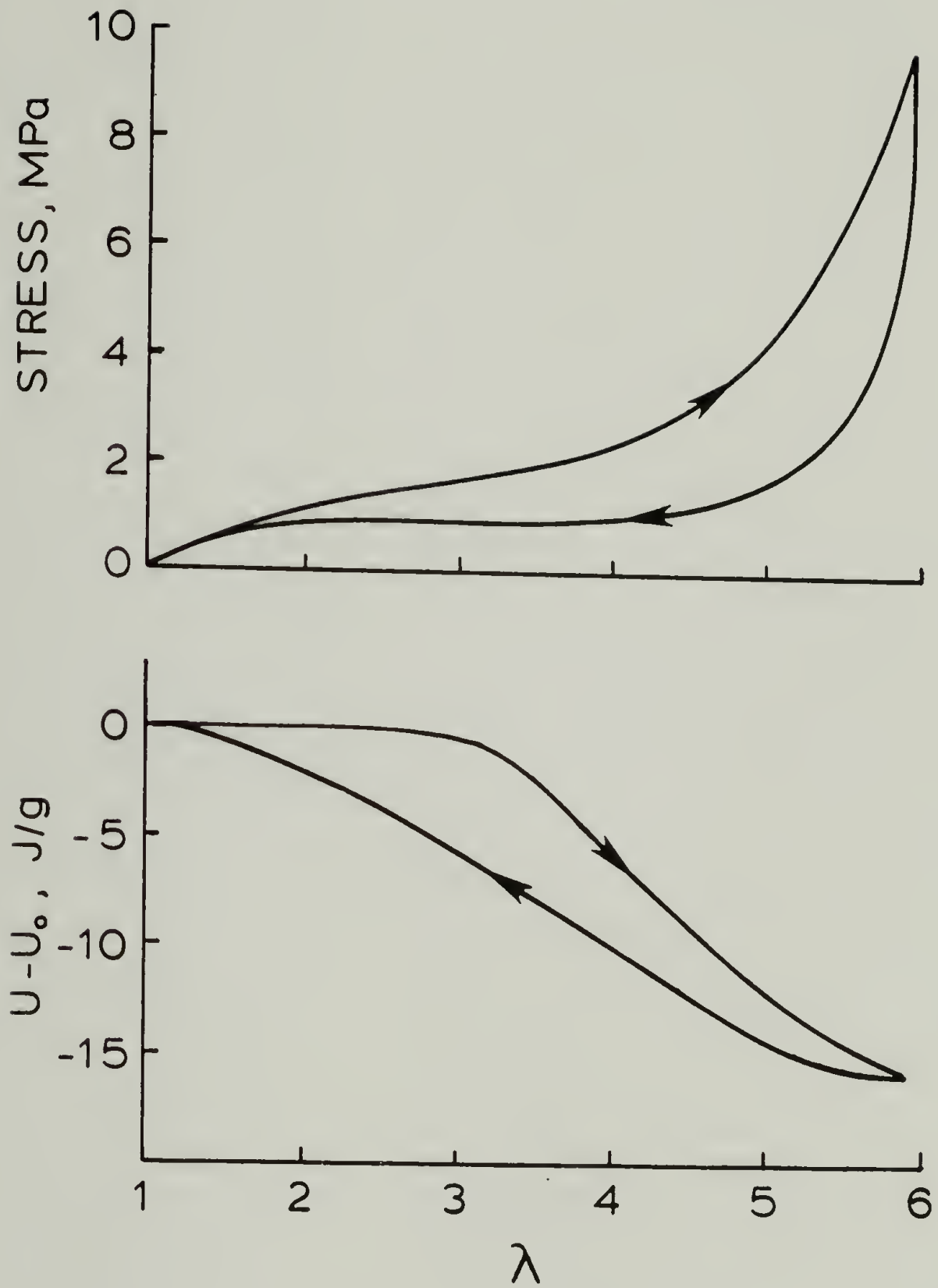


Figure 25. Stress and Internal Energy versus Extension Ratio for Polyester Soft Segment Elastomer

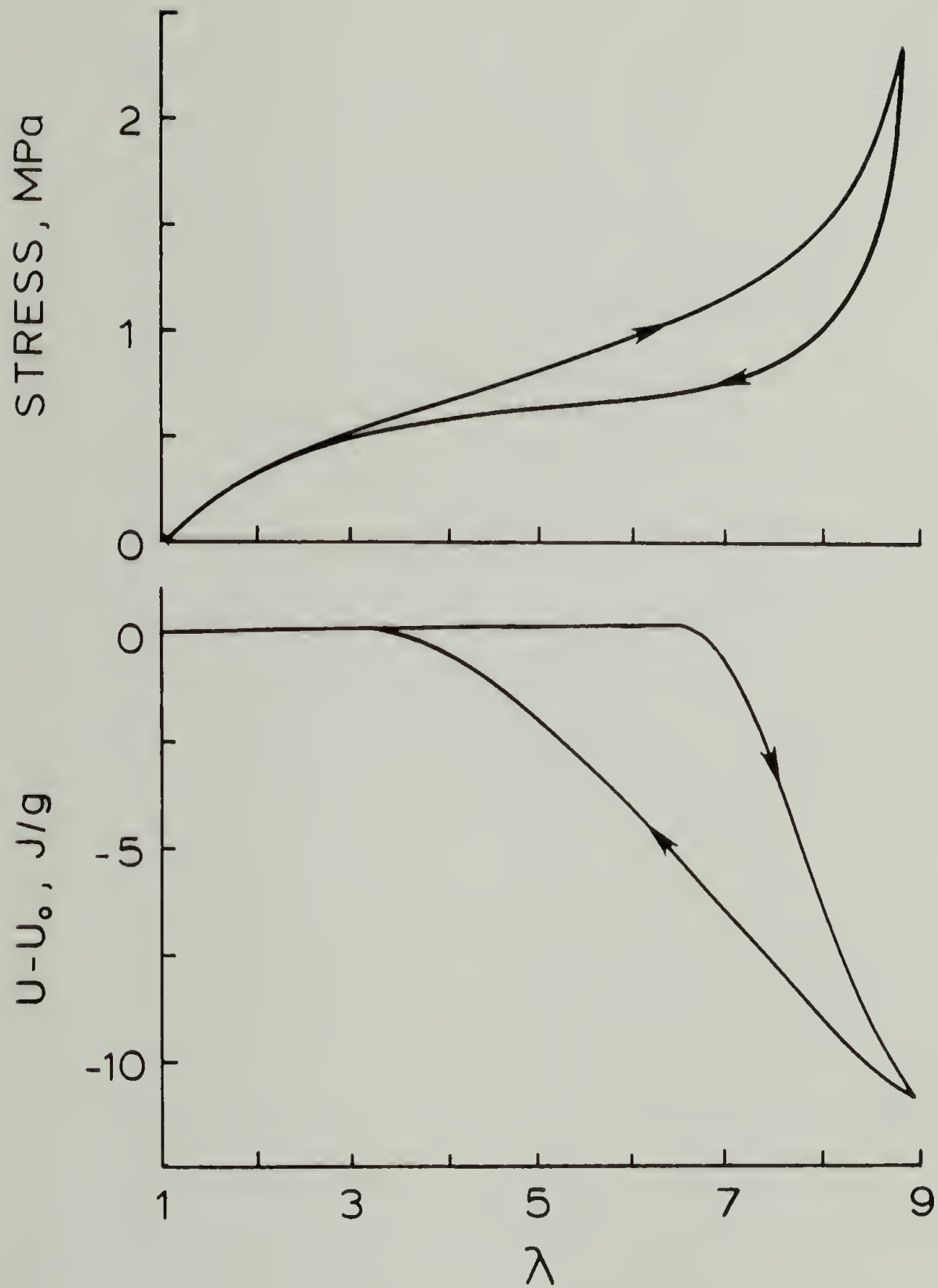


Figure 26. Stress and Internal Energy versus Extension Ratio for Natural Rubber

strain is verified during the loading portion of the curve. The unloading curves, however show that a different relationship to strain characterizes this process. Although the curves are obtained under dynamic conditions, they are essentially strain-rate independent, or quasi-static, since the same behavior was observed in the incremental loading data plotted in Figures 19 and 20.

Having generated the curves for internal energy versus time, $U(t)$, these can be plotted versus stress by utilizing the digital force-time data. Plots of internal energy change versus engineering stress on the sample are shown in Figures 27 , 28 , and 29 for the PTMO, polyester and natural rubber elastomers, respectively. It appears from these plots that the stress correlates better with internal energy than does strain. In particular, the internal energy changes occur over a narrow range of stress, the loading and unloading curves being nearly parallel and separated by about 1-3 Mpa of engineering stress, depending on the elastomer. The fact that melting during unloading occurs at a lower stress than required for crystallization during stretching, implies that an activation energy or free energy barrier must be overcome to initiate the decrystallization or melting process.

Despite the observed hysteresis associated with the non-equilibrium process of stress-induced crystallization and melting, the internal energy changes are recoverable

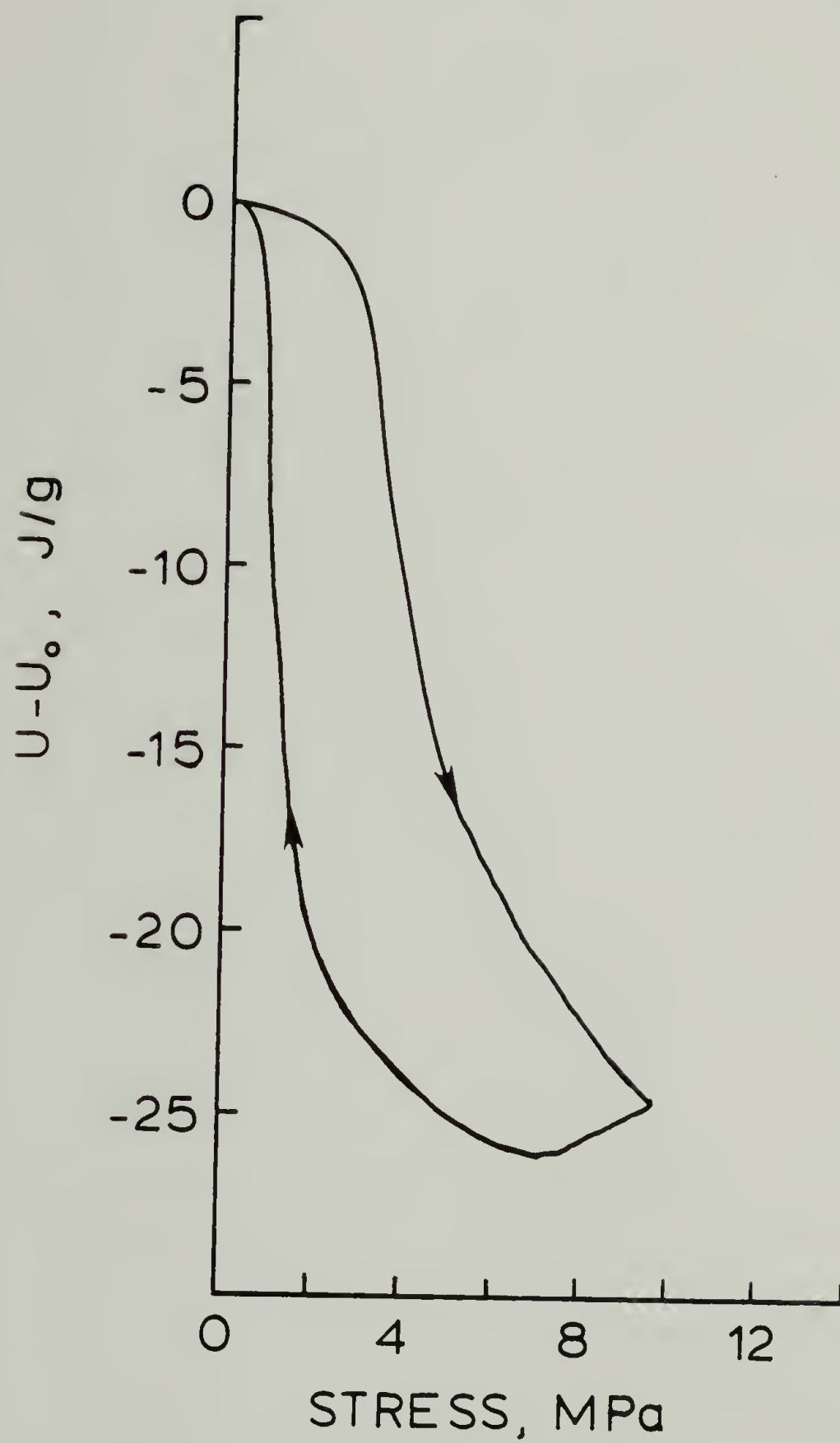


Figure 27. Internal Energy versus Stress for Polyether Soft Segment Elastomer

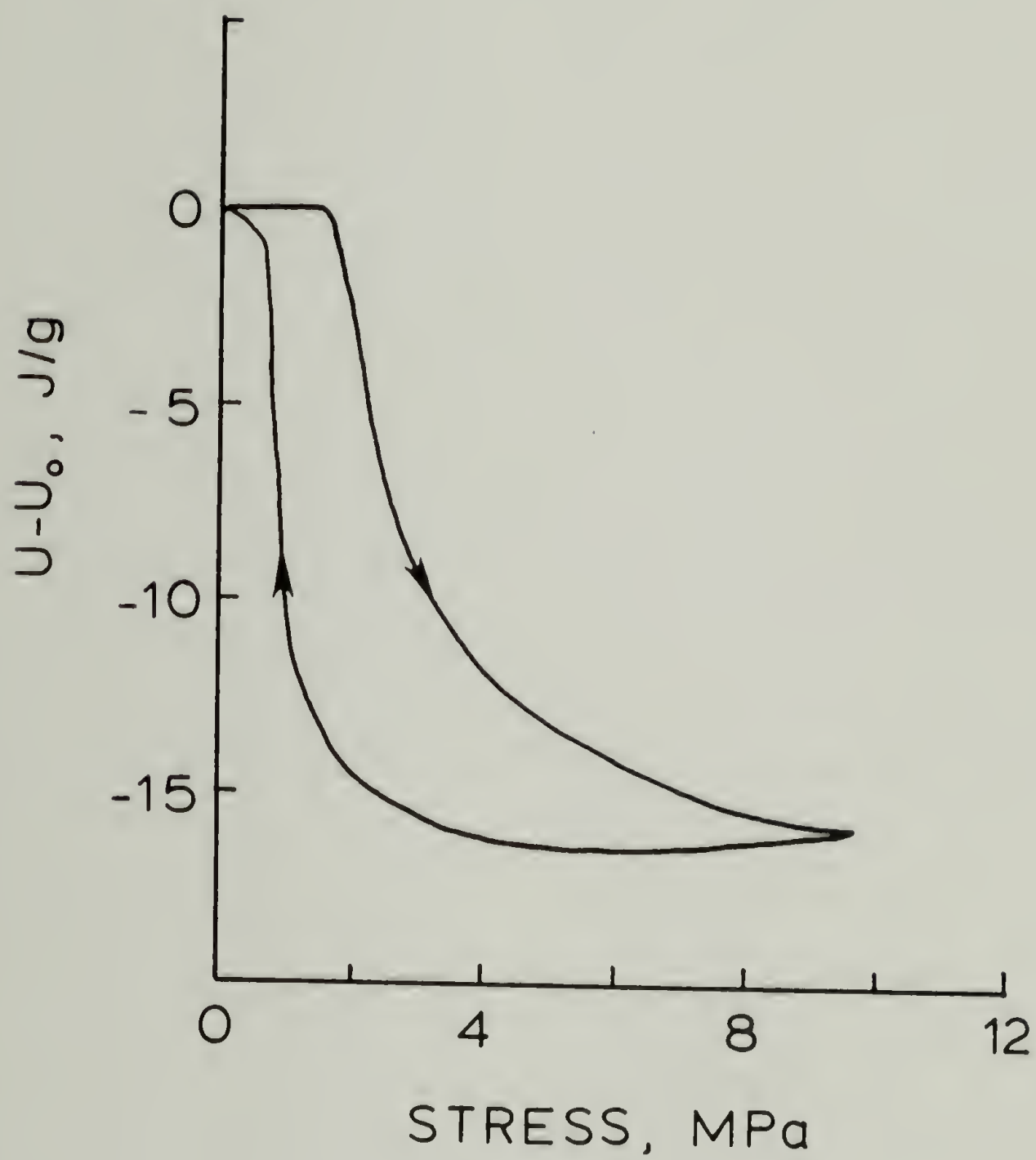


Figure 28. Internal Energy versus Stress for Polyester Soft Segment Elastomer

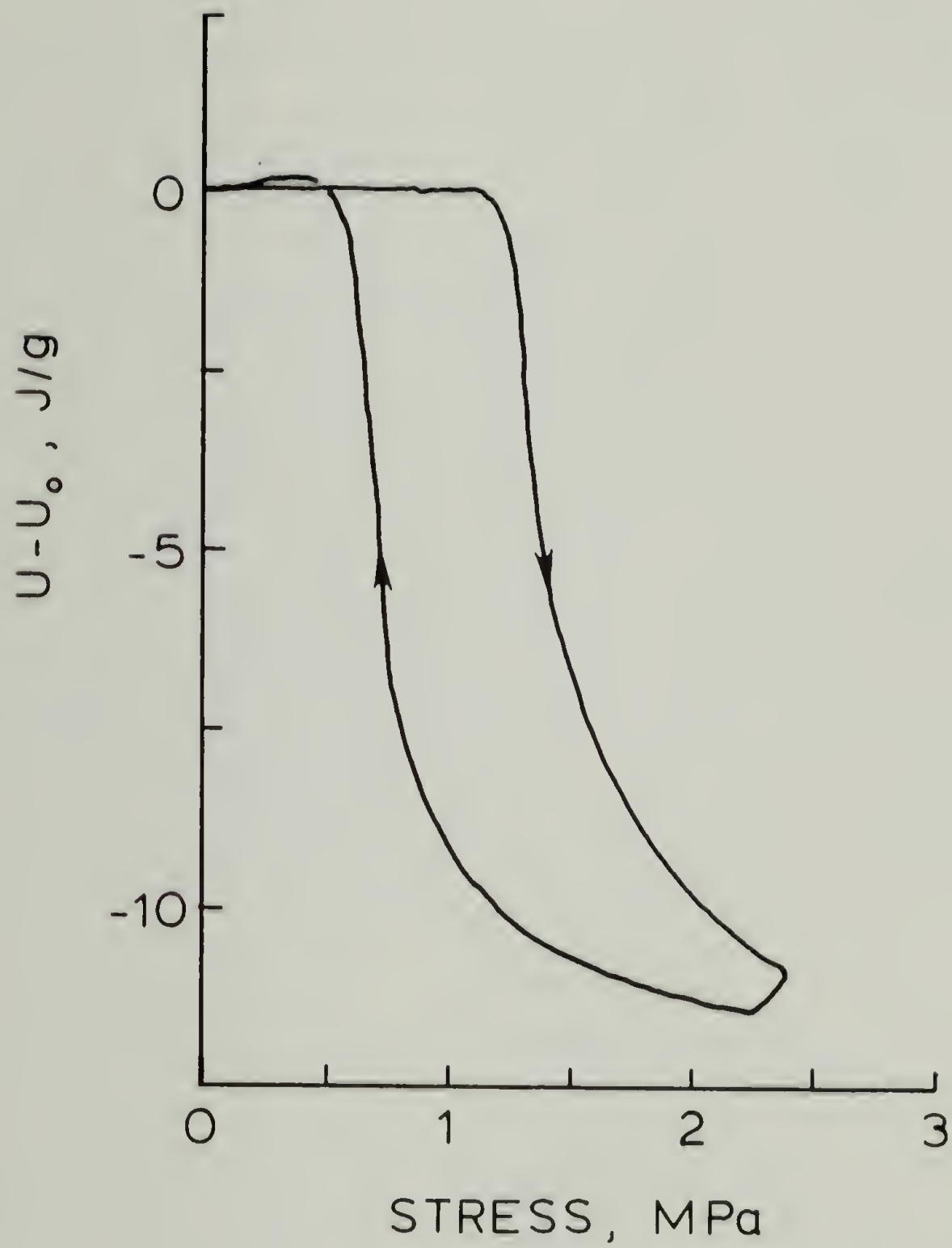


Figure 29. Internal Energy versus Stress for Natural Rubber

in that the cyclic integral is always zero for preworked samples.

Thermoplastic Elastomer

Deformation calorimetry data was obtained at room temperature (292K) for the Hytrel® segmented thermoplastic elastomer at a strain rate of 12%/min. Successive loading/relaxation/unloading cycles to increasing strain levels were used to obtain the data in Table 7. Values reported are the incremental heat, work and internal energy change for the strain interval ($\epsilon = \Delta L/L_0$) indicated.

Force versus temperature curves at a fixed strain of 5% were obtained by cyclic heating and cooling between 19-30 C at 1° C /min. The average slope of these linear curves was -5.58×10^{-3} N/K. The expected heat was calculated from this slope using Equation 27 with $T=292$ K. The measured total heat of loading obtained by summing the incremental heats is compared to the calculated values in Figure 30. It is seen that the measured values exceed the calculated values, i.e. more heat was absorbed during the stretching process than was expected from Equation 27. In addition, the sign of the heat is positive or endothermic for loading, in contrast to the exothermic heats of loading for the polyurethane-urea elastomers and natural

Table 7

Deformation Calorimetry Data for PBT/PTMO Thermoplastic Elastomer: Loading/unloading Cycles to Increasing Strain

STRAIN, %		LOADING			UNLOADING		
MIN	MAX	ΔQ	ΔW	ΔU	ΔQ	ΔW	ΔU
0.0	2.6	.09	.13	.22	-.15	-.07	-.22
2.6	5.2	.18	.36	.54	-.18	-.22	-.40
5.2	7.8	.18	.57	.75	-.33	-.37	-.70
7.8	10.4	.22	.72	.94	-.41	-.51	-.92
10.4	13.0	.25	1.06	1.31	-.47	-.82	-1.29
13.0	15.6	.25	1.08	1.33	-.42	-.83	-1.25
Totals:		1.17	3.92	5.09	-1.96	-2.82	-4.78

ALL VALUES IN JOULES/GRAM ELASTOMER

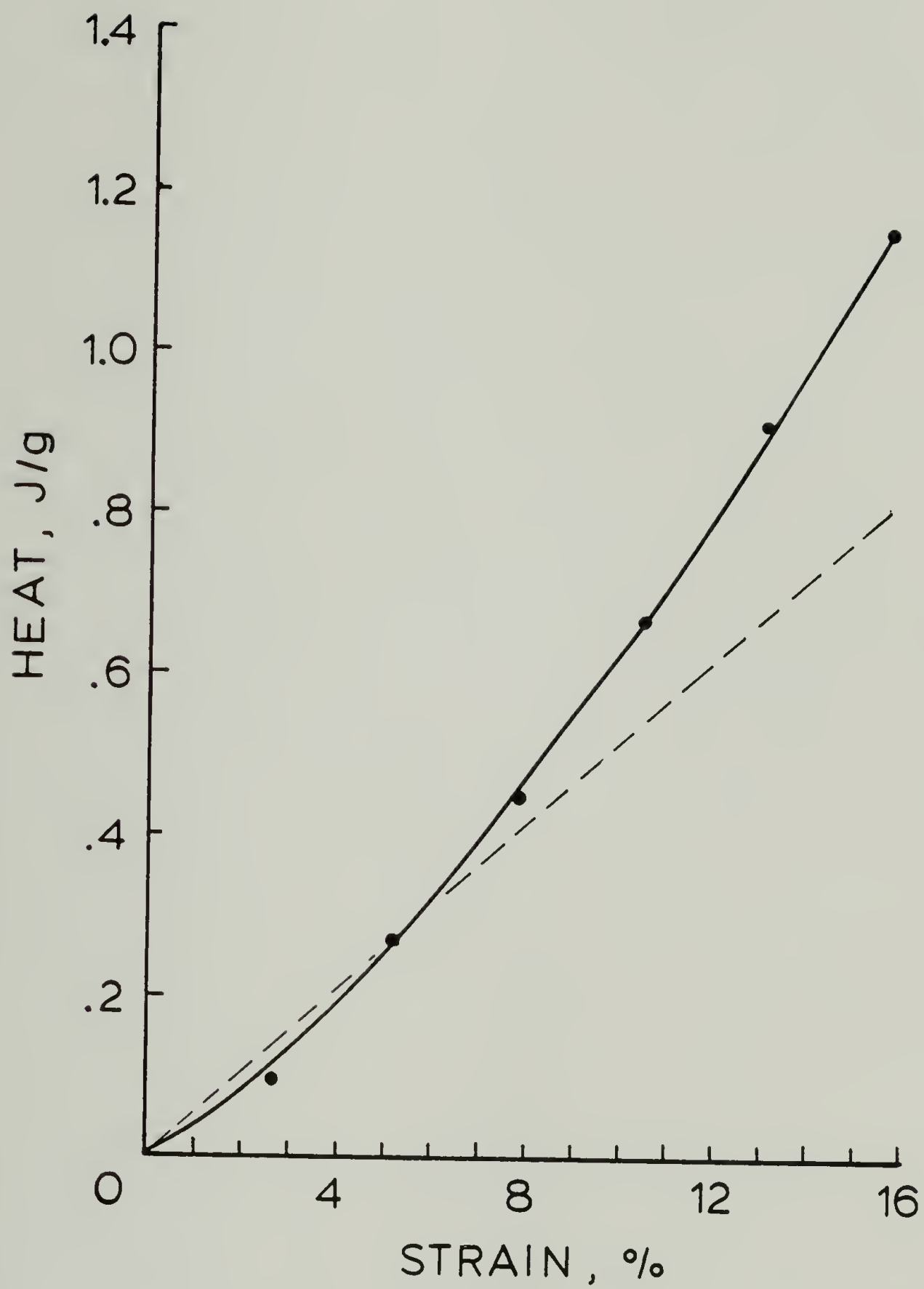


Figure 30. Calculated (----) and Measured (●) Heat versus Strain for PBT/PTMO Thermoplastic Elastomer

rubber. This reflects the different mechanism of energy storage in the PBT/PTMO copolymer which has a continuous PBT glassy phase as opposed to the continuous rubbery phase of the other elastomers.

The internal energy change, $U-U_0$, for incremental extension of the thermoplastic elastomer is shown in Figure 31. The cumulative work and heat are also plotted, showing that the internal energy change is greater than the work but of similar sign while the heat is of much lower magnitude and endothermic. This behavior results from the entropy increase due to dilatation during stretching as shown by Equation 21 and illustrated in Figure 1. It is seen that the PBT/PTMO thermoplastic elastomer with a continuous glassy or semi-crystalline phase stores mechanical energy mainly as changes of internal energy, in contrast to the polyurethane-urea elastomers and natural rubber which store mechanical energy as changes of entropy during small strain isothermal deformations, since $W \approx -Q = -T \Delta S$.

The incremental data indicates that the thermoplastic PBT/PTMO elastomer behaves almost reversibly in small strain deformation cycles to increasing strain levels. However, the true viscoelastic nature of this material is revealed in large strain loading / relaxation / unloading cycles in the calorimeter. Experiments were performed in which the PBT/PTMO fiber was loaded from the rest state to

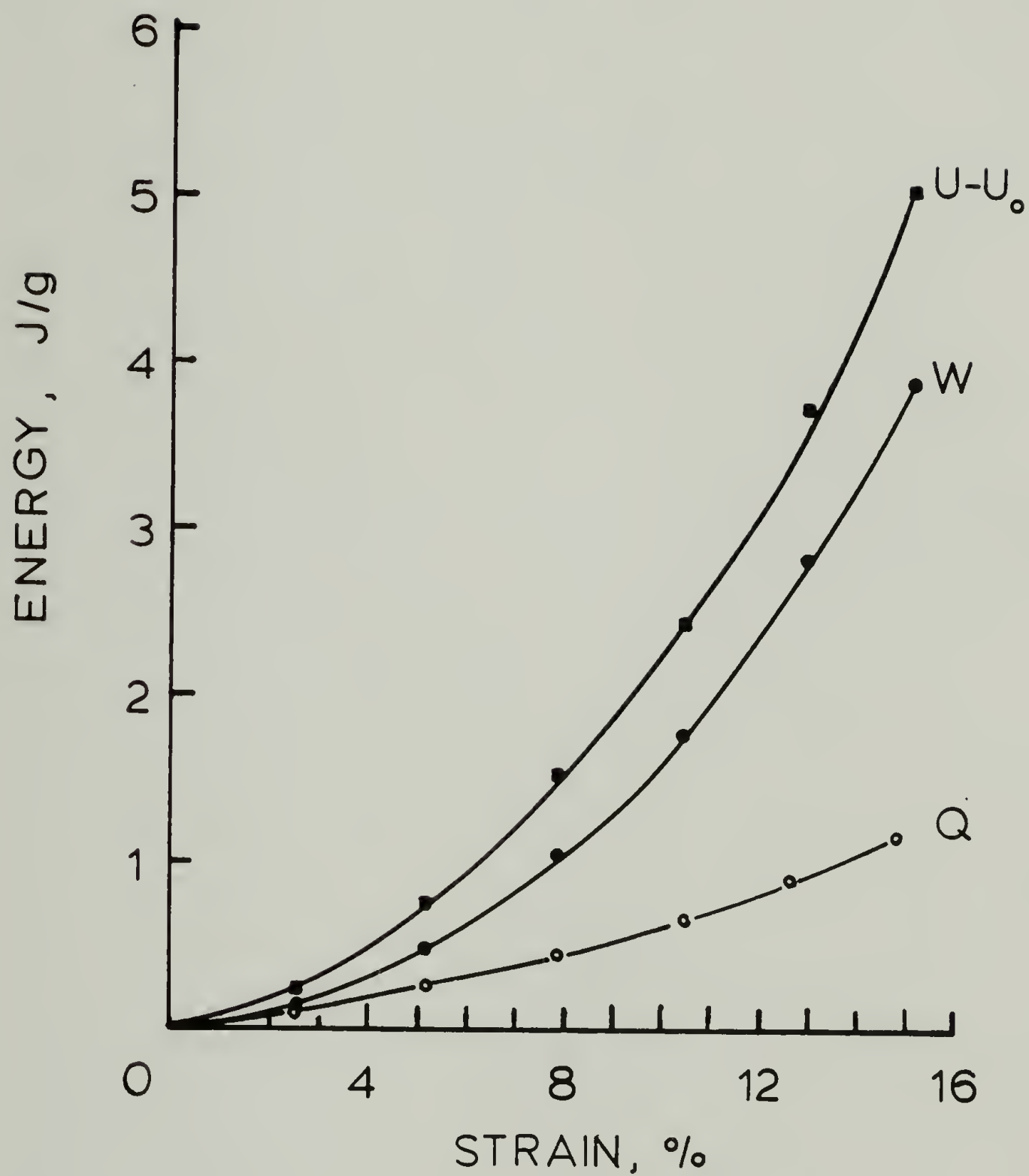


Figure 31. Heat (Q), Work (W) and Internal Energy (U) versus Strain for Incremental Loading of PBT/PTMO Thermoplastic Elastomer

15.3% strain, allowed to relax for 2.5 min and then unloaded to zero stress. The pressure-time and force-time data from the calorimeter obtained at a strain rate of 23%/min are shown in Figure 32 .

This data shows an initial cooling on loading followed by an exotherm which persists during the stress relaxation at fixed strain. Unloading shows only an exotherm persisting to long times with a temporary set at zero force of 2.3% of the initial length. This temporary set is completely recovered after 12 hr in the stress free state.

It has been suggested (89) that the mechanical behavior of the continuous poly(butylene-terephthalate) hard segment phase can be accounted for quantitatively by a standard linear solid model consisting of a spring in series with a Voigt element (spring and dashpot in parallel). According to Chu (90) and Bridgeman (91) the thermodynamic behavior should be similarly described by such a model. Figure 33 shows an idealized stress-strain curve for the standard linear solid, which closely describes the actual behavior of Hytrel.[®] The expected thermal response of such a model to the mechanical process in this figure is qualitatively consistent with the observed heat flow in Figure 32. The individual processes can be described in the following way.

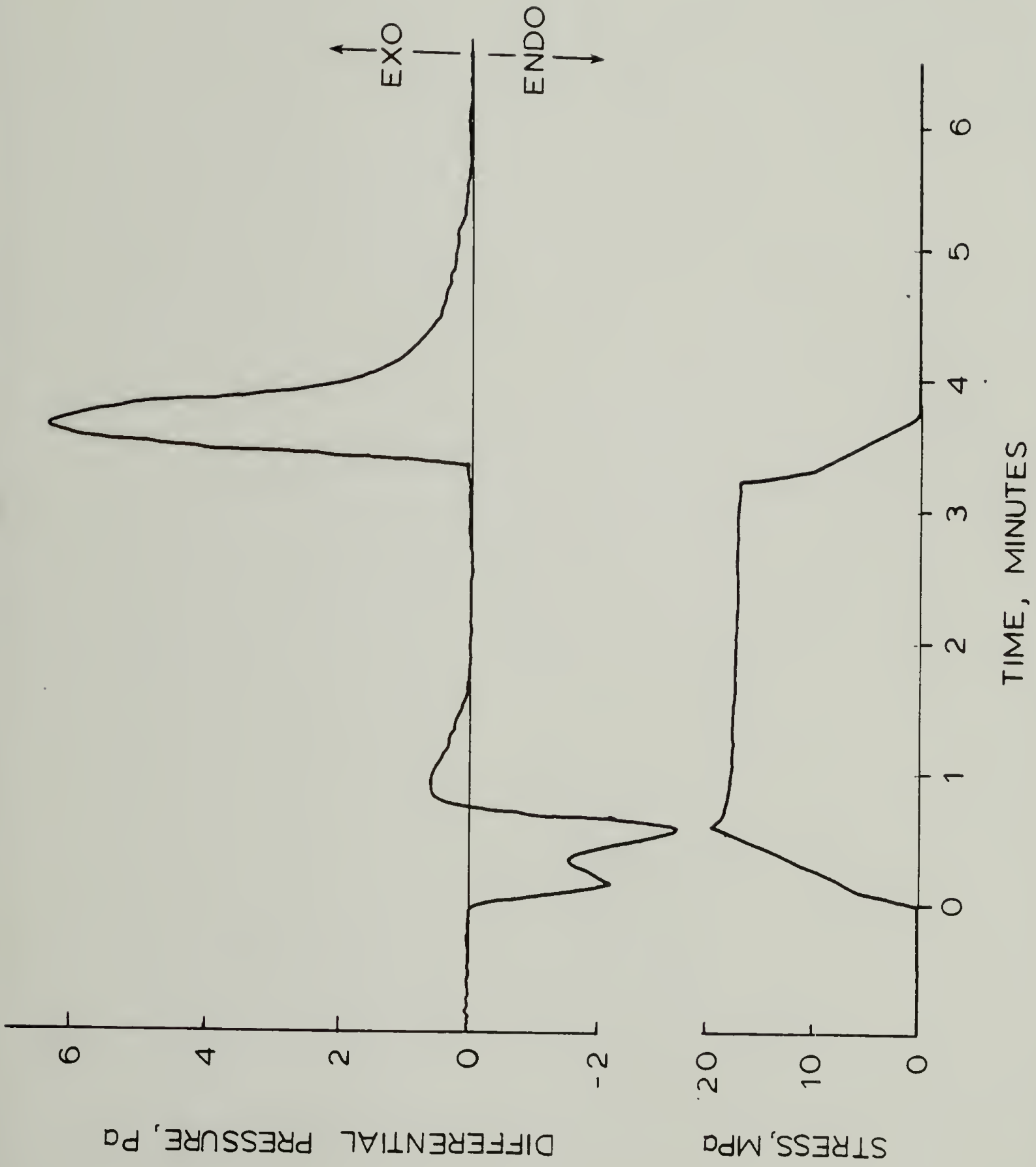


Figure 32. Calorimeter Data for Loading/Relaxation/Unloading of PBT/PTMO Thermoplastic Elastomer Between 0-15.3% Strain

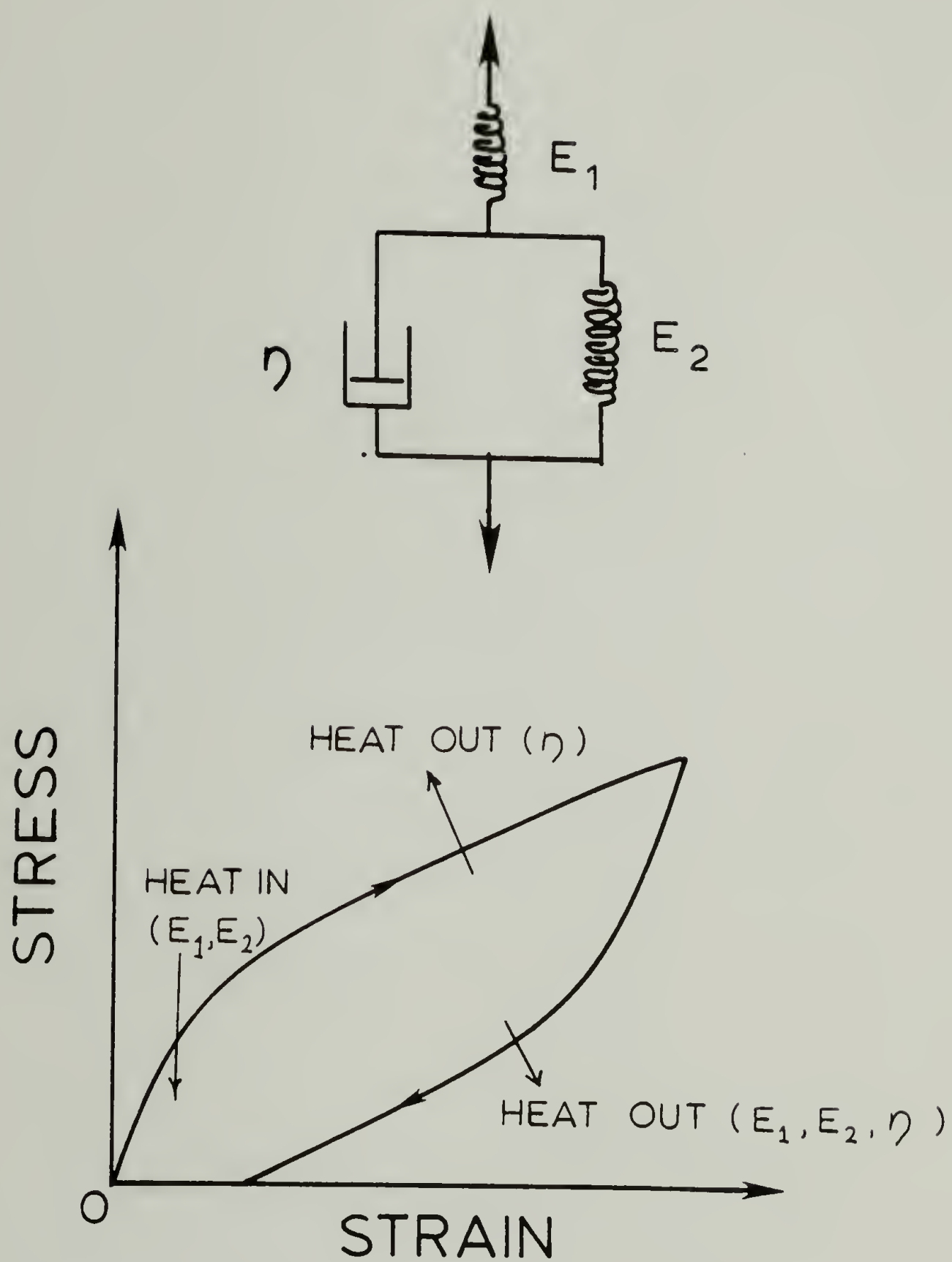


Figure 33. Standard Linear Viscoelastic Solid Model and Typical Stress-Strain Curve Showing Thermal Processes

Initial loading would result in cooling from the instantaneous (dilatational) response of the spring with modulus E_1 , followed closely by an exotherm due to the retarded elastic response of the Voigt element with viscous dissipation (heating) by the dashpot and some cooling by spring E_2 . Viscous dissipation with heat evolution would be expected to characterize the stress relaxation process at fixed strain, as suggested by Equation 55, and shown by Muller and Weiman (26) in deformation calorimetry studies of polycarbonate. The above reasoning suggests that the unloading process should be entirely exothermic as the springs contract, giving off heat, and the dashpot moves back towards its original position dissipating heat in the process. At zero force the initial length is not recovered so that, theoretically, there should be a certain amount of stored elastic energy in the springs which is only slowly released as the length creeps back to its initial value.

In the real polymer, this recovery process is so slow (12 hr) that the thermal effects are undetectable in the calorimeter. From the data in Figure 32 an increase of .47 J/g in the internal energy accompanies the 2.3% temporary set after the deformation cycle. The thermal effects appear to be qualitatively well represented by this simple mechanical model.

Closer inspection of the original data in Figure 32 shows that the actual thermoelastic behavior is somewhat more complicated than this simple model can predict. In particular, a double peak on the endotherm during loading is not suggestive of a purely viscoelastic process. This second peak at about 8.7% strain may be due to the cooperative $\alpha \rightarrow \beta$ transition of the oriented PBT hard segments (89,92,93) which has an associated enthalpy of + 5.1 kJ/mole monomer unit (93). The α crystal form of PBT is thought to be stable in the stress-free state, but undergoes a transition to the more extended, higher energy β crystal form at a critical stress of 7.5 MPa at room temperature. This is in fair agreement with the measured stress of 10 MPa at the onset of the second endotherm on the deformation calorimetry data. The endotherm would be expected for the $\alpha \rightarrow \beta$ transition since the enthalpy is positive and the resulting structure of higher energy. This may account for the excess heat absorbed over that calculated from thermostatic measurements.

Low Density Polyethylene

A sample of the Alathon LDPE was loaded and unloaded between 0 and 6% strain at a strain rate of 200%/min in the calorimeter at 292 K and the heat and work measured. The heat and work of loading were found to be 6.5 and 4.1 mJ respectively, yielding an internal energy change of 10.6 mJ for the loading process. The heat calculated from Equation 26 using the literature value of $24.8 \times 10^{-5} /K$ (94) for the linear thermal expansion coefficient of LDPE is 6.9 mJ, which is close to the measured value. The heat and work of unloading from 6% strain are -4.1 and -2.7 mJ respectively yielding an internal energy change of -6.8 mJ for the unloading process and an overall increase in internal energy of 3.8 mJ for the cycle. Obviously some microstructural processes occur during deformation even at this low level of strain which increase the internal energy of the polymer relative to the value for the initial undeformed specimen.

Samples of LDPE were also subjected to 400% strain loadings at 292 K in the deformation calorimeter at strain rates of .08, .8 and 8 min^{-1} . The samples necked at about 8% strain and exhibited strain hardening on further deformation. The thermodynamic processes dQ/dt , dW/dt and dU/dt accompanying drawing at $.8 \text{ min}^{-1}$ are shown in Figure 34 up to the termination of stretching. From this data it is

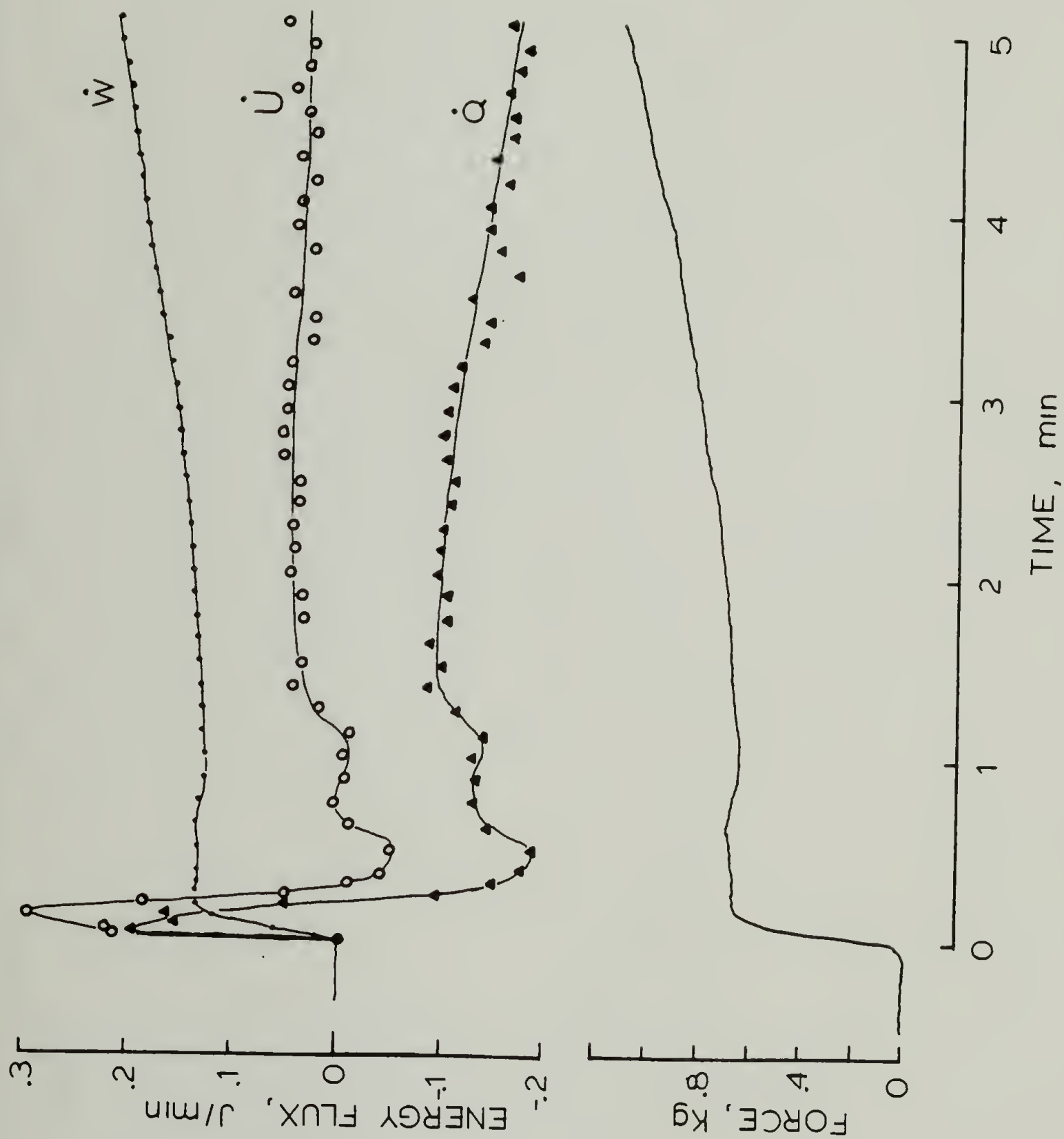


Figure 34. Force-time (strain) Curve and Mechanical Power (\dot{W}), Rate of Change of Internal Energy (\dot{U}) and Heat Flow (\dot{Q}) for Drawing of LDPE at $.8 \text{ min}^{-1}$

clear that the rate of change of internal energy during drawing is positive and relatively constant throughout the entire process, being about 30 % of the mechanical power. This means that 30 % of the mechanical work is stored as internal energy in the LDPE during drawing, in contrast to a purely viscous or rubbery process in which all of the mechanical energy would be transformed into heat with little or no increase in internal energy at constant temperature. Strain rate was found to have no effect on the amount of mechanical energy stored as internal energy during drawing as shown in Figure 35 where a log-log plot of mechanical power versus heat flow shows a slope of 1.0. The individual data and the intercept show that the relationship: $-dQ/dt = .7 dW/dt$ or $dU/dt = .3 dW/dt$ is valid over the entire range of strain rates tested.

This is in agreement with deformation calorimetry studies by Godovskii (55) on polyethylene at a single strain rate, who finds $-dQ/dt = .75 dW/dt$. In a later study with Chvalun et.al. (95) Godovskii studied the reversible small strain thermal effects in drawn and undrawn polyethylene using deformation calorimetry and X-ray diffraction, and found that the sign and magnitude of the thermal effects could be related to changes in the interfibrillar amorphous density and the relative extension of tie chains.

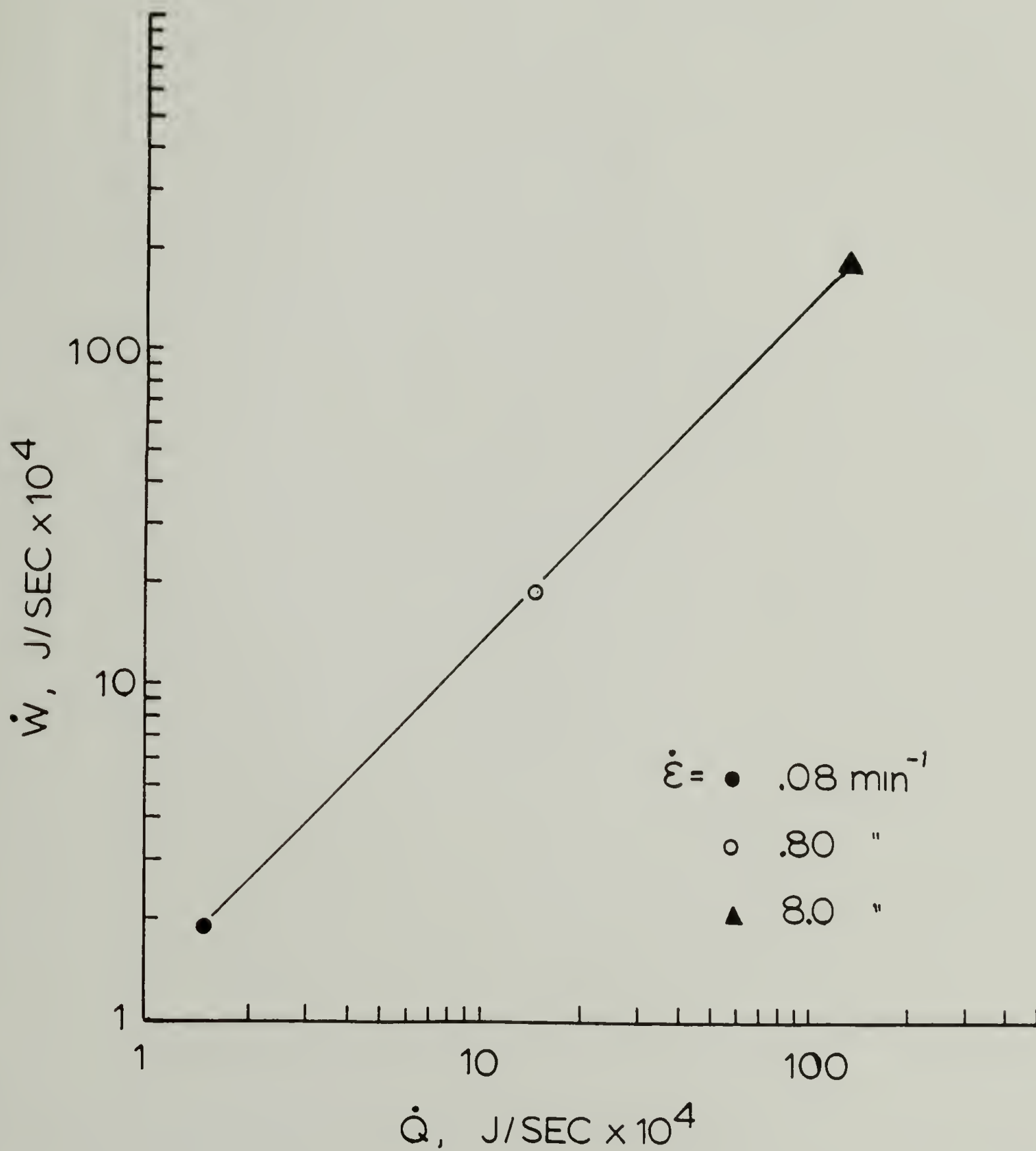


Figure 35. Mechanical Power versus Heat Flow for Drawing of Low Density Polyethylene at Three Strain Rates

Gerth and Muller (96) studied the deformation of radiation crosslinked polyethylene calorimetrically and noted a similar increase of internal energy on first loading to 75% strain which they attributed to "squashing of crystals" or deformation induced decrystallization. Above the melting temperature of 137 C, reversible entropic heats were observed characteristic of the rubbery state.

The decrystallization mechanism for the increase in internal energy during polyethylene drawing is consistent with proposed molecular models of solid state deformation which consider breakup of crystalline lamellae, subsequent orientation in the stretching direction and the pulling out of chain folds. Perkins and Porter (97) have given an in-depth review of solid state deformation mechanisms for polyethylene.

Duvdevani, Biesenberger and Gogos (58) studied the drawing of spherulitic polybutene-1 using their flow calorimeter and found an increase in internal energy of 7 J/g after drawing. Elongation of spherulites was observed in the deformed samples with the aid of a polarized microscope, which suggested distortional energy as the source of the observed internal energy increase.

Goritz and Muller (98) studied the drawing of polypropylene and noted a similar increase in internal energy of the sample caused by deformation which was found to be

directly proportional to the increase in specific surface area, implying that surface free energy is the source of the internal energy change in this polymer.

In summary, it appears that a variety of explanations have been proposed for the observed increase in internal energy of drawn semi-crystalline polymers. Future work by Adams in this laboratory using deformation calorimetry to study the drawing of various types of polyethylene should shed some light on this problem.

DIFFERENTIAL SCANNING CALORIMETRY OF STRETCHED ELASTOMERS

Differential scanning calorimetry studies on stretched yarns of the polyurethane-urea elastomers were performed according to the method given in the Experimental section, in order to characterize the melting behavior of stress-induced crystallinity assumed to be responsible for the decrease in internal energy at high elongations.

A composite of normalized DSC heating scans obtained at a heating rate of $10^{\circ}\text{C}/\text{min}$ are shown in Figure 36 for the PTMO soft segment elastomer held at the indicated extension ratio during the scan. It is seen that the melting endotherm of the PTMO soft segments centered at about 280 K in the isotropic sample ($\lambda = 1$) is broadened

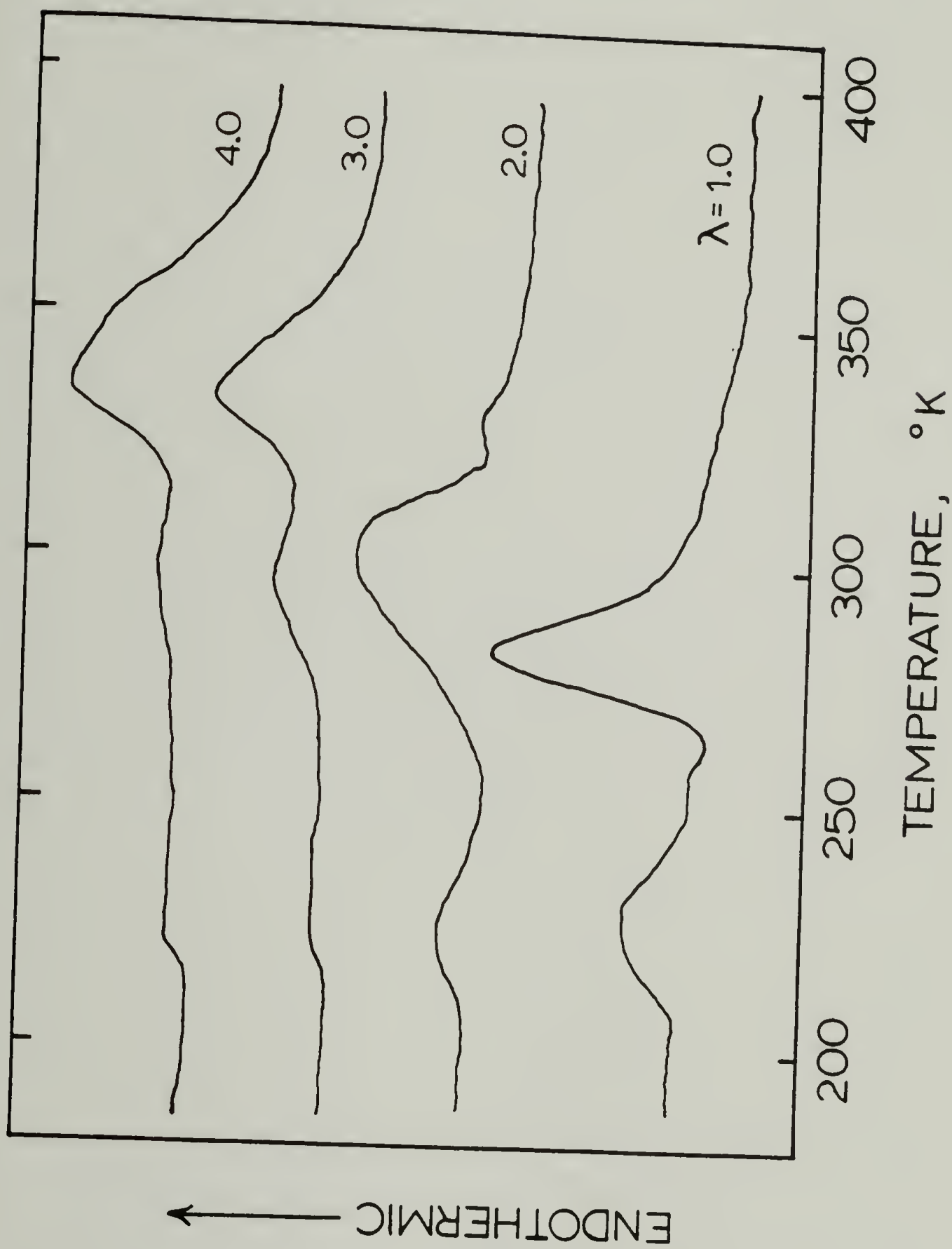


Figure 36. First DSC Heating Scans of Polyether Soft Segment Elastomer Held at the Indicated Extension Ratios

and shifted to higher temperature with increasing elongation. At an extension ratio between 2 and 3, a second endotherm forms which is centered around the equilibrium melting temperature of 330 K. This second peak at high elongations has an end of melting above 100 C and results from stress-induced crystallization during stretching. It is unstable with respect to melting and does not reform after heating and subsequent cooling at fixed length. This is shown clearly in Figure 37 for the PTMO soft-segment elastomer at an extension ratio of 3. Irreversible melting occurs up to the highest temperature of the first heating scan, subsequent scans showing only a broadened low temperature endotherm resulting from thermally-induced crystallization formed by cooling in the DSC at fixed length. This thermally-induced crystallinity is stable in the strained state and melts and recrystallizes reversibly in all successive scans, having an end of melting around the equilibrium melting temperature of 323K.

The heat of fusion for the high temperature, stress-induced crystallinity (SIC) was estimated by computer subtraction of the second scan DSC data from the first scan data, and subsequent integration. Values for the heat of fusion of SIC in J/g, are plotted in Figure 38 along with the internal energy change measured by deformation calorimetry during the stretching process. The agreement, which is seen to be very good, is perhaps

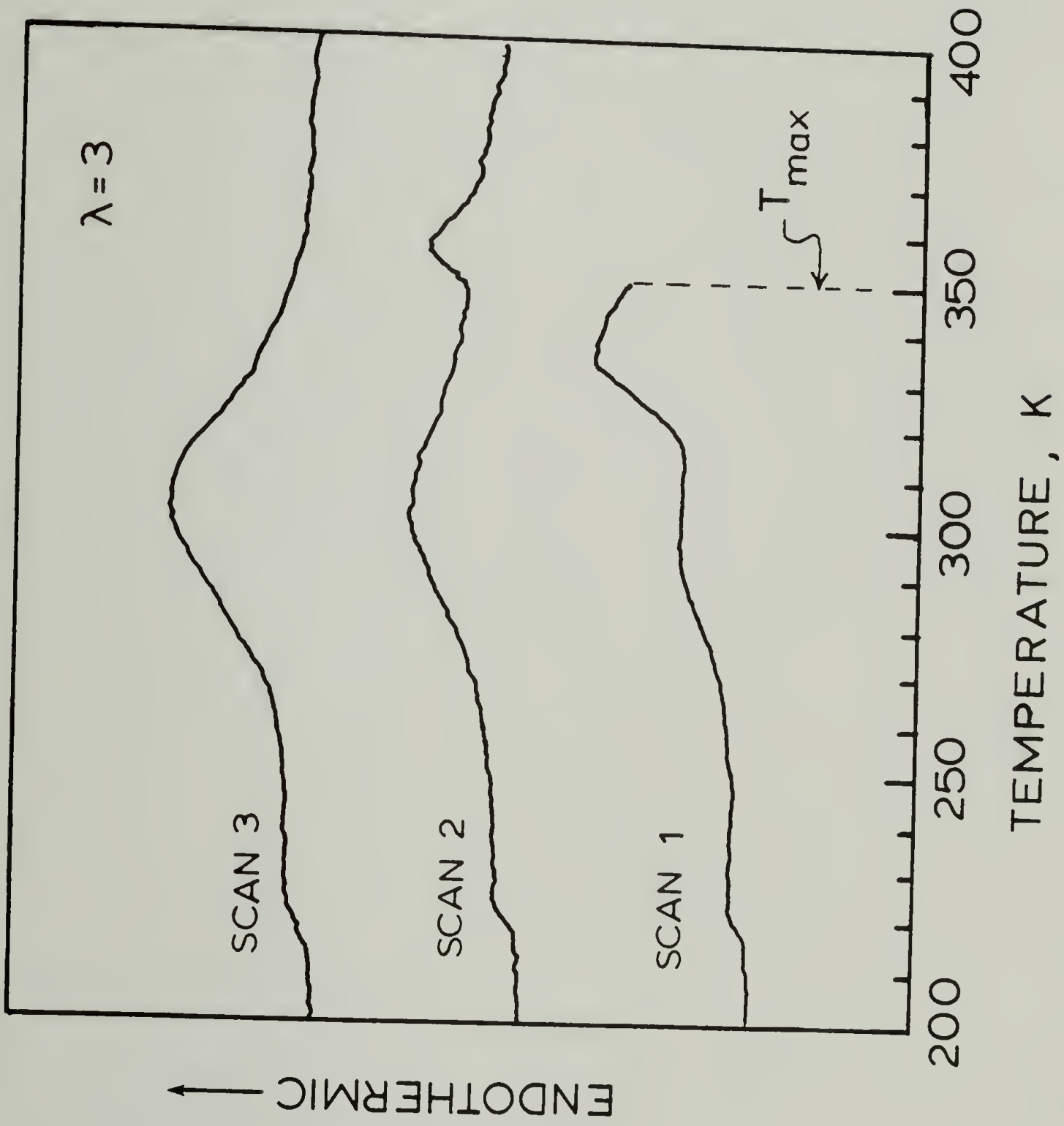


Figure 37. First, Second and Third DSC Heating Scans of Polyether Soft Segment Elastomer Held at $\lambda = 3$

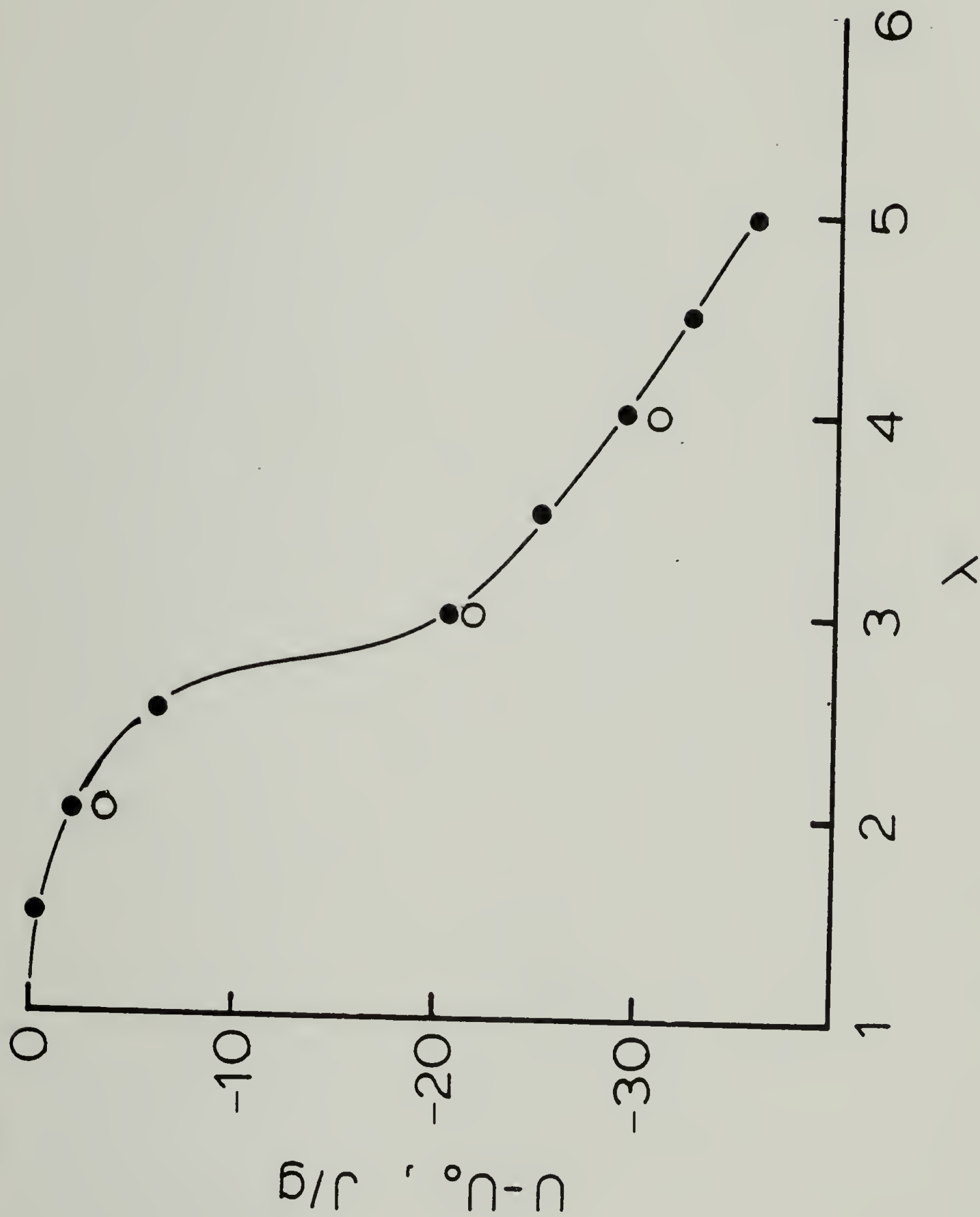


Figure 38. Internal Energy Change versus Extension Ratio for Polyether Soft Segment Elastomer. Deformation Calorimetry (●) and Heat of Fusion from DSC (○).

fortuitous considering the crudeness of the DSC method. The data does suggest, however, that the internal energy change measured by deformation calorimetry is in close agreement with the heat liberated by crystallization of the soft-segments during stretching.

Similar results to those shown for the PTMO soft-segment elastomer were also obtained for the mixed polyester soft-segment elastomer as shown in the composite of normalized first scan DSC thermograms in Figure 39. Conspicuously absent in these data, however, is the melting of thermally-induced soft-segment crystallinity in the isotropic, unstretched state. This is undoubtedly due to the irregular chemical structure of the mixed polyester soft-segments. At an extension ratio of 2.3, however, melting of thermally-induced crystallinity is observed, indicating that perhaps the crystallization kinetics change from homogeneous nucleation to heterogeneous nucleation on preformed nuclei consisting of a small fraction of highly extended soft-segment chains. This is consistent with the appearance of a small high temperature shoulder for SIC at the extension ratio where thermally-induced crystallinity (TIC) is first observed. The same behavior is found for the PTMO elastomer, whereby the first sign of SIC corresponds to the extension ratio at which significant changes in TIC are observed. The effect of strain in general, is known to greatly increase the

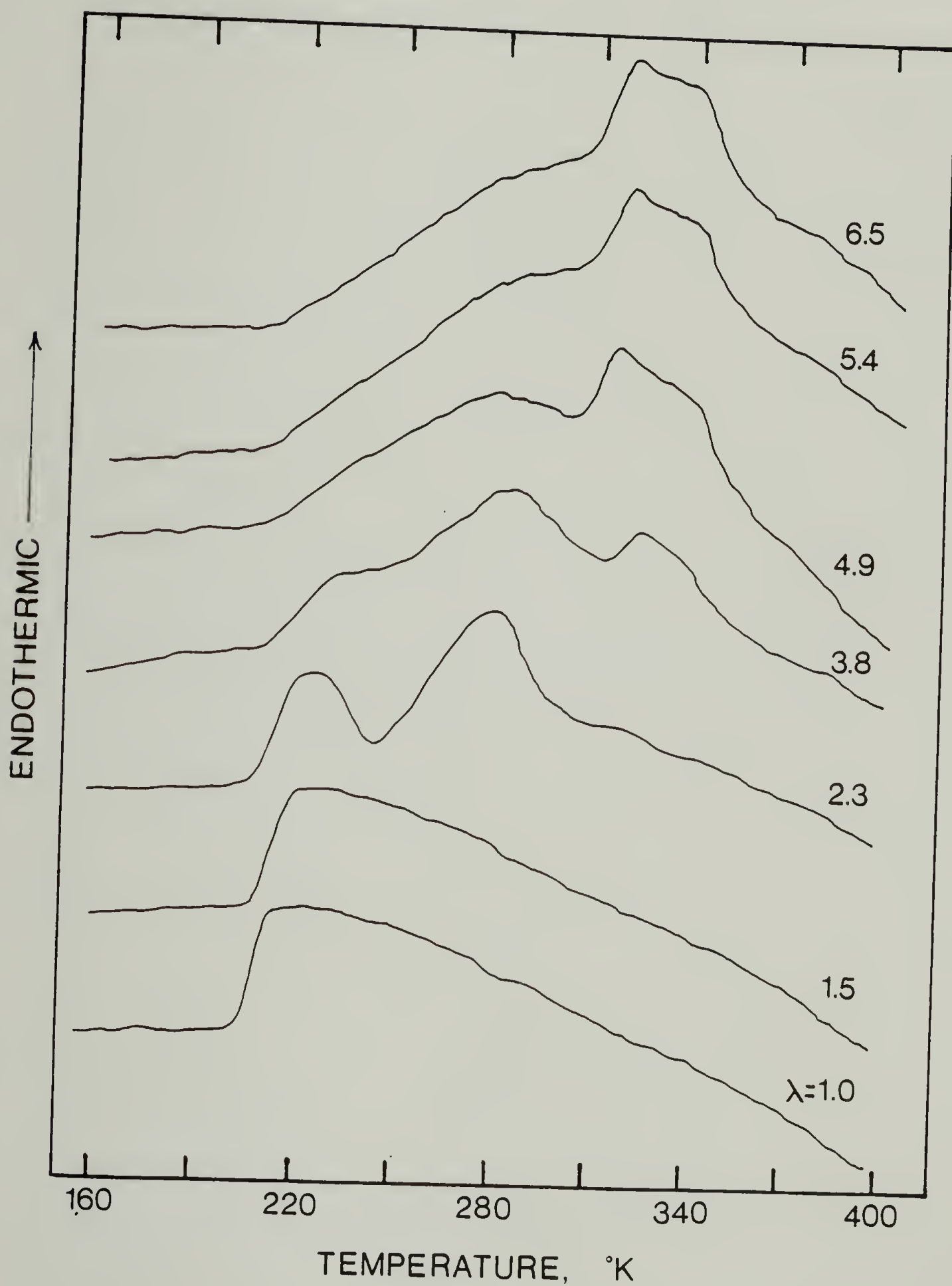


Figure 39. First DSC Heating Scans of Polyester Soft Segment Elastomer Held at Indicated Extension Ratios

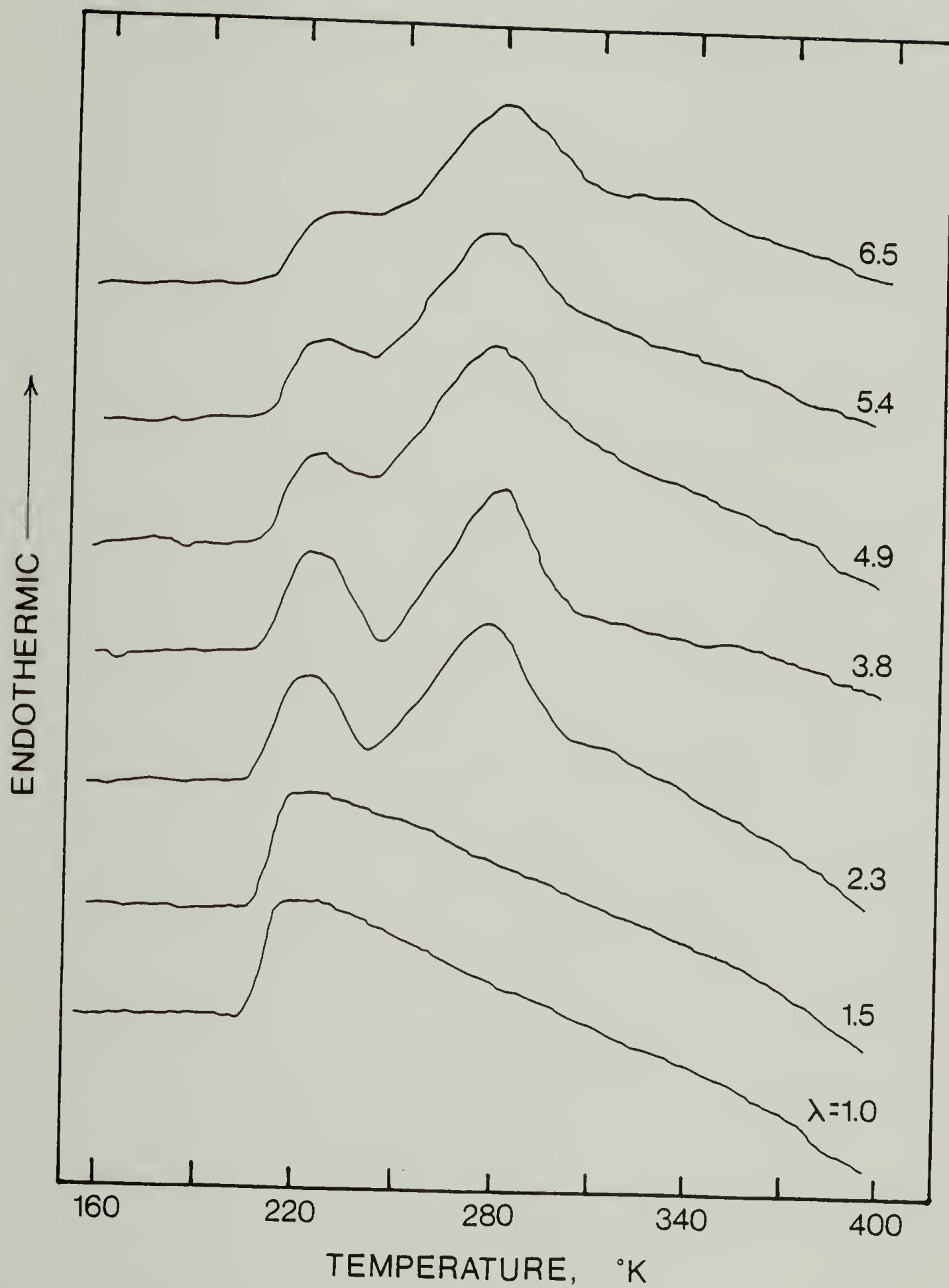


Figure 40. Second DSC Heating Scans of Polyester Soft Segment Elastomer Held at Indicated Extension Ratios (after First Heating to 400 K)

kinetics of crystallization in elastomers (74,76,77,99).

At higher elongations the polyester soft-segment elastomer shows the melting of fully developed stress-induced crystallinity centered around 338 K which is the equilibrium melting temperature of the predominant adipic acid/ethylene glycol sequences of the soft-segments. The end of melting at about 400K is significantly higher than the equilibrium melting temperature of 338K. Second scan DSC thermograms of the same samples at the indicated extension ratios are shown in Figure 40. Again the high temperature endotherm is erased by the thermal treatment of heating to 400 K during the first scan. A pronounced dependence of morphology, and presumably mechanical properties, on the thermal history of the stretched elastomers is inferred from these data.

The apparently two-stage nature of crystallization observed in the DSC data has been the subject of previous studies concerned with the crystallization behavior of stretched elastomers. Cesari, Perego Zazzetta and Gargani (100,101) studied crystallization in cis-1,4 polybutadiene networks stretched at room temperature and cooled to -50 C before crystallinity and crystallite orientation were determined at various temperatures using WAXS and SAXS. These authors concluded that all of the experimental data was consistent with the formation of two types of crystals: one depending mainly on stretching, the

other on temperature. The former is characterized by extended chain crystals with T_m higher than the isotropic melting point, while the latter possessed a lamellar or bulk-like morphology which is stable only below the isotropic melting point. Consistent with the present study, a slight increase of T_m was observed for extension ratios less than 3, when the axes of the crystallites were tilted with respect to the stretching direction. At extension ratios above 3, when untilted crystals were formed, a dramatic increase in melting temperature was observed with an end of melting at 345 K, which is 75 degrees higher than the isotropic melting temperature of 276 K. The qualitative interpretation of the two-stage mechanism for crystallization under strain was that non-uniform extension of the rubbery segments between crosslinks provided ample flexibility for lamellar-type crystallization below the isotropic melting temperature even in the highly extended state.

Essentially the same conclusions as those of Cesari et.al., regarding the two stage nature of oriented crystallization were reached by Goritz and Muller (21) in kinetic studies of crystallization in natural rubber using deformation calorimetry. Goritz and Muller found that the final degree of crystallinity depended on temperature and elongation, as observed in the present study. Moreover, these authors concluded that crystallization could not be

described by a single uniform process using Avrami kinetics. However, all of the data could be reduced to two separate processes- one consisting of three dimensional growth during stretching, and a second assigned to one dimensional growth of existing crystallites in the direction of stress after stretching and during cooling.

Goritz, Muller and Sietz (65) are the only authors to publish differential scanning calorimetry data for an elastomer held in the extended state during the DSC scan. These authors studied the melting behavior of natural rubber which had been stretched at room temperature and cooled to the maximum crystallization temperature (248 K) before heating at fixed length. The thermograms are qualitatively similar to those presented in this section, in that two distinct melting processes were observed: one below room temperature induced by cooling (TIC) and a broad endotherm above room temperature (SIC) with an end of melting near 333 K. Consequently, the two-stage melting process in elastomers which have been stretched at room temperature is not unique to the polyurethane-urea elastomers of the present study. Moreover, a distinction should be made between the type of crystallites generated during the (non-equilibrium) stretching process and those formed under equilibrium conditions by cooling from an oriented melt. These have been referred to as stress- and thermally-induced crystallinity respectively, the former being

primarily responsible for the internal energy change measured in deformation calorimetry experiments at room temperature.

The melting point increase from 280 K in the isotropic PTMO elastomer to over 330 K at high elongation, and similar behavior in the polyester soft-segment elastomer, can be due to a number of reasons including an increase in crystallite size. Additionally, the observed increase in stress accompanying the formation of SIC during stretching suggests an unusually high degree of amorphous orientation which can elevate the melting point above the equilibrium, isotropic value by reducing the configurational entropy sacrificed on melting. The extremely broad melting range of both TIC and SIC suggests a wide distribution of crystallite size, tension or perfection. Smearing of the thermogram is not considered to be responsible for this broadening, since the glass transition of the soft-segments at about 220 K shows a sharp discontinuity in heat capacity over only a few degrees of temperature.

An approximate relation between crystallite size, amorphous orientation and observed melting point can be derived by considering the individual crystallites to possess sufficient surface free energy that the Gibbs free energy, G , of the system is no longer a bulk quantity, but must contain surface free energy terms. Following the

derivation of Hill (102) for small systems where size effects become important, the free energy of fusion, ΔG_f , for the system of small crystallites embedded in an amorphous matrix can be written:

$$\Delta G_f = \Delta G_f^\circ + \Sigma \gamma A \quad (90)$$

where γ , is the interfacial free energy between the crystallite and the amorphous matrix and A is the interfacial area. The quantity ΔG_f° , is the bulk free energy for the infinitely large system (i.e. 100% crystalline solid). To obtain an expression for the melting point from Equation 90, the assumption must be made that the melting process can be treated locally as an equilibrium process. With this assumption Equation 90 becomes-

$$\Delta H_f - T \Delta S_f = \Delta H_f^\circ - T \Delta S_f^\circ + \Sigma \gamma A \quad (91)$$

Including elongation effects, the entropy of fusion becomes: $\Delta S_f = \Delta S_f^\circ + \Delta S_{el}$, and if the enthalpy of fusion is a constant, $\Delta H_f = \Delta H_f^\circ$, then the melting point T_m , of the crystallite can be written

$$T_m = T_m^\circ \left[1 - T_m \frac{\Delta S_{el}}{\Delta H} - \frac{1}{V} \frac{\Sigma \gamma A}{\Delta h} \right] \quad (92)$$

where $T_m^\circ = \Delta H_f^\circ / \Delta S_f^\circ$ is the equilibrium melting

temperature of an infinite sized crystal. For a crystallite of square crosssection with end area, a^2 and sides of length, l , the volume, v , of the crystallite is a^2l , and Equation 92 becomes

$$T_m = T_m^{\circ} \left[1 - T_m \frac{\Delta S_{el}}{\Delta H} - \frac{2 \gamma_e}{l \Delta h} - \frac{4 \gamma_s}{a \Delta h} \right] \quad (93)$$

where γ_e , γ_s are the end and side surface free energy and Δh the bulk enthalpy of fusion per unit volume for an infinite sized crystal. Neglecting the elongational entropy term, this equation is commonly used to interpret melting point elevation of polyethylene crystals with increasing fold period, l , the usual assumption being that the end surface area is so large for folded chain crystals that the free energy term in l/a can be neglected. For fringed micelle or fibrillar crystals however, the lateral (a) dimensions would be expected to be small relative to the crystal length (l), so that for this morphology the side surface free energy term would be comparable to the end surface term. In general, the effect of increasing crystallite dimensions, a, l , is to cause a decrease in the ratio of the surface/bulk free energies and an elevation of the melting point towards the equilibrium value for a 100 % crystalline solid.

The configurational entropy term in Equation 93 is negative resulting in an increase of the equilibrium mel-

ting temperature above that observed for the isotropic network. In the case of infinitely large crystals or negligible surface free energy the configurational entropy term alone survives, and the equilibrium melting point elevation becomes

$$\frac{1}{T_m} - \frac{1}{T_m^\circ} = \frac{\Delta S_{el}}{\Delta H} \quad (94)$$

which is the equation derived by Flory (8) for the equilibrium melting point elevation of an oriented network with

$$\Delta S_{el} = -R \left[\frac{\lambda^2}{n} + \frac{1}{\lambda n} - \sqrt{6/n\pi} \lambda \right]$$

the decrease in entropy of the amorphous phase at an elongation λ , for chains of n statistical segments between crosslinks. In Flory's equation ΔH is the bulk enthalpy of fusion per mole and T_m° is the incipient crystallization temperature in the undeformed state, which for a reversible, equilibrium process must be equal to the melting temperature.

Qualitatively, an expression such as Equation 93, accounts for the dual melting behavior observed in stretch DSC scans solely in terms of two crystallite size distributions and differing amounts of local amorphous orientation without the need for invoking folded and extended

chain structures. Although the equilibrium expression is invalid for the irreversible melting of SIC at high temperatures, it nevertheless shows in a qualitative way how melting temperatures in excess of the equilibrium melting temperature are possible under local conditions of high amorphous orientation and increasing crystallite width. Experimentally, the former is confirmed by the rapid rise in stress once crystallization has commenced, and the latter by WAXS, as will be shown in the following section.

WIDE-ANGLE X-RAY SCATTERING STUDIES

Wide-angle X-ray equatorial scans were obtained in conjunction with D.X. Wang (103) on solvent cast films of the polyurethane-urea elastomers and fiber bundles of natural rubber at various extension ratios to confirm the presence of stress-induced crystallinity at room temperature, and obtain an estimate of the lateral dimensions of crystallites oriented in the stretching direction. Flat-film exposures were made of the PTMO elastomer in order to compare unit cell dimensions with published values.

Figures 41 , 42 and 43 are composites of room temperature equatorial scans at the indicated extension

ratio for the polyether soft-segment elastomer, the polyester soft-segment elastomer and natural rubber, respectively. The occurrence of reflections at an extension ratio between 2-3 denoting measurable crystallinity in the PTMO elastomer is in good agreement with DSC melting curves for SIC, and with deformation calorimetry estimates for the decrease in internal energy during stretching of this elastomer. The effect of heating on the WAXS equatorial scan of the PTMO soft-segment elastomer is shown in Figure 44, where the room temperature scan at $\lambda = 5$ is compared to the scan obtained after heating the stretched sample to 400 K for 15 min. A significant reduction in intensity is observed after heating at fixed length, in agreement with the second scan DSC data.

Flat-film exposures were made at room temperature over a 24 hr period for the PTMO elastomer in order to obtain an estimate of the unit cell for SIC. Measured spacings yielded unit cell parameters that were in perfect agreement with literature values by Cesari, et.al. (104) and Imada (105) for poly(tetramethylene-oxide) in the unstressed state, as well as those of Bonart (106) for stress-induced crystallinity in PTMO soft-segment polyurethane-ureas.

Room temperature small-angle X-ray scattering data by Wang (103) for the PTMO soft-segment elastomer in this study showed a long period of 140 \AA up to an extension

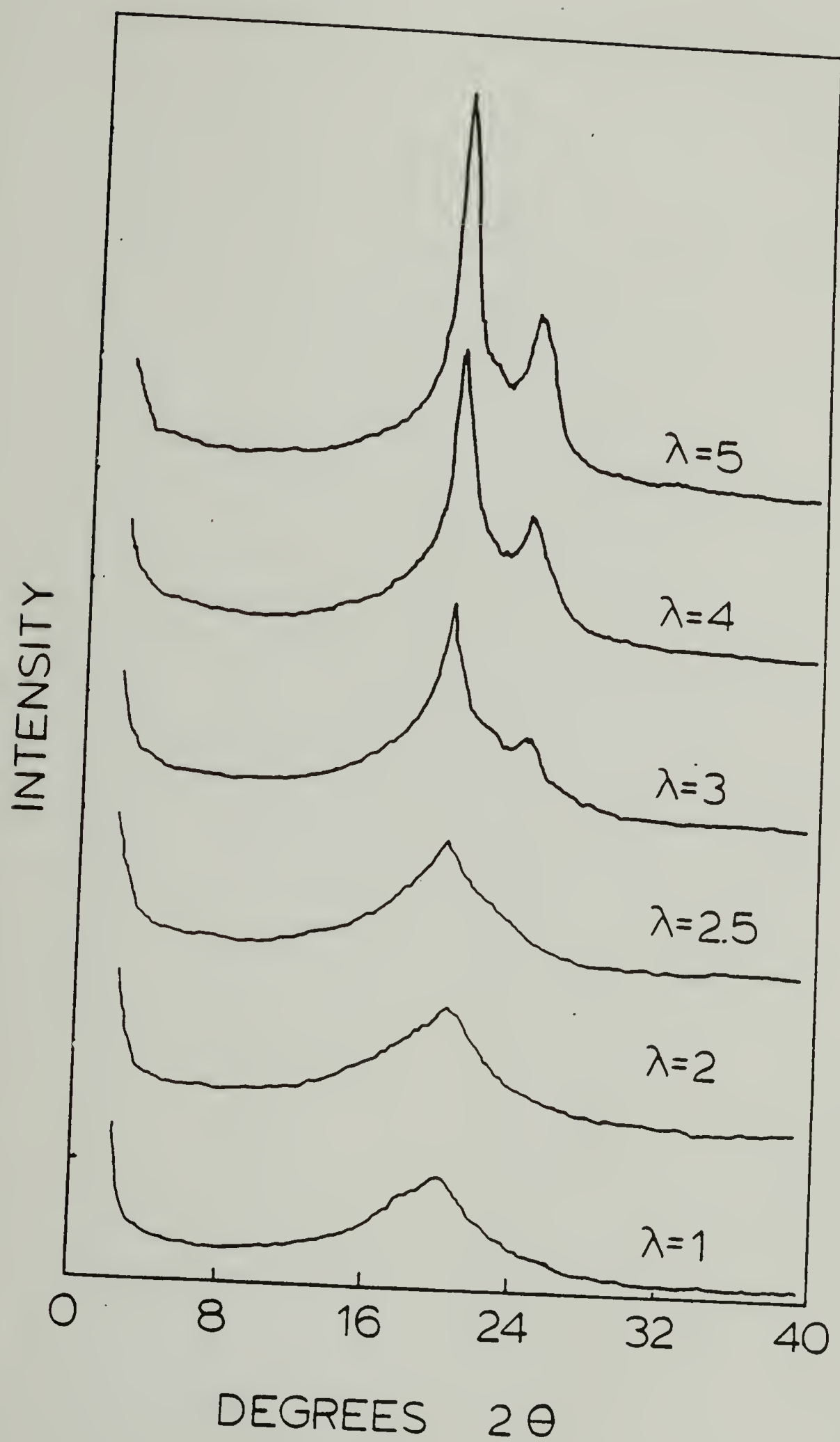


Figure 41. Wide Angle X-Ray Equatorial Scans of Polyether Soft Segment Elastomer Held at Indicated Extension Ratios

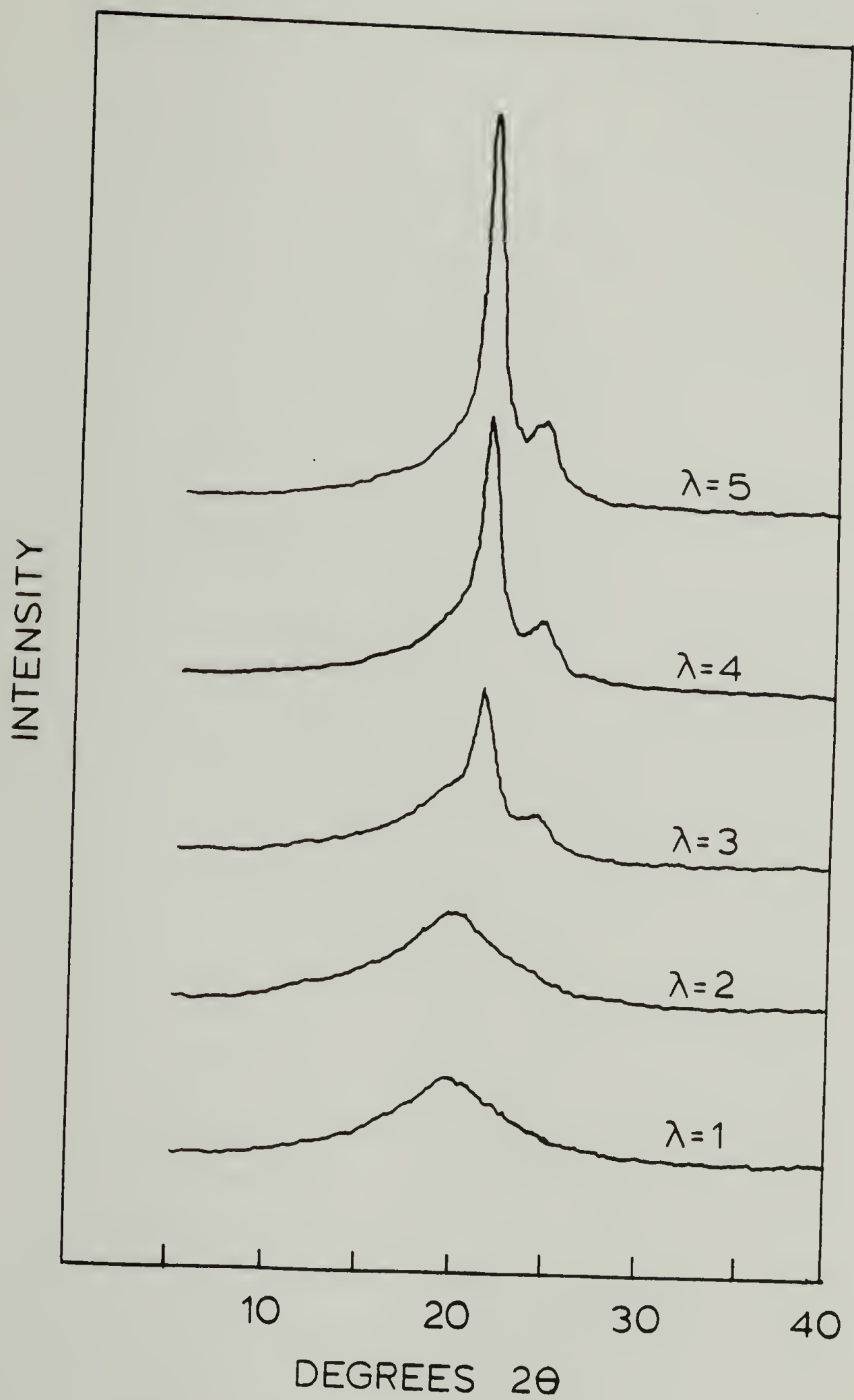


Figure 42. Wide Angle X-Ray Equatorial Scans of Polyester Soft Segment Elastomer Held at Indicated Extension Ratios

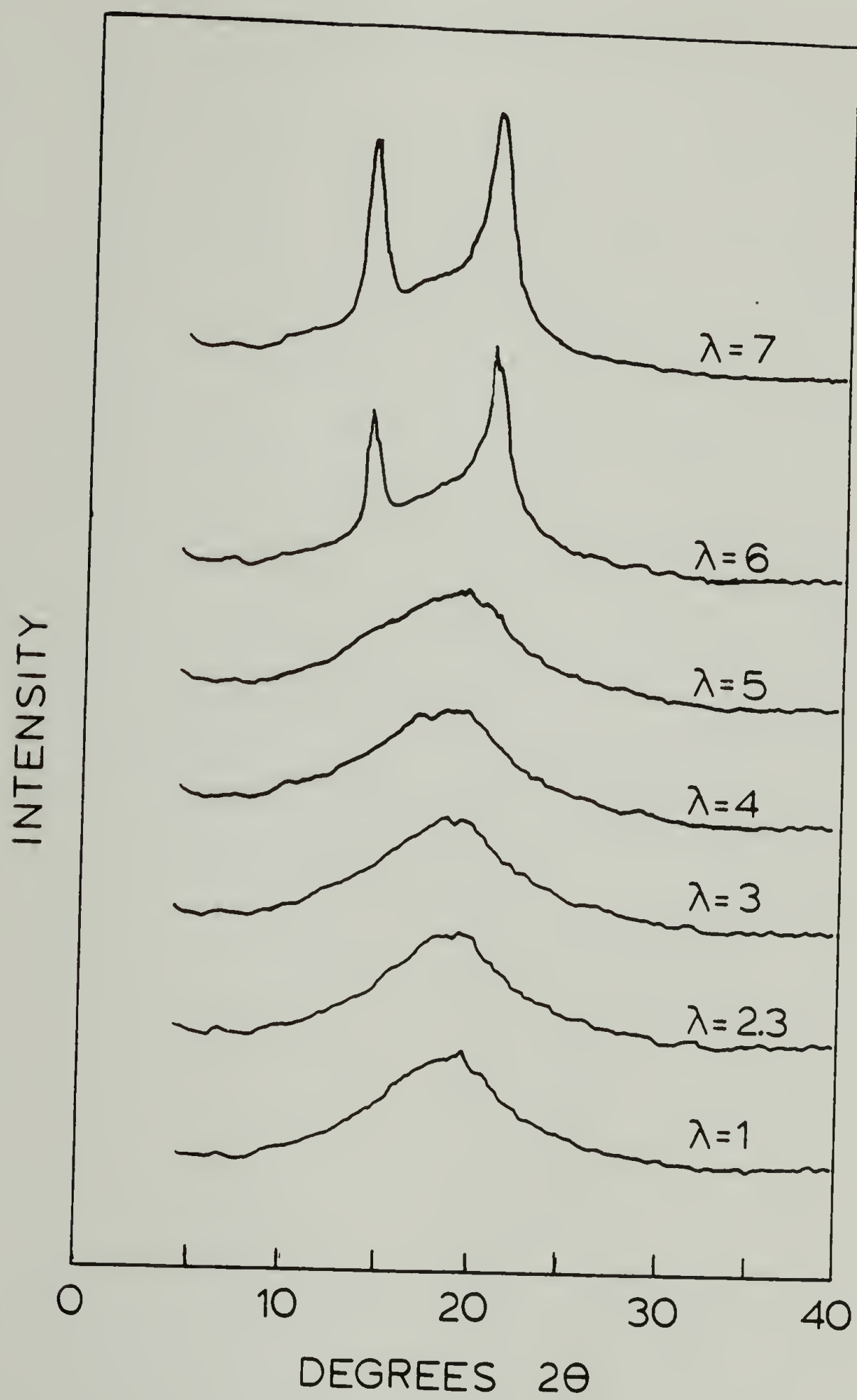


Figure 43. Wide Angle X-Ray Equatorial Scans of Natural Rubber Held at Indicated Extension Ratios

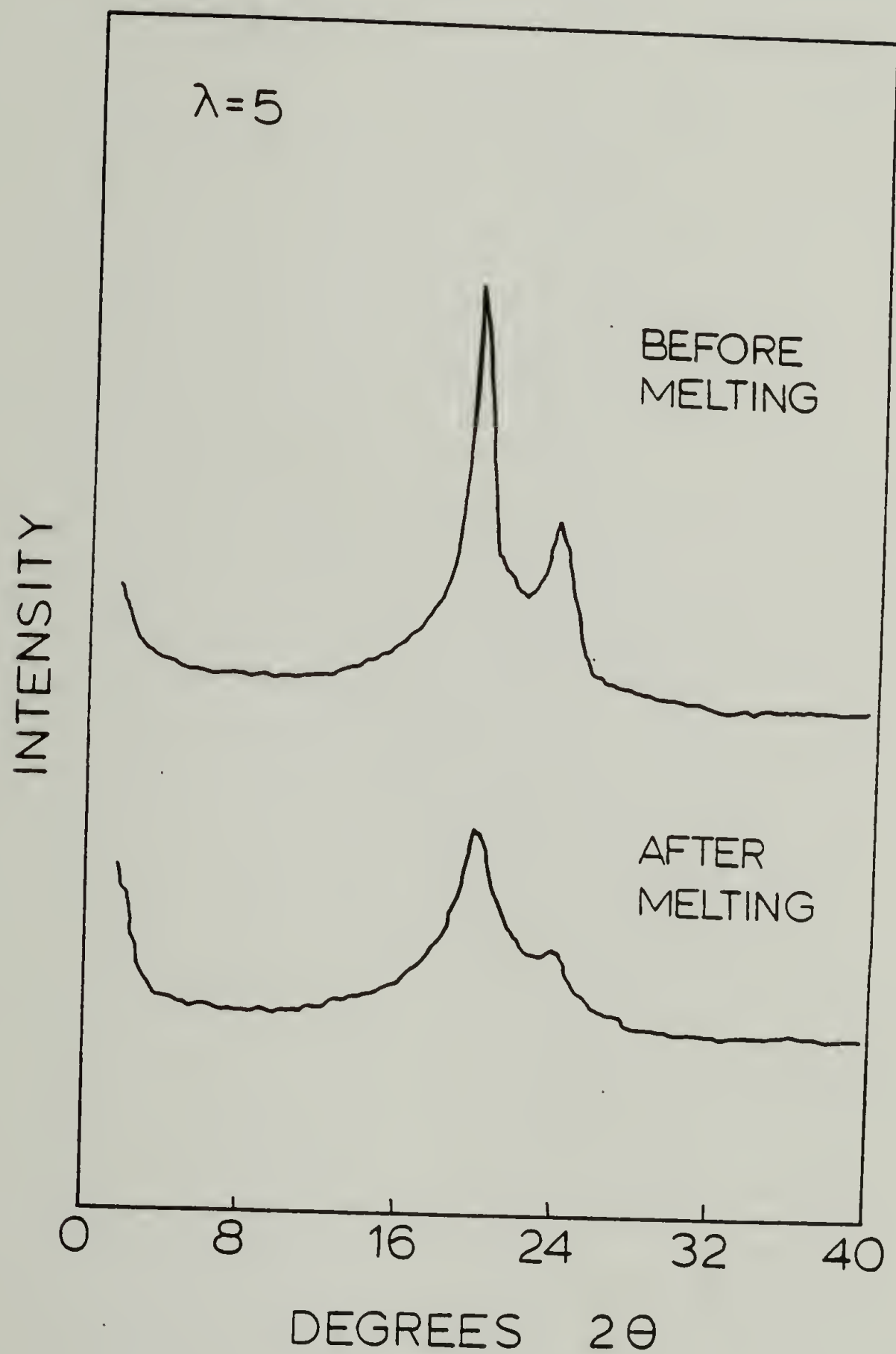


Figure 44. Wide Angle X-Ray Equatorial Scans of Polyether Soft Segment Elastomer Held at $\lambda = 5$, Before and After Heating to 400 K.

ratio of 2, changing to a long period of 190 \AA which remained constant for extension ratios of 3, 4 and 5. The constant long period at high elongation where crystallinity is increasing suggests that growth is not in the direction of stretching.

Equatorial scans of the polyester soft-segment elastomer show significant crystallinity is already present at an extension ratio of 3, which is in good agreement with DSC and deformation calorimetry estimates of $\lambda = 2.6$ for the onset of crystallization during room temperature stretching.

Natural rubber is seen to exhibit strong crystalline reflections at $\lambda = 6$, which coincides with the value obtained in deformation calorimetry studies. Consequently, WAXS, DSC and deformation calorimetry are in qualitative agreement with regard to the onset and magnitude of stress-induced crystallization in all of the elastomers studied.

Crystallite dimensions perpendicular to the stretching direction were estimated from the equatorial scans of this section using the simplified Scherrer equation and the method described in the experimental section. These data for the crystallite width, a , are plotted in Figure 45 versus extension ratio for both polyurethane-ureas and natural rubber. It is seen that the crystallite width or thickness perpendicular to the stret-

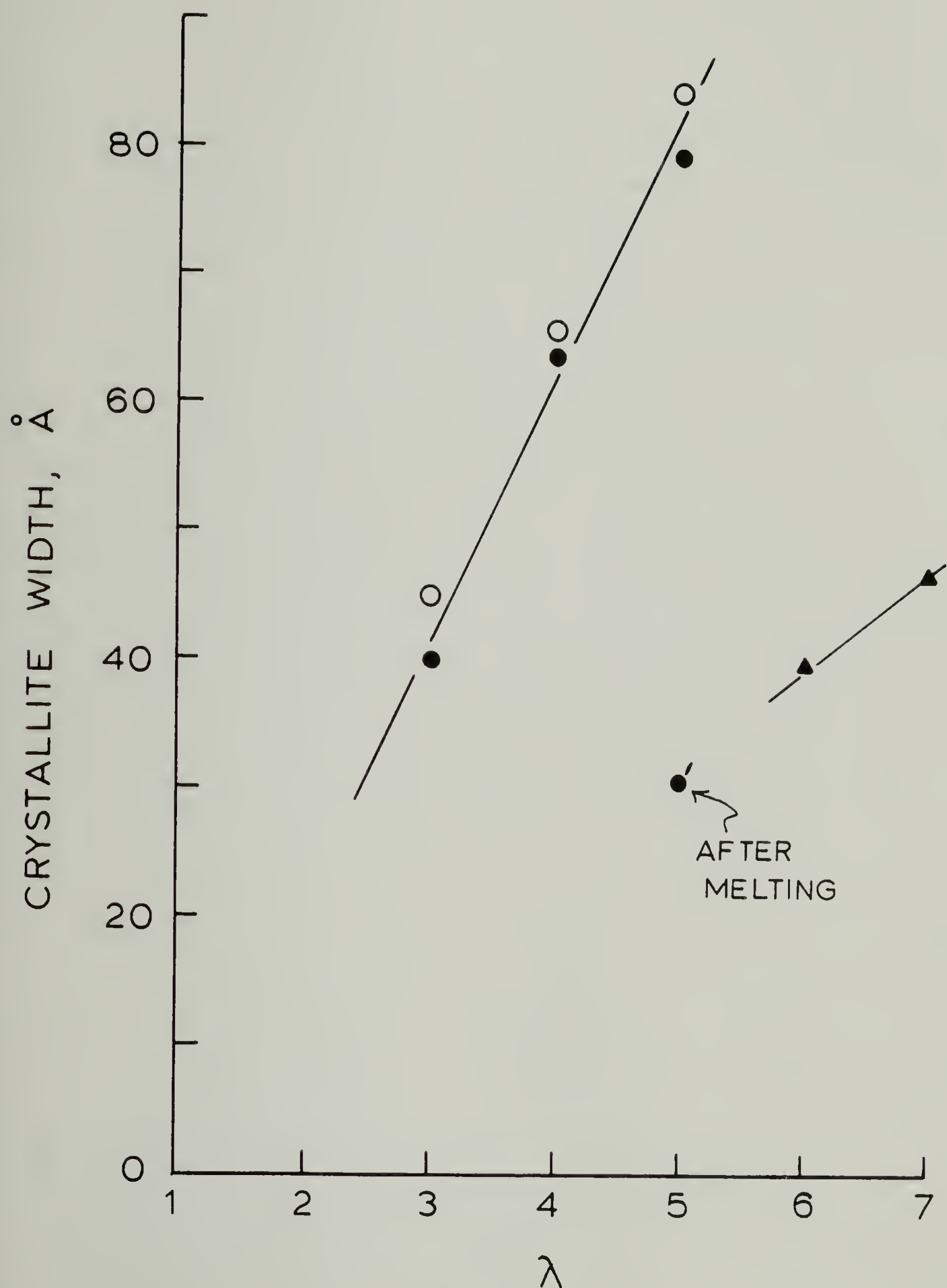


Figure 45. Crystallite Width (a) Perpendicular to Stretching Direction. Polyether (●), Polyester (○) Soft Segment Elastomers and Natural Rubber (▲).

ching direction increases almost linearly with strain over the region where stress-induced crystallinity is also increasing linearly in the polyurethane-ureas. As mentioned previously, the long period remains essentially constant over this same range of extension, implying that crystallites are growing transverse to the stretching direction by an intermolecular process. This is in contrast to the commonly encountered one-dimensional growth process for thermally-induced crystallization of oriented crosslinked melts at high extensions (74,107). After melting at 400 K at fixed length and cooling back to room temperature, the PTMO soft-segment crystallites show a reduction in crossection from 90\AA to 35\AA , corresponding to the lower melting point observed on DSC thermograms. This may be due to crystallite size alone or to the reduction in amorphous orientation after initial melting of the SIC network formed during stretching.

Experimental studies of the morphology of stress-induced crystallinity are scarce. Most notable are the earlier electron microscopy studies by Andrews (108) on cis-polyisoprene, which showed that crystallization occurs by a two dimensional growth of lamellae perpendicular to the fiber axis when the extension ratio is less than 4, but that growth is one-dimensional yielding needle-like crystals above this extension. Luch and Yeh (109) reported electron microscopy results for stress-induced crys-

tallization of uncrosslinked natural rubber thin films. These authors found that films stretched to extension ratios of between 6 and 10 at room temperature showed a particulate texture with small nodular crystallites having an apparent core diameter of 100-130 \AA . The crystallites showed a tendency to align in the stretch direction, although this was not a necessary condition of the morphology. Aging of highly stretched films at room temperature for up to five months resulted in a slight increase in definition with no detectable change in size. The effect of heating the stretched films to 328 K for two minutes and then cooling to room temperature was to decrease the degree of crystallinity, as deduced from the number of fibrils remaining after the heat treatment, with no large change in the details of the particulate fibrillar structure. This was interpreted as direct evidence for the lack of folded-chain-type crystal overgrowth, which would not be expected to survive such a heat treatment. Cooling of the highly stretched films to 245 K for 20 minutes showed crystallite growth perpendicular to the stretch direction, eventually resulting in a lamellar texture with no evidence of the original fibrous texture.

In summary, Luch and Yeh conclude that stress-induced crystallinity stable above room temperature is limited to about 150 \AA in size, regardless of the degree of elongation, although the population density increases

with strain. This is consistent with the constant long period or lamellar periodicity for SIC of PTMO in the present study. Luch and Yeh suggest the the crystallites might consist of micellar-type extended chain crystals, but are restricted in growth due to the rapidity of the crystallization process- a postulate which is agrees with the deformation calorimetry data of the present study and the kinetic studies of crystallization during stretching by Mitchell and Meier.

The fringed micelle structure for stress-induced crystallinity proposed by Luch and Yeh is consistent with the narrow crystallite widths observed in WAXS, but represents an energetically unfavorable structure, since calculations by Zachman (110,111) suggest that the end surface free energy for the fringed micelle is at least an order of magnitude higher than the side surface free energy. If this is correct, the minimum free energy route for crystallization would be in the c-axis or fiber direction- as expected (and experimentally verified) for equilibrium crystallization of stretched networks. In contrast, the observations of Luch and Yeh and the WAXS in this study show increasing lateral width at constant crystal length, revealing the relative instability of crystals formed in this manner. Undoubtedly the rapid rate of stress-induced crystallization at room temperature dictates the formation of the high energy structure over

the thermodynamically favored one-dimensional growth mode. Thermostatic measurements presented in the following section confirm the metastable nature of SIC.

A pictorial representation of the process of stress-induced crystallization at room temperature leading to this high energy metastable structure, which is consistent with the lateral growth mode, observed melting temperature increase and deformation calorimetry data is shown in Figure 46. Initial deformation of the amorphous network results in sporadic crystallization in the direction of stress of the most highly extended chains. This may result in a slight depression of the stress-strain curve during the initial stages of crystallization. Since the kinetics of further one-dimensional growth are presumably slow, fringed micelle-type crystallites grow transverse to the stretching direction by lateral accretion of adjacent chains. This greatly increases the crosslink density causing an upswing in the stress-strain curve. At high extension the crystallites may coalesce forming a semi-continuous three-dimensional structure which eventually bears all of the load. Further deformation would distort or destroy this structure resulting in an increase in internal energy observed in the deformation calorimetry experiments on natural rubber at ultimate elongations. Similar models have been proposed by Morbitzer and Bonart (81) and Bosley (112).

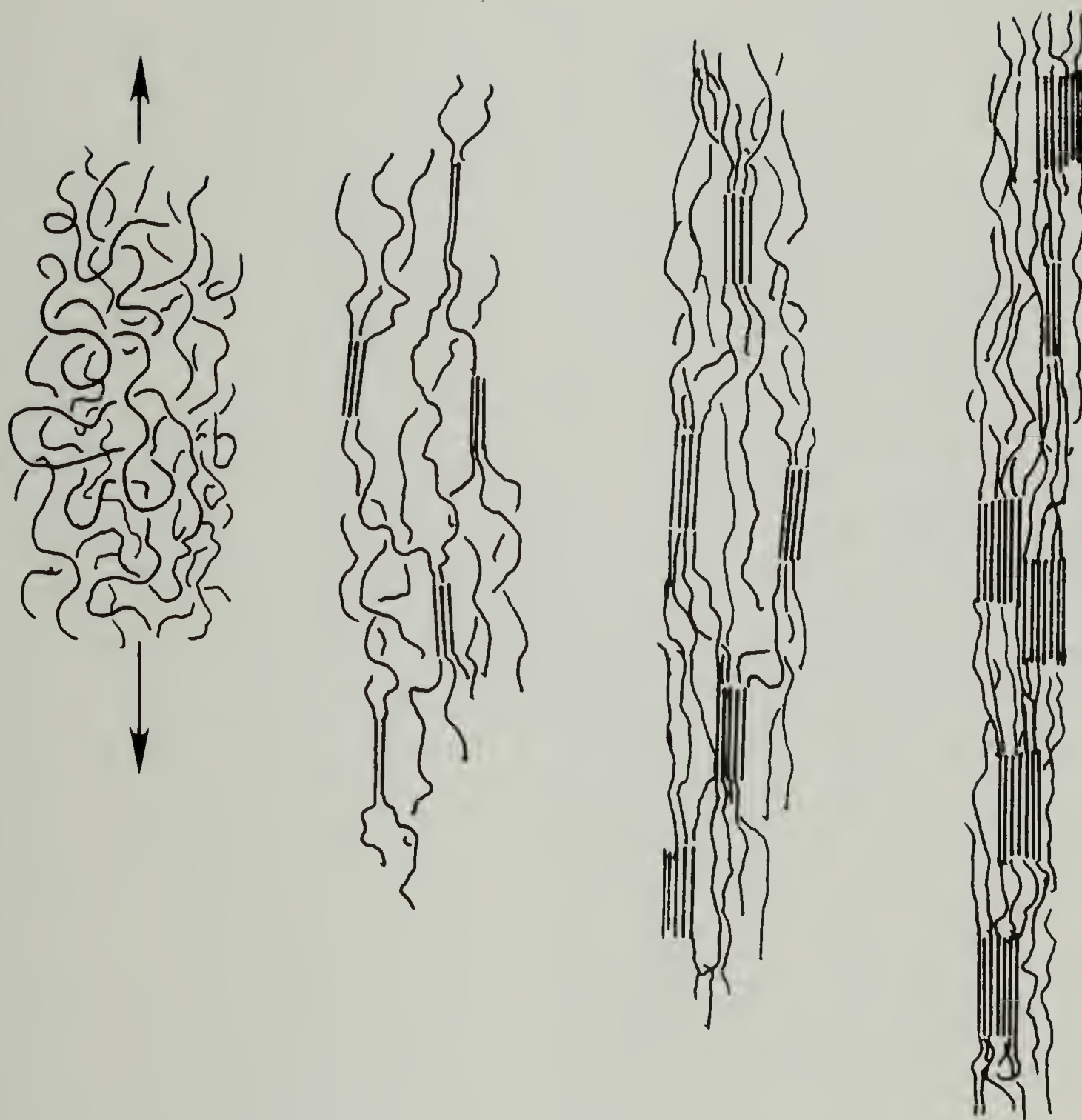


Figure 46. Model for Stress-Induced Crystallization Showing Crystallite Growth Perpendicular to Stretching Direction and Limited Axial Growth in the Direction of Stress

THERMOSTATIC MEASUREMENTS AND STRESS-STRAIN CURVES

The retractive force at various temperatures was measured for the polyurethane-urea elastomers which had been stretched at room temperature and held at constant length during cooling and subsequent heating at $5^{\circ}\text{C}/\text{min}$ between 210-450 K. These experiments were conducted to study the thermoelastic behavior and any thermal transitions which could occur at large static strains and high temperature where the heat engine operates most effectively.

Figures 47 and 48 show composite data for retractive stress versus temperature for the polyether and polyester soft-segment elastomers, respectively. Both sets of data are qualitatively similar, showing three definite regions of thermomechanical behavior- 1) the glassy region below about 220 K characterized by a negative force-temperature slope, 2) the rubbery region above 220 K having a positive force-temperature slope, and 3) the relaxation region where thermal softening occurs with an irreversible drop in stress. At high extension ratios (high stress) this thermal softening begins at or slightly below room temperature, while at an extension ratio of 1.5 thermal softening does not occur until 60 C.

The low temperature region below 220 K exhibits the positive thermal expansion coefficient characteristic of

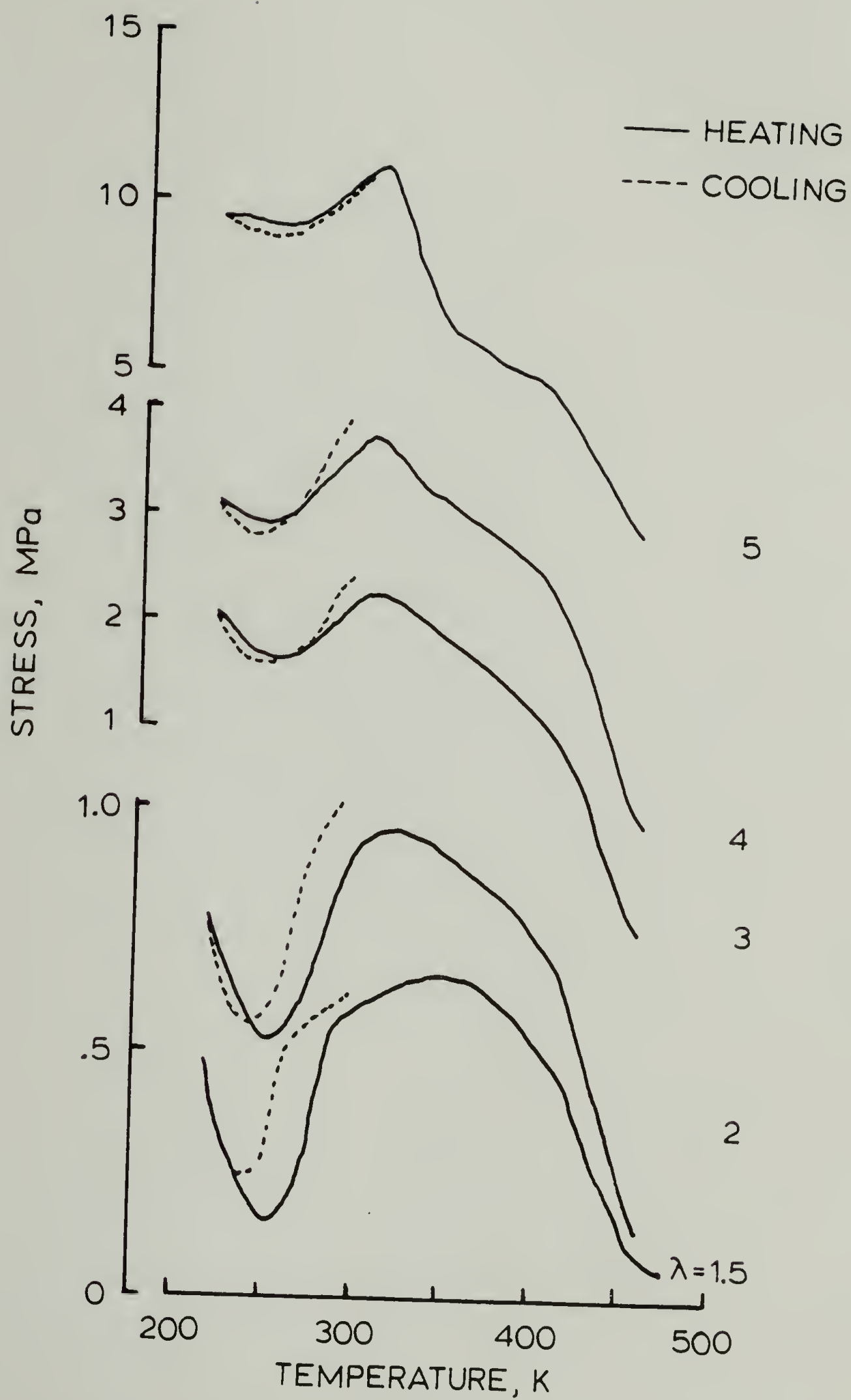


Figure 47. Stress versus Temperature Scans of Polyether Soft Segment Elastomer at Indicated Extension Ratios

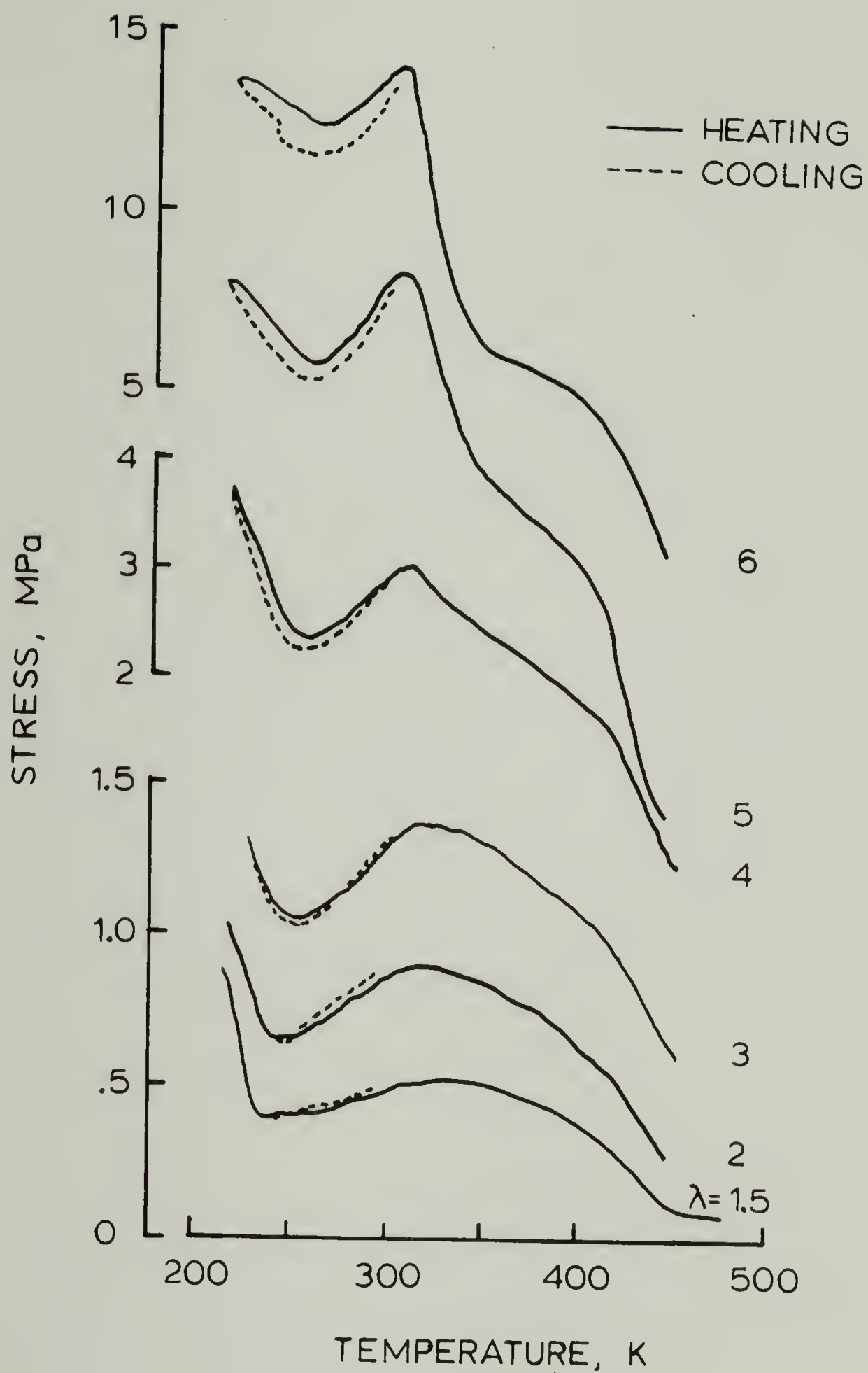


Figure 48. Stress versus Temperature Scans of Polyester Soft Segment Elastomer at Indicated Extension Ratios

the glassy state, resulting in a decrease in stress with increasing temperature. At the glass transition temperature the force-temperature slope changes sign due to the increased mobility of the extended rubbery soft-segment phase, which has a negative thermal expansion coefficient. Consequently this inflection temperature represents the glass transition temperature of the rubbery, soft-segment phase in the polymer.

The glass transition at about 210-220 K for the PTMO soft-segment elastomer is in good agreement with the stretch DSC data given in a previous section, but is somewhat higher than the value of 204 K reported for this polymer by Wang and Cooper (113) using dynamic mechanical analysis and DSC. A value of 185 K is reported for the pure PTMO polymer (114), suggesting some phase mixing.

Broadening of the low temperature transition from glassy to rubbery behavior in both polymers was suggested by the DSC data, which showed a decrease in sharpness of ΔC_p at the glass transition for high extension ratios. It is clear from the force-temperature data that this is due to the distribution of thermal events over a range of almost 25 C at high elongations, in contrast to the sharp change in slope for the isotropic unstretched material. Since these studies were performed, a commercial instrument has been reported for determining the glass transition temperature of stretched elastomers using force-

temperature measurements (115). Nose (116) and Wall (117) have studied the hysteresis in force-temperature curves caused by heating and cooling through the glass transition temperature of chemically crosslinked elastomers.

At temperatures above the glass transition temperature, a positive force-temperature slope is observed which is typical of stretched elastomers. The slope increases dramatically with increasing elongation. This positive force-temperature slope is reversible provided a certain maximum temperature is not exceeded—this temperature being determined by the stress on the elastomer. In particular, increasing stress lowers the softening temperature.

At temperatures between the stretching temperature (room temperature) and about 60 C, an irreversible drop in stress is noted on force-temperature curves, the onset of which decreases with increasing extension ratio. Cooling from temperatures above the softening temperature results in reversible force-temperature behavior at a lower stress level, provided the previous maximum temperature is not exceeded. Figure 49 shows a series of force-temperature cycles to increasingly higher maximum temperature for the polyether soft-segment elastomer at a fixed extension ratio of 4. Low temperature hysteresis increases while the mean stress drops with each successive cycle to higher temperature. The force-temperature slope at 292 K does

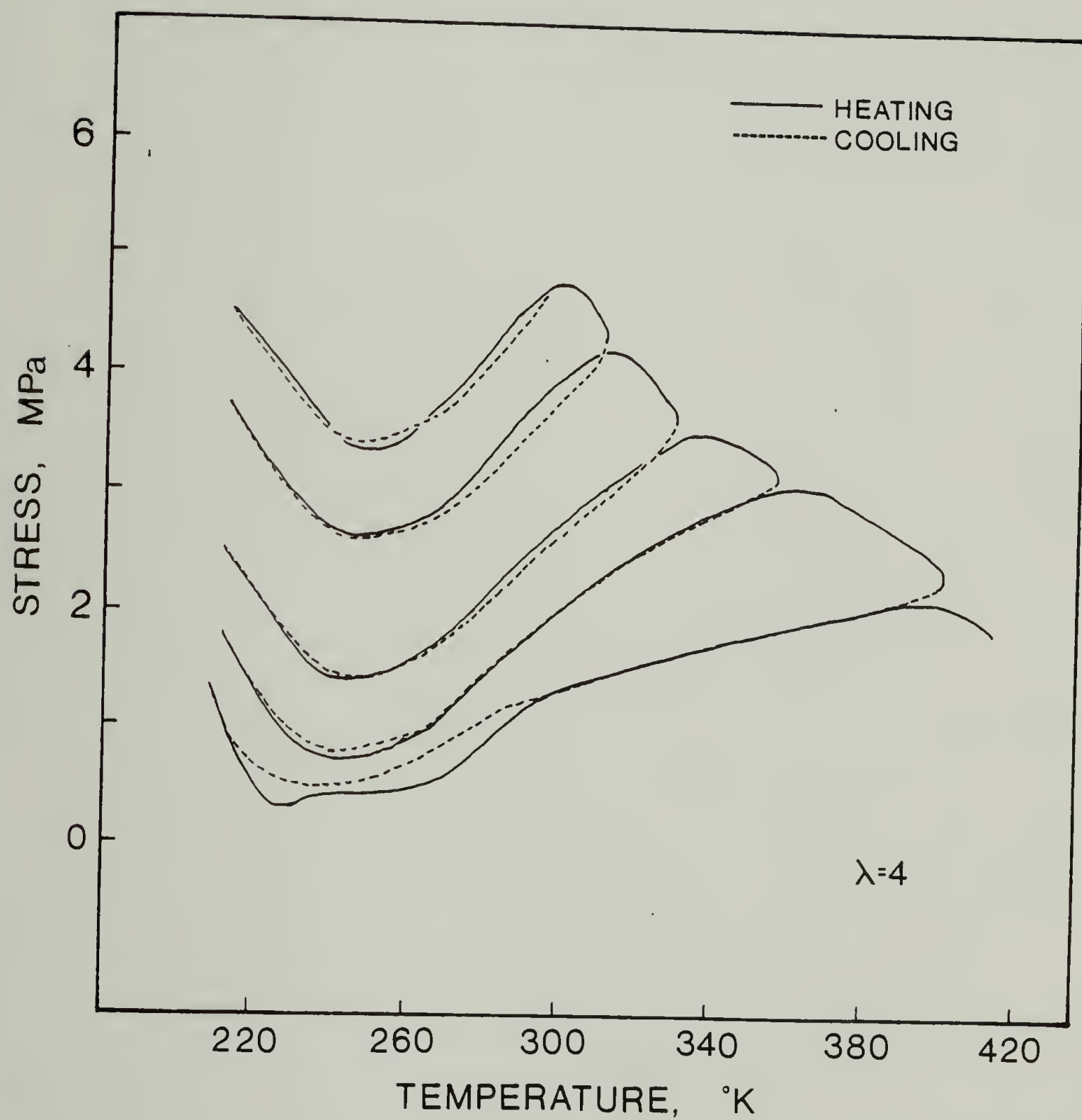


Figure 49. Stress versus Temperature Scans to Increasing Maximum Temperature for Polyether Soft Segment Elastomer at $\lambda = 4$

not change significantly until a maximum temperature of about 400 K is reached. However, the force-temperature slope above 292 K decreases steadily with each increasing maximum temperature, T_{\max} .

Morphological studies by Luch and Yeh (109) show evidence for irreversible melting of stress-induced crystallinity in natural rubber. Decandia, Russo, Vittoria and Peterlin (118) measured shrinkage and retractive forces in room temperature drawn low density polyethylene, and found the same irreversible stress drop, beginning at about 330K in polyethylene held at fixed length. These authors suggested that the crystalline structure generated during drawing was far from thermodynamic equilibrium and represents a frozen-in morphology which moves to a more stable state of lower free energy as soon as the constituent parts possess sufficient thermal energy to effect the change. Stein, Krimm and Tobolsky (119) in earlier studies of deformed polyethylene which was heated and cooled at fixed length, observed similar stress drops and postulated that increasing temperature released distortional energy stored in the crystalline regions. Subsequent cooling regenerated the crystalline structure at a lower level of internal energy, as suggested by reversible birefringence data during heating and cooling, regardless of the maximum temperature. Consequently, the energetic contribution to the stress, $(\partial U/\partial L)_{T,V}$ was seen to de-

crease with increasing T_{\max} .

Explanations of irreversible stress drops in stretched crystalline polymers by deCandia and Stein are seen to be equivalent in that non-equilibrium effects are attributed to thermally induced irreversible processes in highly stressed crystalline regions. The situation becomes considerably more complicated in the segmented elastomers of this study because a certain amount of crystalline or glassy structure is sure to exist in the hard segment phase, in addition to the stress-induced crystallinity which accompanies deformation.

Evidence for hard segment yielding comes from thermomechanical analysis by Schneider and Sung (120), which shows a distribution of hard segment glass transition temperatures ranging from 20-60 C in unstrained TDI/BDO hard segment, PTMO soft-segment polyurethanes. During the current investigations, force-temperature studies of MDI/BDO hard segment elastomers with non-crystallizable poly(propylene-oxide) soft segments, as well as terephthalic acid/ethylene glycol hard segment/PTMO 2000 soft-segment both showed the same thermally induced softening and yielding observed in the present polyurethane-urea elastomers, suggesting that the hard segments may be the primary yielding structures at low strain, but at higher elongations the secondary network resulting from stress-induced crystallization undoubtedly

plays a role.

The final feature of the force-temperature curves for the polyurethane-ureas is the complete loss of structural integrity beginning at about 423 K for both elastomers. This is associated with a flow process due to melting of the hard segments, since irreversible permanent set increases dramatically at this temperature. Ishihara, et.al. (121) studying PTMO soft-segment polyurethane-ureas with 40% MDI/ppropylene diamine hard segments have shown that complete scission of interurea and interurethane hydrogen bonding occurs in the hard segments at these temperatures, although true melting does not occur until about 450 K. Wang and Cooper (113) studying polyurethane-ureas identical to the PTMO soft-segment elastomer of this study, have shown that the storage modulus in dynamic mechanical analysis begins to drop off at about 420 K, which they attribute to melting at that temperature. This value agrees with the observed flow temperature of the polyurethane-ureas of the present study in force-temperature curves.

Stress-strain loading curves for the polyurethane-urea elastomers are shown in Figures 50 and 51 for the PTMO and polyester soft-segment materials, respectively. A strain rate of 100 % /min was used to obtain the loading curves at 22, 40, 60, 80 and 125 C. It is clear that the stress at a particular level of strain decreases with

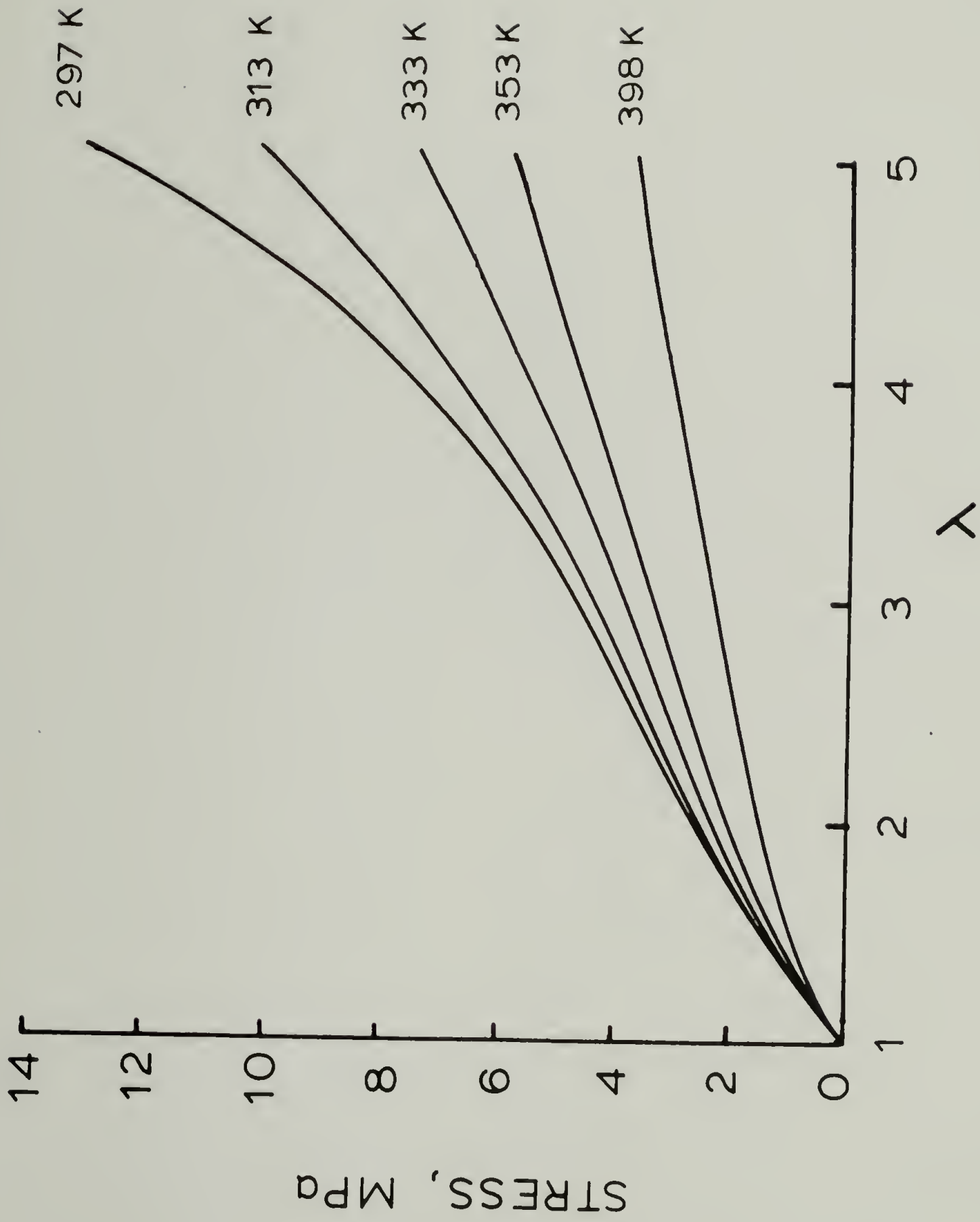


Figure 50. Stress-Strain Loading Curves for Polyether Soft Segment Elastomer at Indicated Temperatures

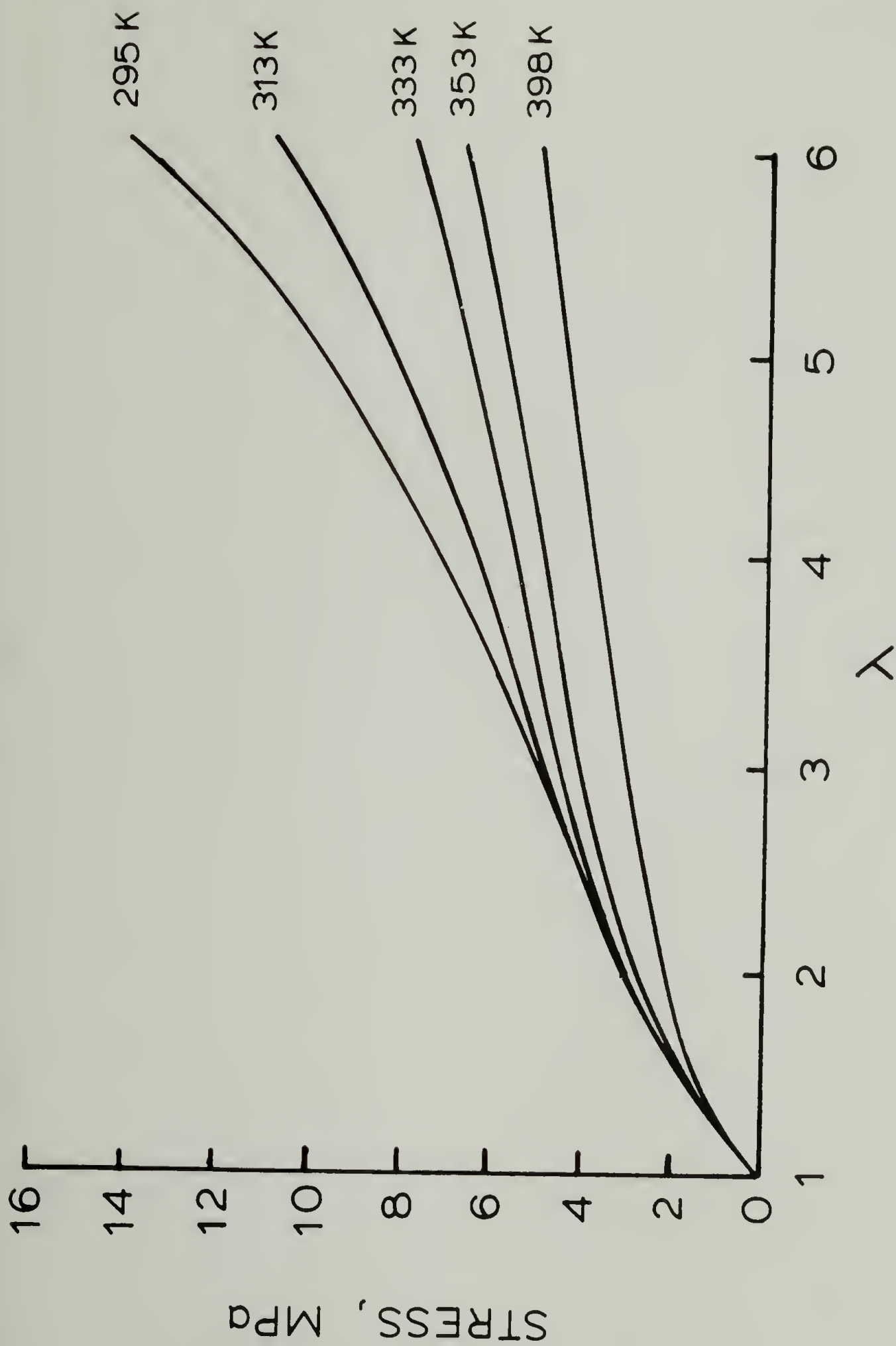


Figure 51. Stress-Strain Loading Curves for Polyester Soft Segment Elastomer at Indicated Temperatures

increasing temperature, i.e thermal softening is observed. This is in contrast to ideal rubber behavior, where increasing temperature increases the modulus of the elastomer. Thermally-induced yielding of the hard segments and the reduced tendency to stress-crystallize at higher temperatures both contribute to softening of the stress-strain curves with increasing test temperature.

A static loading/ unloading curve for natural rubber at 292 K is shown in Figure 52 . This curve was obtained over a period of 48 hours with at least one hour allowed at each elongation for mechanical equilibrium to be achieved, as deduced from the time-independent stress. Also plotted on this curve are values of stress obtained by stretching the natural rubber at 350 K, and slowly cooling back to room temperature. These experiments, which were only performed for the strain region where stress-induced crystallization is known to occur, show that significantly lower stresses are achieved in this way compared to the process of stretching isothermally at room temperature. In fact, the stress appears to be almost invariant during the crystallization region. Consequently, the previous suggestion that thermally-induced crystallization represents an approach to thermodynamic equilibrium, while stress-induced crystallization proceeds by a kinetically favored high energy route, appears to be substantiated by the mechanical data.

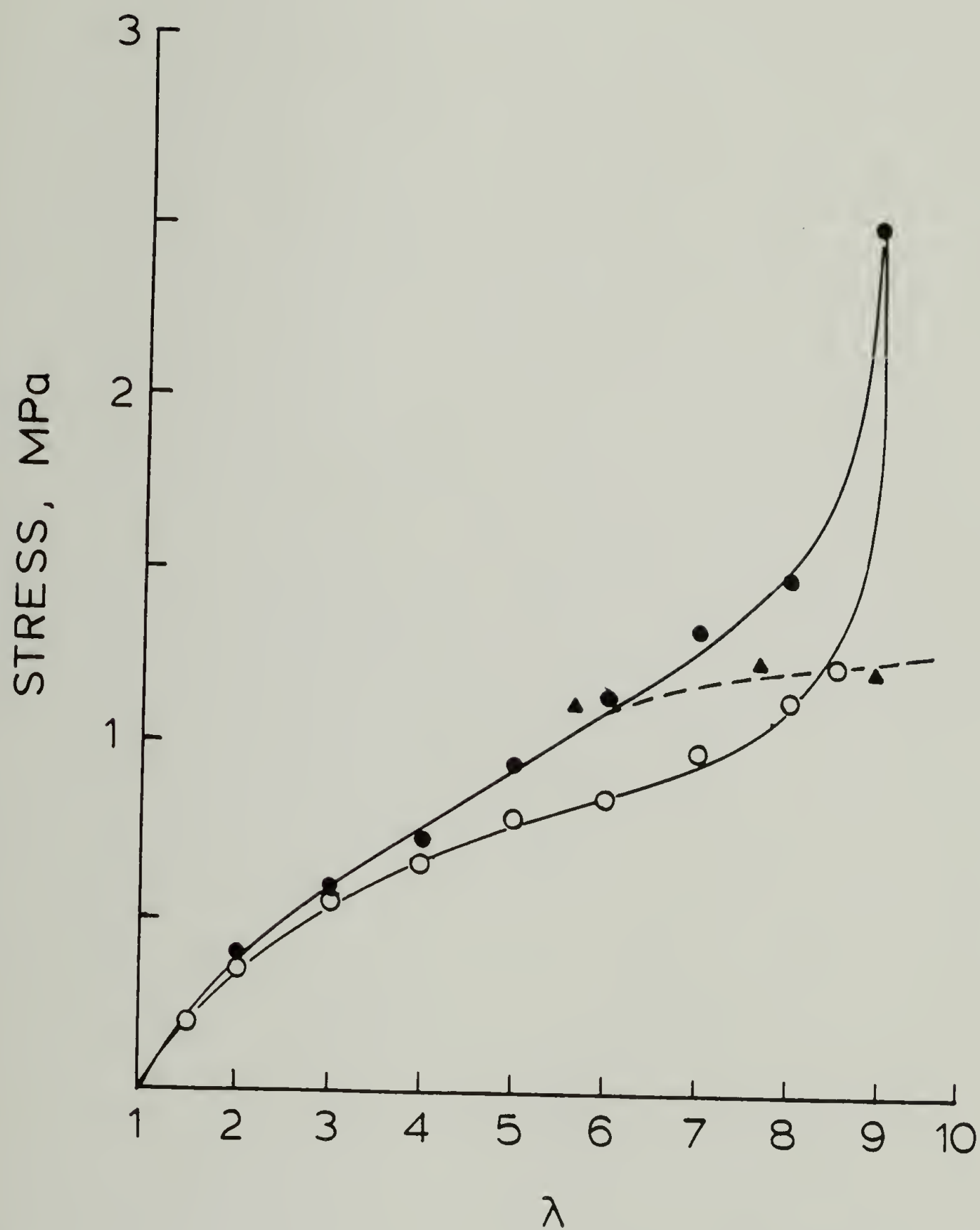


Figure 52. Static Stress versus Extension Ratio for Natural Rubber; Loading at 292 K (solid circles); Unloading at 292 K (open circles); Loading at 350 K and Cooling to 292 K (solid triangles)

HEAT ENGINE CYCLES OF POLYURETHANE-UREA ELASTOMERS

Heat engine cycles were performed using the two polyurethane-urea elastomers as working substances according to the method described in the experimental section. Values of the available work per cycle per gram of elastomer in units of J/g, are given in Table 8 for the PTMO soft-segment elastomer, and in Table 9 for the mixed polyester soft-segment material. The sign convention used for this data is that positive values represent work done by the elastomer on the surroundings during one complete cycle (as would be required in a heat engine), whereas negative values mean that the surroundings, i.e. the Instron, had to do work on the elastomer in order to complete the cycle under the given conditions.

A general trend in the data of both elastomers is that the maximum work per cycle (1 J/g) is obtained at small strain perturbations on top of large static strains at a maximum temperature of 100 C. Above this temperature there is a decrease in available work due to the enhanced flow process accompanying partial melting of the hard segments as observed in force-temperature studies, which effectively lowers the mean stress.

The effect of mean strain level and strain-perturbation on the available work at 100 C is shown most clearly

Table 8

Polyether Soft Segment Elastomer

λ_{\min}	λ_{\max}	T_{L0}	T_{HI}	W_c	T_{HI}	W_c	T_{HI}	W_c	T_{HI}	W_c	T_{HI}	W_c	T_{HI}	W_c	T_{HI}	W_c
2.0	2.5	10	40	0.25	60	0.25	80	0.31	100	0.21	120	—	—	—	—	—
2.0	3.0	10	40	0.13	60	0.29	80	0.25	100	0.22	120	—	—	—	—	—
2.0	3.5	10	40	-0.26	60	-0.17	80	0.03	100	0.07	120	—	—	—	—	—
2.0	4.0	10	40	-1.00	60	-0.45	80	-0.15	100	-0.59	120	—	—	—	—	—
2.0	4.5	10	40	-1.94	60	-1.61	80	-1.5	100	-1.60	120	—	—	—	—	—
2.0	5.0	10	40	-2.45	60	-2.88	80	-3.07	100	-2.60	120	—	—	—	—	—
2.5	3.0	10	40	0.34	60	0.37	80	0.42	100	0.41	120	—	—	—	—	—
2.5	3.5	10	40	0.33	60	0.30	80	0.57	100	0.57	120	—	—	—	—	—
2.5	4.0	10	40	-0.20	60	-0.08	80	-0.08	100	0.36	120	—	—	—	—	—
2.5	4.5	10	40	-1.03	60	-0.56	80	-0.17	100	0	120	—	—	—	—	—
2.5	5.0	10	40	-2.10	60	-1.40	80	-1.70	100	-0.47	120	—	—	—	—	—
3.0	3.5	10	40	0.36	60	0.49	80	0.51	100	0.48	120	—	—	—	—	—
3.0	4.0	10	40	0.10	60	0.50	80	0.57	100	0.72	120	—	—	—	—	—
3.0	4.5	10	40	-0.16	60	0.12	80	0.40	100	0.68	120	—	—	—	—	—
3.0	5.0	10	40	-0.92	60	-0.97	80	-1.01	100	0.27	120	—	—	—	—	—
3.5	4.0	10	40	0.37	60	0.55	80	0.62	100	0.51	120	—	—	—	—	—
3.5	4.5	10	40	0.14	60	0.48	80	0.76	100	0.81	120	—	—	—	—	—
3.5	5.0	10	40	-0.97	60	-0.54	80	-0.11	100	0.62	120	—	—	—	—	—
4.0	4.5	10	40	0.41	60	0.62	80	0.72	100	0.62	120	—	—	—	—	—
4.0	5.0	10	40	0.15	60	0.38	80	0.84	100	0.93	120	—	—	—	—	—
4.5	5.0	10	40	0.50	60	0.66	80	0.71	100	0.80	120	—	—	—	—	—

All values in Joules/gram elastomer

Table 9

Polyester Soft Segment Elastomer

λ_{\min}	λ_{\max}	T_{L0}	T_{H1}	W_c	T_{H1}	W_c	T_{H1}	W_c	T_{H1}	W_c	T_{H1}	W_c	T_{H1}	W_c
2.0	2.5	10	40	0.14	60	0.17	80	0.10	100	0.09	120	—	—	—
2.0	3.0	10	40	0.24	60	0.27	80	0.21	100	0.09	120	—	—	—
2.0	3.5	10	40	0.26	60	0.19	80	0.26	100	0.01	120	—	—	—
2.0	4.0	10	40	-0.06	60	0.16	80	-0.07	100	0.07	120	—	—	—
2.0	4.5	10	40	-0.90	60	0.16	80	0.23	100	-0.38	120	—	—	—
2.0	5.0	10	40	-0.51	60	-0.42	80	-0.19	100	-0.68	120	—	—	—
2.0	5.5	10	40	-2.50	60	-1.30	80	-0.80	100	-0.74	120	—	—	—
2.0	6.0	10	40	-2.81	60	-3.54	80	-1.33	100	—	120	—	—	—
2.5	3.0	10	40	0.25	60	0.21	80	0.23	100	0.12	120	—	—	—
2.5	3.5	10	40	0.38	60	0.38	80	0.30	100	0.26	120	—	—	—
2.5	4.0	10	40	0.34	60	0.38	80	0.53	100	0.31	120	—	—	—
2.5	4.5	10	40	0.21	60	0.35	80	0.34	100	0.18	120	—	—	—
2.5	5.0	10	40	-0.16	60	0.03	80	0.27	100	0.08	120	—	—	-0.09
2.5	5.5	10	40	-2.00	60	-0.44	80	-0.06	100	-0.22	120	—	—	-0.11
2.5	6.0	10	40	-2.60	60	-1.65	80	-0.36	100	-0.43	120	—	—	-0.50
3.0	3.5	10	40	0.28	60	0.26	80	0.28	100	0.24	120	—	—	—
3.0	4.0	10	40	0.39	60	0.45	80	0.35	100	0.37	120	—	—	0.13
3.0	4.5	10	40	0.21	60	0.68	80	0.63	100	0.27	120	—	—	0.20
3.0	5.0	10	40	0.11	60	0.29	80	0.68	100	0.55	120	—	—	0.13
3.0	5.5	10	40	-1.20	60	0.36	80	0.31	100	0.47	120	—	—	0.06
3.0	6.0	10	40	-2.34	60	-1.0	80	0.14	100	0.23	120	—	—	-0.07
3.5	4.0	10	40	0.28	60	0.35	80	0.32	100	0.27	120	—	—	0.24
3.5	4.5	10	40	0.39	60	0.60	80	0.64	100	0.32	120	—	—	0.24
3.5	5.0	10	40	0.29	60	0.70	80	0.73	100	0.51	120	—	—	0.45
3.5	5.5	10	40	-1.20	60	0.19	80	0.71	100	0.65	120	—	—	0.53
3.5	6.0	10	40	-2.30	60	-1.30	80	0.54	100	0.65	120	—	—	0.55
4.0	4.5	10	40	0.26	60	0.33	80	0.39	100	0.19	120	—	—	0.21
4.0	5.0	10	40	0.50	60	0.61	80	0.61	100	0.53	120	—	—	0.37
4.0	5.5	10	40	-0.66	60	0.42	80	0.62	100	0.72	120	—	—	0.55
4.0	6.0	10	40	-1.50	60	-0.71	80	0.72	100	0.98	120	—	—	0.81
4.5	5.0	10	40	0.30	60	0.47	80	0.42	100	0.34	120	—	—	0.24
4.5	5.5	10	40	-0.36	60	0.33	80	0.68	100	0.66	120	—	—	0.46
4.5	6.0	10	40	-1.10	60	-0.82	80	0.68	100	0.76	120	—	—	0.65
5.0	5.5	10	40	0.20	60	0.31	80	0.41	100	0.45	120	—	—	0.39
5.0	6.0	10	40	-0.21	60	0.34	80	0.61	100	0.70	120	—	—	0.61
5.5	6.0	10	40	0.04	60	0.32	80	0.48	100	0.49	120	—	—	0.36

All values in Joules/gram elastomer

by constructing an energy contour map of the work per cycle, W_c , against the minimum λ_{\min} , and maximum λ_{\max} extension ratio for the cycle. This type of plot is shown in Figure 53 for the polyester soft-segment elastomer at the optimum high temperature of 100 C.

It is seen that negative or dissipative power cycles are observed at large strain perturbations, which occur along the lower horizontals of the contour map. The maximum work/cycle is obtained in a small region in the upper right corner, corresponding to small strain perturbations on top of large static strains.

Graphical recordings of the heat engine cycles for the polyether soft-segment elastomer at a fixed temperature differential of 50 K are shown in Figure 54. The cycles have been vertically shifted for clarity, and illustrate the complex thermomechanical behavior of this elastomer at large strain perturbations. Arrows in the figure indicate the direction of the process with time. Useful work is obtained from the elastomer in counter-clockwise processes, whereas clockwise cycles or portions of cycles indicate that the Instron is doing work on the elastomer. It is seen that a transition from net mechanical loss to net mechanical gain during a cycle occurs with decreasing strain perturbation at fixed temperature differential.

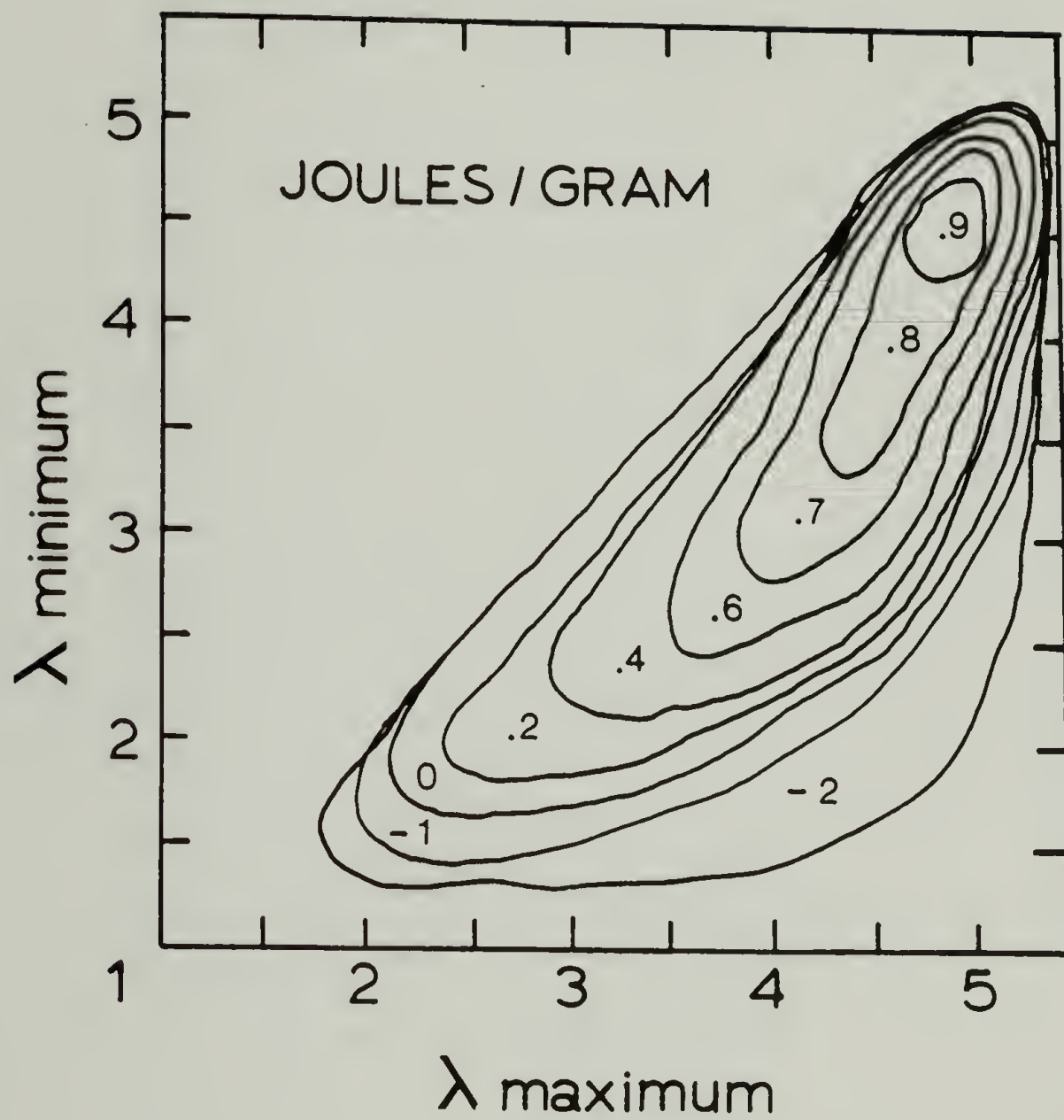


Figure 53. Power Contour Map for Polyester Soft Segment Elastomer for $\Delta T = 90^\circ\text{K}$

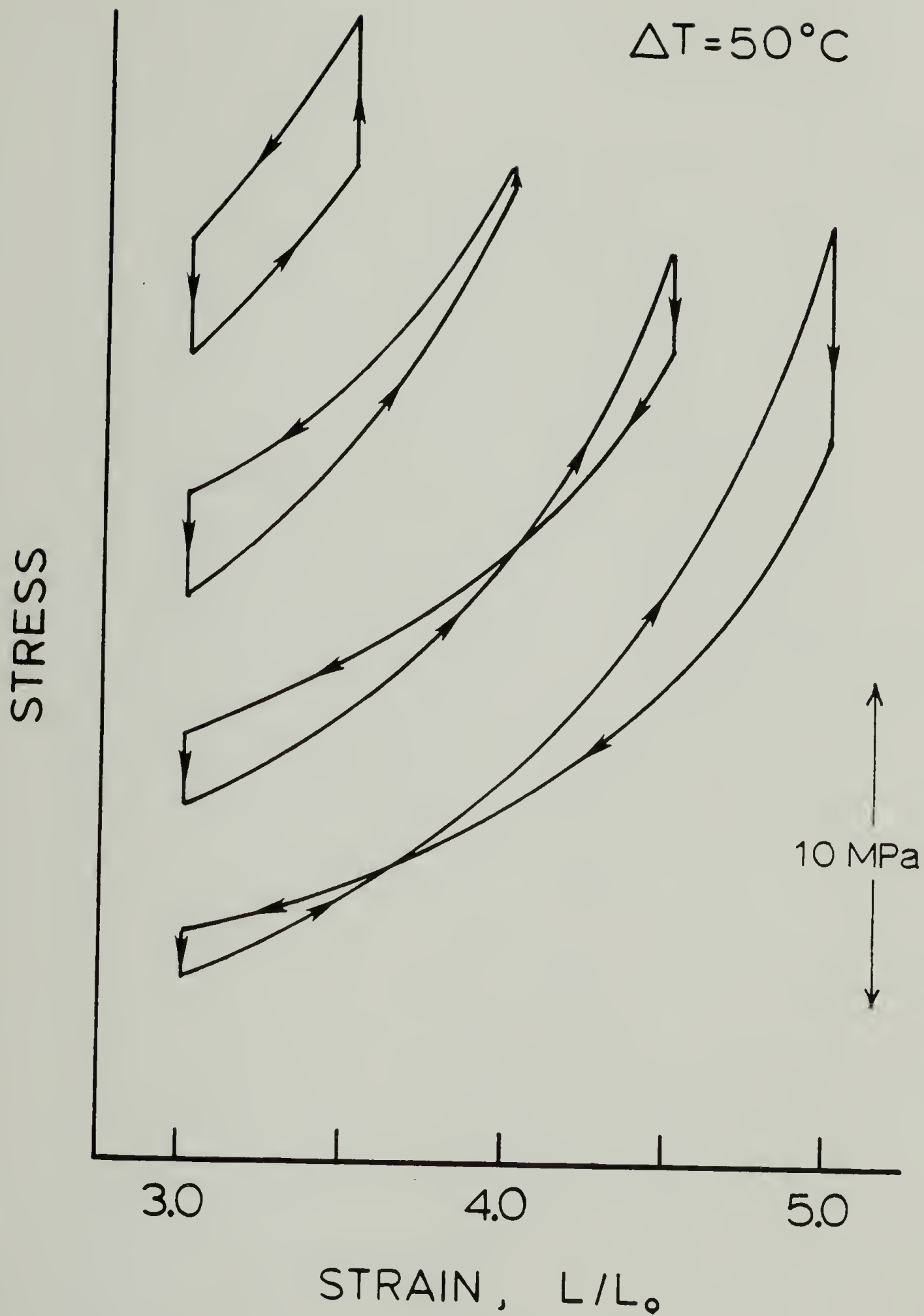


Figure 54. Power Cycles of Polyether Soft Segment Elastomer at Fixed ΔT and Various Strain Perturbation (Data Vertically Shifted for Clarity)

The dissipative figure-8 cycles at large maximum extension reflect the hysteresis normally observed in this elastomer during isothermal stress-strain cycles, and can be directly related to the process of crystallization during stretching (SIC). Heating to 330 K at the maximum strain does not cause an increase in stress, but instead results in a stress drop as the metastable load bearing SIC network is melted out, as observed in the force-temperature studies. Consequently, the unloading curve, although at higher temperature, is along a path of lower stress and lower crystallinity resulting in a net loss of mechanical energy for the cycle. Decreasing the strain perturbation at constant temperature differential reduces the amount of SIC which can be generated during stretching while leaving TIC relatively unaffected, since the latter depends only on the minimum and maximum temperature of the cycle as indicated by DSC. The low and high temperatures of 283 K and 333 K used for these cycles bracket the melting range of thermally-induced crystallization in DSC thermograms, so that at small strain perturbations at large static strains, reversible thermally-induced melting and crystallization during the isomechanical portions of the cycle can be utilized to increase the available work per cycle.

The effect of changing the temperature differential at fixed strain perturbation on the heat engine cycles of

the polyester soft-segment elastomer is shown in Figure 55. In this figure the elastomer is cycled between $\lambda = 5$ and $\lambda = 6$ at $T_{hi} = 40, 60, 80$ and 100 C. The same transition from dissipative to available work/cycle is seen to occur with increasing T_{hi} as was observed for decreasing strain perturbation. Again, this can be linked to SIC which was shown to melt irreversibly in DSC thermograms. Increasing the maximum cycle temperature at fixed maximum strain has the effect of permanently eliminating successively greater amounts of the high melting SIC during the first excursion to T_{hi} , with a concomitant increase in TIC which forms in its absence and melts and crystallizes reversibly in subsequent cycles.

The preliminary conclusion based on these observations and the tabulated data is that hysteresis or mechanical losses which detract from the available work/cycle can be suppressed by high maximum cycle temperatures and/or decreasing strain perturbation.

The decrease in cycle work at large strain perturbations where SIC is forming during the mechanical portions of the cycle is in contrast to that which would be expected for an enthalpy cycle in which oriented crystallization and melting could occur in a reversible manner. Mandelkern (6) has discussed the possibility of using an enthalpy cycle for elastomers in heat engine applications, wherein the elastomer is made to undergo

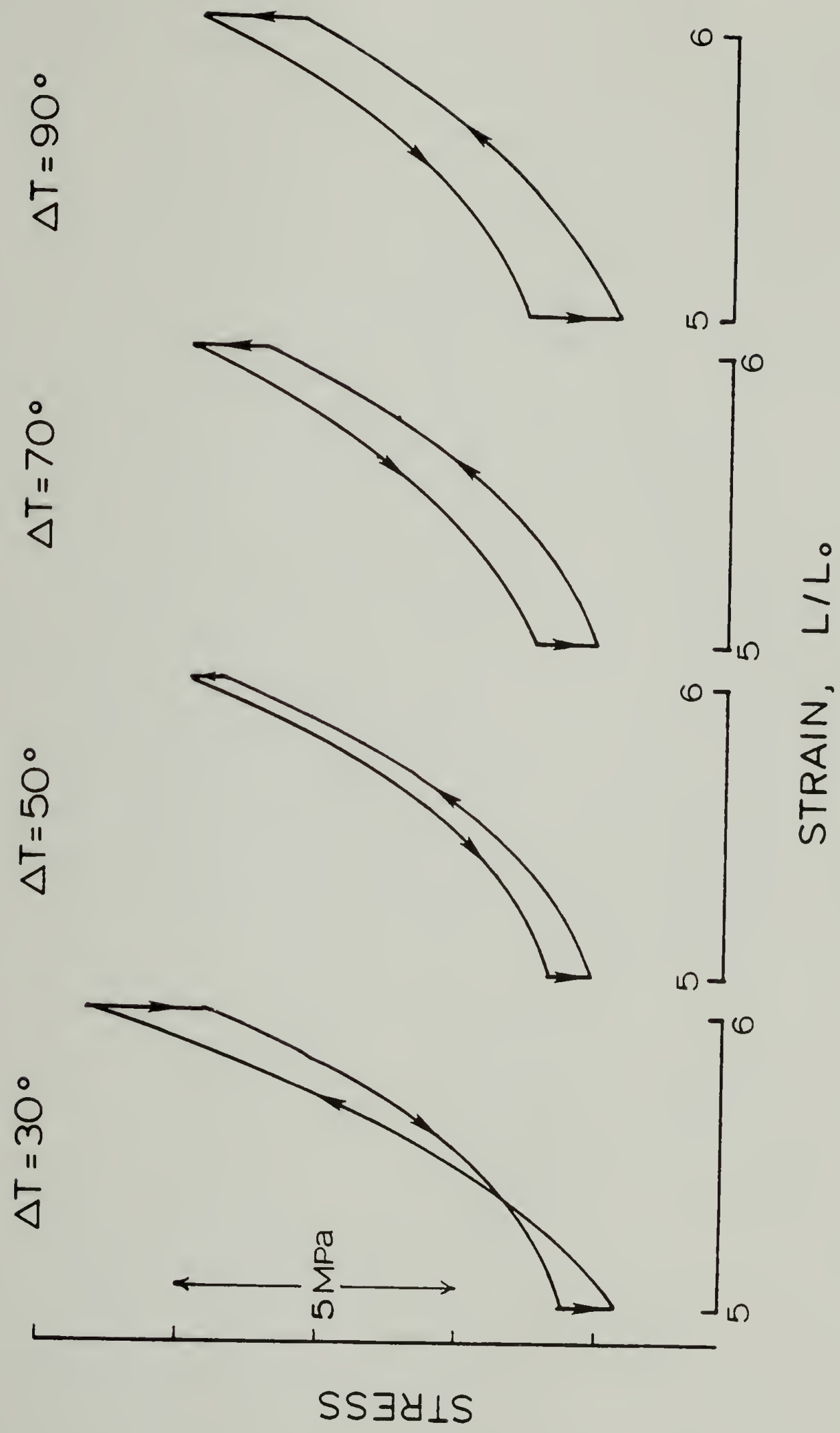


Figure 55. Power Cycles of Polyester Soft Segment Elastomer at Fixed Strain Perturbation and Various ΔT

reversible crystallization and melting during the isothermal mechanical processes of a Carnot cycle. The advantage of such a cycle derives from the decrease in stress expected to accompany equilibrium, oriented crystallization during the low temperature mechanical stroke, and the proportionally large stress rise during melting at fixed length. The results of this and numerous other studies (4,76,83,85) show however, that the simultaneous processes of crystallization and stretching are mutually incompatible with regard to the attainment of equilibrium. The cycle envisioned by Mandelkern is therefore difficult to achieve in practice.

An enthalpy cycle could of course be constructed by a series of processes whereby the elastomer is heated, stretched and cooled to T_{10} at a particular level of strain in order to achieve true equilibrium between the crystalline and amorphous phases. Repeating this succession of steps over the strain perturbation of interest, between the appropriate high and low temperatures would undoubtedly yield more useful work than the same cycle conducted reversibly for a non-crystallizable elastomer. This is shown graphically in Figure 56 where is plotted isothermal stress-strain curves for the polyester soft-segment elastomer at $T_{10} = 292$ K and $T_{hi} = 382$ K, calculated from the ideal rubber equation of state using the measured shear modulus of this elastomer. Also plotted is the

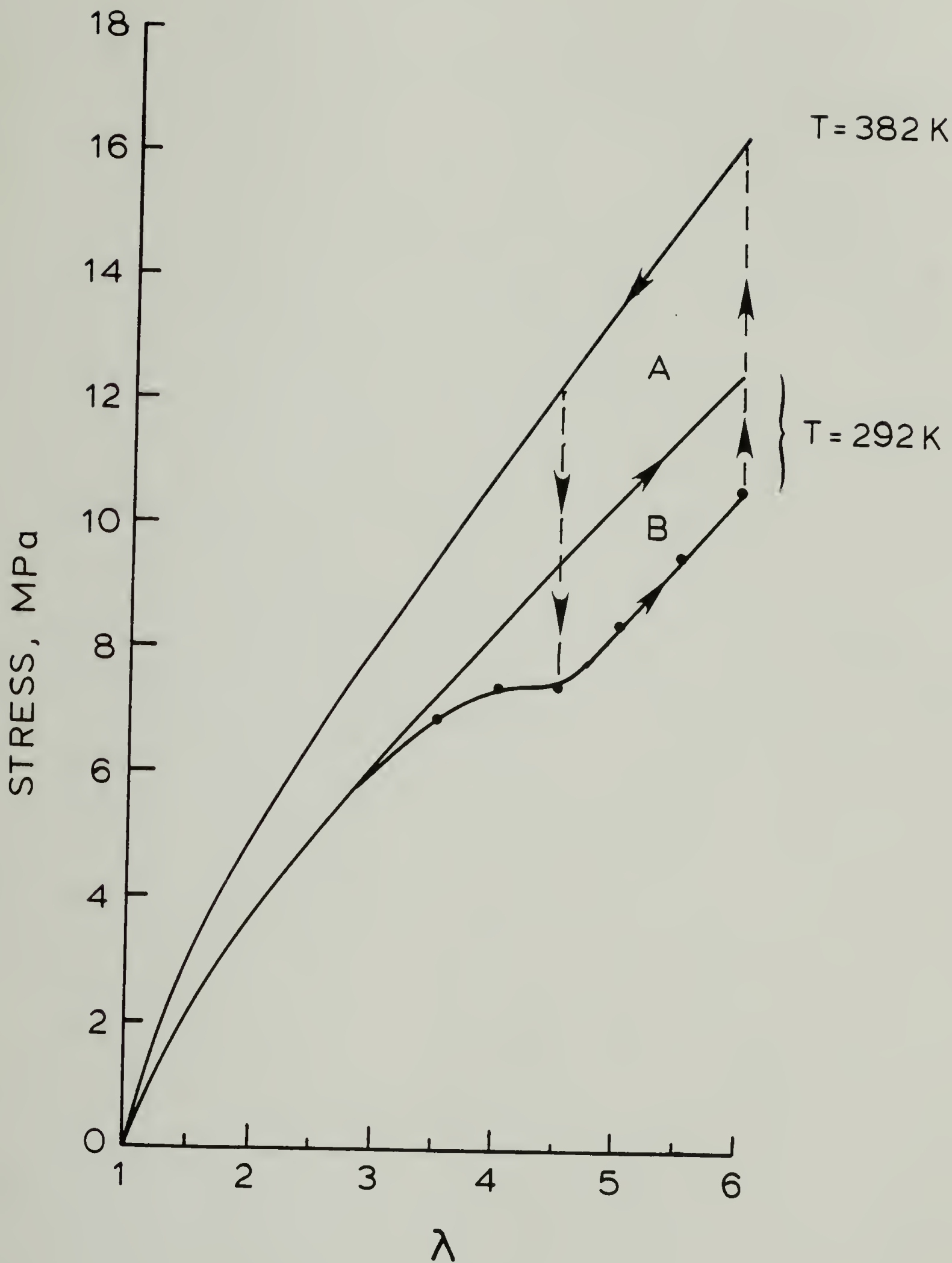


Figure 56. Stress-Strain Curves Calculated for Polyester Soft Segment Elastomer at 292K and 382K Using Ideal Rubber Equation of State. Lower Curve (solid circles) at 292K Calculated Using Flory's Theory(Ref.8) and Measured Crystallinity.

equilibrium stress-strain curve for a crystallizable elastomer calculated using Flory's (8) theory and the measured degree of crystallinity obtained from deformation calorimetry data using a heat of fusion of 104 J/g elastomer. It is clear from this figure that if crystallization could occur in an equilibrium manner so as to decrease the stress during the stretching process, significantly more work per cycle could be obtained between extension ratios of 4.5 and 6 for the given temperature difference.

In reality, stress-induced crystallization proceeds via a kinetically determined high energy route, so that the optimum situation appears to be the minimization of SIC during the mechanical portions of the cycle, and the utilization of essentially strain-independent TIC during the change in temperature at constant strain.

Wiegand and Snyder (5) were the first to consider using rubber as a working substance in a heat engine. These authors constructed two operating heat engines which demonstrated that useful work could be obtained from natural rubber in such devices. In characterizing the thermomechanical properties of rubber, Wiegand and Snyder constructed pseudo-power cycles by superimposing isothermal stress-strain perturbation curves at 24 and 75C for a change in strain of 100%. The samples were severely worked at each temperature and strain to achieve a degree of reversibility. The results, in conjunction with stress

and temperature values taken from the same data which were used to calculate $(\delta U / \delta L)_{T,P}$, indicated that under the conditions of these experiments the most work per cycle could be obtained in the region of strain where $(\delta U / \delta L)_{T,P}$ was at a minimum, i.e. the rate of change of crystallinity with strain was at a maximum. This is in contrast to the results of the present study which showed that changing stress-induced crystallinity during stretching reduces the available work per cycle due to the non-equilibrium nature of the process. The discrepancy is due to the way in which Wiegand and Snyder constructed the hypothetical power cycles. The samples were severely worked by performing 5-6 loading / unloading cycles at the low temperature (the stress decreasing with each cycle) before reproducible curves were shown. Deformation calorimetry studies reported in a previous section of this study, showed that preworking a sample over a particular strain interval at room temperature could remove any non-equilibrium effects, and in particular result in melting and recrystallization into a thermodynamically stable structure as evidenced by the absence of stress-temperature yielding (not reported). Consequently, the conclusions of Wiegand and Snyder connecting SIC to the enhanced performance of natural rubber in heat engine cycles was correct for the ideal case in which crystallinity could be reduced to its equilibrium configuration by preworking (or premelting) at the low

temperature of the cycle. Unfortunately, real cycles traverse a deformation state at a particular temperature only one time, so that the subsequent portions of the cycle reflect the history of events that occur during the single (non-equilibrium) loading process.

In addition to the type of heat engines envisioned by Wiegand and Snyder and later improved upon by Farris (7), heat engines have been developed using contractile polymers as working substances. Contractile polymers are those such as natural rubber (122) and polyethylene (123) which can be crosslinked in the extended state and undergo small reversible dimensional changes on melting and recrystallization of the oriented network. These reversible dimensional changes occur in the absence of an applied load, but can be harnessed to do useful work by attaching the polymer to a lever arm, as was done by Mandelkern (124). Contractile polymers used in such a device operate purely on an enthalpy cycle, the high and low temperatures of the cycle being determined by the melting and crystallization temperatures of the polymer. The magnitude of the work obtainable from these devices is estimated to be on the order of .1 J/g by Mandelkern. This is about an order of magnitude less than the cycles used in this study which combine elements of both an entropy and enthalpy cycle.

Since the first law of thermodynamics places no restrictions on the type of material that can be used in a heat engine, provided it can traverse a complete cycle and return to the initial state, it is worthwhile to estimate the potential of a non-rubbery material such as steel in such a device. This can be done most easily in the temperature-entropy plane. For a reversible entropy cycle in which the internal energy change over the cycle is zero, the work per cycle is simply

$$W_c = \oint dW = \oint dQ = - (T_{hi} - T_{lo}) \Delta S$$

where ΔS is the reversible entropy change during an isothermal portion of the cycle. From equations derived in the Theory section, the entropy change for tensile deformation of steel at constant temperature between zero strain and the breaking strain of .001, is approximately $\Delta S = E \alpha \epsilon = (10^{11} \text{ Pa})(10^{-6} / \text{K})(.001)(10^{-6} \text{ M}^3 / \text{cc}) = 10^{-4} \text{ J/cc-K}$. For a temperature difference of 100 K, with the requirement that loading take place at T_{hi} and unloading at T_{lo} due to the positive entropy of loading, the work per cycle is $W_c = (100 \text{ K})(10^{-4} \text{ J/cc-K}) = .01 \text{ J/cc}$. For rubber with a breaking extension of 10, from the ideal rubber equation of state and the same temperature difference the work per cycle is 16 J/cc, or approximately 1000 times greater than steel. This reflects the fact that rubber stores and

releases large amounts of mechanical energy as (configurational) entropy, while entropy changes in hard elastic solids are exceedingly small and result solely from volume dilatation.

The power density, P , for a rubber heat engine turning typically at 100 RPM (125,126) using the polyurethane-urea elastomers in this study under optimum conditions is

$$P = 1 \text{ J/g} \times 1000 \text{ g/Kg} \times 100 \text{ RPM} \times 1/60 \text{ min/sec}$$

$$= 1.7 \text{ Kilowatts/Kg elastomer}$$

The efficiency, η , is just W_c / Q_{in} . For the cycle of Figure 18 with a temperature difference of 100 K, $Q_{23} = C_p \Delta T$, and with Q_{34} estimated from deformation calorimetry-

$$\eta = \frac{W_c}{Q_{23} + Q_{34}} = \frac{1 \text{ J/g}}{(1.6 \text{ J/g})(100 \text{ K}) + (10 \text{ J/g})} = .06$$

which is about 3% of Carnot efficiency for the same temperature difference. This is typical of heat engines used for converting low grade heat as would be obtained from waste heat reclamation or environmental sources such as solar, geothermal or ocean thermal.

C H A P T E R V

CONCLUSIONS

Deformation Calorimetry as a Tool for Studying Polymer Deformation Processes

The new deformation calorimeter which has been developed provides a sensitive and reliable means of simultaneously measuring the heat and work of polymer deformations. The internal energy change in the material can then be determined by difference according to the first law of thermodynamics. The high sensitivity and low detection limit of this instrument allows for deformations to be conducted essentially isothermally, since temperature changes of only 10^{-6} K in the solid are required to produce a detectable heat flow in the instrument during deformation. Under isothermal, reversible conditions the entropy change is directly related to the heat flow according to the second law of thermodynamics.

In contrast to the condition of reversibility imposed on thermostatic measurements, deformation calorimetry provides a complete energy balance, regardless of whether the deformation proceeds via an equilibrium or non-equilibrium process. This facilitates a thermodynamic analysis of many polymer deformation processes which are inherently

non-equilibrium such as yielding or necking, viscoelastic phenomenon and stress-induced crystallization. Models for the deformation mechanisms of these processes should conform to the measured thermal, mechanical and internal energies obtained by deformation calorimetry.

Internal Energy Changes and Stress-Induced Crystallization in Polyurethane-urea Elastomers and Natural Rubber

Data from WAXS, stretch DSC and deformation calorimetry are in good qualitative agreement with regard to the onset and magnitude of stress-induced crystallinity in the polyurethane-urea elastomers and natural rubber. It has been assumed throughout this thesis that internal energy changes measured by deformation calorimetry are proportional to the degree of crystallinity induced by stretching. The semi-quantitative agreement between DSC melting endotherms and measured internal energy changes during deformation support this conclusion. A quantitative analysis of the fraction of crystallinity at a particular elongation requires that the proportionality between internal energy changes and degree of crystallinity be known. Typically this proportionality constant is the heat of fusion, determined from independent, equilibrium measurements. The validity of using this heat of fusion

to estimate a crystalline fraction for stress-induced crystallinity is subject to the same constraints as those which apply to DSC determinations of polymer crystallinity in general. Since the unit cell for PTMO stress-induced crystallinity is identical to the isotropic unit cell for this polymer, the assumption of a constant heat of fusion may be reasonable.

The main source of uncertainty arises from the assumption that the internal energy changes measured in deformation calorimetry experiments are solely due to crystallization, i.e. quasi-ideal elastomer behavior is assumed even in the presence of crystallinity. As discussed in Chapter 2, volume contributions to the internal energy of elastomers are extremely small, and are justifiably negligible at large strains compared to the energy of crystallization. In the case of the two (or more) phase polyurethane-ureas, heats of phase mixing or hydrogen bonding need to be considered. However, calculations showed that these latter effects are on the order of 1/100 of the heat of fusion of the soft-segments.

All of the above arguments in hand, deformation calorimetry estimates of the degree of crystallinity based on tabulated heats of fusion suggest that a maximum of about 20 % w/w crystallinity, based on the weight of the polymer, can be generated by stretching the polyurethane-urea elastomers and natural rubber at room temperature,

this value increasing at lower temperatures and decreasing at higher temperatures.

Thermomechanical Behavior of Polyurethane-urea Elastomers and Natural Rubber

Isothermal Mechanical Behavior

At low elongations both of the polyurethane-urea elastomers exhibit essentially reversible behavior characterized by the absence of mechanical hysteresis and small reversible internal energy changes. Although the internal energy changes are small, some differences between the polyether and polyester soft-segment elastomers can be observed. In particular, it is found that the polyether elastomer exhibits zero order internal energy changes, while the polyester elastomer shows consistently negative internal energy changes on loading which are recovered on unloading for extension ratios less than 2. This has been tentatively assigned to reversible changes in the domain structure of the polyester elastomer which is thought to be less phase separated than the PTMO soft-segment elastomer judging from solubility parameter calculations. This conclusion is supported by dynamic mechanical analysis by

D.X. Wang (127) which shows an initial decrease in the glass transition of the polyester soft-segment phase at low elongations followed by an increase at an extension ratio of about 2. The decrease in T_g of the polyester soft-segments at extension ratios less than 2 can be interpreted to suggest phase demixing at low elongations, which was not observed in dynamic mechanical data of the PTMO soft-segment elastomer.

In contrast to the zero or slightly negative internal energy changes observed during extension of the polyurethane-urea elastomers, the single phase natural rubber shows reversible increases of internal energy with stretching to extension ratios less than 5, and an absence of mechanical hysteresis up to this extension. As suggested in the theory section, volume changes alone can be responsible for the internal energy changes in homogeneous rubbery solids. This further strengthens the phase demixing hypothesis for the polyurethane-ureas, which would be expected to exhibit the same dilatational behavior as natural rubber during deformation, resulting in an apparent increase in internal energy during stretching as opposed to the decrease typically observed.

Above critical extension ratios of 2, 2.5 and 6 for the polyether, polyester and natural rubber elastomers respectively a severe internal energy hysteresis is

observed which coincides with the onset of mechanical hysteresis. A sharp decrease in internal energy is seen to occur during isothermal loading at the above critical extension ratios, which indicates that stress-induced crystallization has begun. Unloading isothermally from strains within the stress-induced crystallization region traverses a completely different sequence of quasi-static stress and internal energy states, which reflect the persistence of stress-induced crystallinity to much lower strains than those required to initiate crystallization during loading. The observed hysteresis of stress and internal energy is quasi-static in the sense that the same stress-strain curve and internal energy path is obtained whether the isothermal loading / unloading process is achieved in an incremental or continuous manner. Deformation calorimetry data for both incremental and continuous loading/unloading confirm the relationship between mechanical hysteresis and the cumulative internal energy of the elastomer (as an indication of crystallinity) for all of the elastomers studied. A direct proportionality is in fact observed between the work lost in an isothermal stress-strain cycle and the change of internal energy between the two states of deformation, this appearing to hold for all strains and temperatures for all of the elastomers tested. The proportionality factor of $1/5$ suggests that this fraction of the heat of crystallization is

lost to the environment as unrecoverable work during each of the loading and unloading processes in which crystallization during stretching can occur. However, the internal energy is recoverable since the cyclic integral is zero for preworked samples.

Both the static and dynamic stress-strain curves of the elastomers in this study show an upswing during loading at about 8% crystallinity, implying that an unusually high degree of amorphous orientation accompanies the process of crystallization during stretching. This is thought to result from the increase in effective crosslinking as the initially long and thin crystallites grow perpendicular to the stretching direction, as indicated by WAXS. Constrained orientation of the hard segments due to this increased crosslinking or the formation of a three dimensional interconnected crystalline network during stretching cannot be discounted as perhaps primary sources of the upswing in stress. The rapid increase in internal energy of natural rubber at strains approaching break suggests an increase in distortional energy in the stress-induced crystallites or mechanical decrystallization of an interconnected crystalline network analogous to the drawing of polyethylene.

The lateral growth mode of stress-induced crystallinity during stretching appears to be a high energy route as deduced from thermodynamic arguments which favor a one-

dimensional growth mode in the direction of stress due to the apparent high end-surface free energy relative to the side-surface free energy of fringed micelle type crystallites. Morphological studies by other authors confirm the fringed micelle type structure for stress-induced crystallization, with axial growth limited to about 150 \AA . Consequently, equilibrium one-dimensional growth, though thermodynamically favored, is suppressed by the relatively slow kinetics of this process. The observed rapid nucleation and growth of stress-induced crystallization suggests that kinetic factors dictate the lateral growth mode in an effort to minimize the free energy of deformation, although this is only partially accomplished due to increased distortional energy in the preformed crystallites at higher extensions. The stress-strain curve during unloading follows a path of much reduced stress (compared to the loading curve) with evidence of a continuous melting/recrystallization process which delays complete decrystallization to much lower strain. A tentative explanation, consistent with the presence of a high energy metastable structure formed during stretching, would be that the unloading sequence facilitates a continuous restructurization whereby thermodynamically stable crystals are formed at the expense of the metastable phase. This is in agreement with the observed increase in thermal stability of the unloading states, and the fact that

preworking the sample at constant temperature results in a significant stress drop-implying one-dimensional recrystallization from an initially two or three dimensional structure. The unloading process therefor appears to release distortional energy bound in the metastable stress-induced crystallites and facilitates the approach to thermodynamic equilibrium as would occur by stretching the elastomer at high temperature and cooling slowly. The observed stress reduction of 1-3 MPa required to initiate decrystallization during isothermal unloading is consistent with these arguments, in that a certain amount of distortional energy must be released before melting and recrystallization can begin.

The above conclusions support the widely held belief that crystallization during stretching is an inherently non-equilibrium phenomenon. However, the formation of this secondary crosslinking network is responsible for the increased strength and energy to break of elastomers in general, and segmented elastomers in particular, which have a relatively weak system of physical crosslinking at low hard segment content.

Isomechanical Thermal Behavior

The thermal behavior of the polyurethane-urea elastomers was studied at fixed strain using stretch DSC and force versus temperature measurements. The following conclusions are obtained from these data.

Two distinct melting regions are observed on DSC thermograms of elastomers stretched at room temperature and held at fixed length during the DSC scan. One endotherm is centered around room temperature, and is essentially independent of strain. Melting of this type of crystallinity is reversible at fixed length. The term thermally-induced crystallinity (TIC) has been used to describe this structure, which is identical to the equilibrium oriented crystallinity normally obtained by cooling a stretched elastomer from above the melting temperature.

A second endotherm is observed on first scans of elastomers stretched at room temperature to above extension ratios of 2-2.5. The melting range of this type of crystallinity is between room temperature and 400 K, which is significantly higher than the equilibrium melting temperature of about 335 K reported for the polyether and polyester soft-segments in the pure state. This type of crystallinity which forms only during stretching has been referred to as stress-induced crystallinity (SIC), and accounts for the internal energy changes measured in room

temperature deformation calorimetry studies. Stress-induced crystallinity melts irreversibly and does not reappear on thermograms after first melting at fixed length, consistent with the above conclusions about the metastable nature of this type of crystallinity. However, stress-induced crystallinity does form and melt in a recoverable manner during loading and unloading at constant temperature, yielding no net internal energy change for the stress-strain cycle as observed from deformation calorimetry data.

The unusually high melting temperature of stress-induced crystallinity may be due to the high degree of local amorphous orientation which would accompany (or be responsible for) the upswing in the stress-strain curve during isothermal loading. In addition, the increased crystallite size observed on WAXS may contribute to the melting temperature elevation by decreasing the ratio of the surface/ bulk free energy of fusion.

Force versus temperature measurements at fixed length show , in order of increasing temperature: the glass transition of the polyurethane-urea elastomer soft-segments at about 220 K; a non-recoverable thermal yielding region beginning at room temperature in highly stretched elastomers; and the final loss of all mechanical integrity at 420 K, the latter being due to the melting of crystalline polyurea hard segments. The region of temperature

between about 330-420 K where the stress drops irreversibly at low elongations is probably due to the softening of glassy hard segments which should have a T_g around 330 to 350K. At high elongations, thermal softening can occur as low as room temperature, and is thought to be due to melting out of the metastable load-bearing SIC secondary network which forms at extension ratios above 2-3.

Polyurethane-urea Elastomers as Working Substances in Rubber Heat Engines

The two polyurethane-urea elastomers investigated in this study did not show any significant differences with regard to their ability to function as working substances in rubber heat engines. Under optimum conditions of small strain perturbation on top of large static strain, and at temperature differentials of 100 C, both of these elastomers can yield 1 J/g of useful work in the heat engine cycles used in this study. This translates into a power density of about 1.7 kilowatts/Kg elastomer in pilot scale heat engines turning typically at 100 RPM. Although the conversion efficiency of heat to work is only 3% of theoretical, it is typical of engines utilizing low-grade heat. Conversely, these materials functioning in

reversed cycles as heat pumps would be very efficient, especially in view of the large amount of heat transported by stress-induced crystallization and melting.

It was observed that power cycles obtained under conditions which promote stress-induced crystallization during the mechanical portions of the cycle do not yield useful work. This is not due to the phase transformation itself, which if conducted reversibly should increase the available work per cycle. Instead, it is the inherent non-equilibrium nature of the process which is responsible for the lost work.

Reversible thermally-induced crystallization and melting during the isomechanical portions of the cycle contributes to the available work at large static strains and small strain perturbations where stress-induced crystallization is avoided. Consequently, the phase change advantage of an enthalpy cycle is realized only under conditions which approach mechanical and phase equilibrium, as expected. The actual heat engine cycles of the polyurethane-urea elastomers can best be described as enthalpy-assisted entropy cycles.

Polyurethane-urea elastomers, by virtue of their chemical composition are ideally suited to repeated exposure to hot and cold water during actual heat engine operation. The best elastomer for heat engine applications, based on the previous conclusions would be composed

of crystallizable, moisture insensitive, stabilized rubbery segments such as the polyether or polyester soft-segments studied, which have a melting range for thermally-induced crystallinity between the source and sink temperatures. A narrow melting range would be most efficient. In addition, the elastomer should be free of thermally labile hard segments which promote softening at high cycle temperatures. Chemical crosslinking would be desirable, the optimum degree being a tradeoff between enhanced modulus and decreasing crystallizability.

Thermomechanical Behavior of the PBT/PTMO Thermoplastic Elastomer

The heat flows measured by deformation calorimetry during stress-strain loading of Hytrel are consistent with the standard linear viscoelastic solid model which has been used to describe the mechanical behavior of the continuous poly(butylene-terephthalate) hard-segment phase of this polymer. In contrast to the continuous soft-segment phase of the polyurethane-ureas, the continuous PBT hard segment phase deforms by an energy elastic mechanism, whereby mechanical energy is stored primarily as an increase of internal energy in the material. The possibility of a crystal-crystal transition contributing

to the unrecoverable internal energy after a deformation cycle is suggested from the calorimetric data.

Thermomechanics of Polyethylene Drawing

Deformation calorimetry shows that only 70% of the mechanical power during drawing of low density is evolved as heat. Consequently, 30% of this power is stored in the material as an increase of internal energy. Various mechanisms for the increase of internal energy of drawn polymers have been proposed by other authors who have studied drawing processes calorimetrically. These include crystallite distortion, increased surface area of crystallites and decreased amorphous density. Some general conclusions can be drawn from the present study with regard to possible deformation mechanisms. First, it is observed that over three decades of strain rate the heat flow varies as the first power of the mechanical energy. Since the yield and drawing stress are found to be independent of strain rate, this means that the heat flow is linearly proportional to the strain rate. This suggests that viscous dissipation, in which the heat flow should go as some higher power of the strain rate (Newtonian = 2), is not operable. This is not surprising considering that cold drawn polymers, when heated above

the glass or melting temperature, recover essentially 100% of their initial length.

Complete recovery or memory in drawn polymers implies a rubber elastic deformation process, for which the heat flow would be expected to go as the first power of the strain rate. This is in fact observed for polyethylene which is essentially a semi-crystalline rubber.

From the magnitude of the pressure changes in the calorimeter, a temperature rise in the necking zone of .01-1 degree centigrade are inferred. Clearly, melting in the sense of thermally induced fusion is not a necessary condition for restructurization of the crystalline morphology in passing through the necking zone. An alternative explanation could be deformation induced isothermal decrystallization as is observed in the elastomers of this study at ultimate elongations. If decrystallization were not followed by an identical amount of crystallization, an internal energy change in the material would be expected. The increase in internal energy suggests that recrystallization is incomplete. Calculations show that a decrease in polyethylene crystallinity of only about 2-3% can account for all of the internal energy increase in this polymer.

REFERENCES

1. J.E. Mark, Polym.Eng.& Sci., 19(6). 409 (1979)
2. T.L. Smith, Polym.Eng.& Sci., 17(3),129 (1977)
3. R. Caspary and H.W. Schnecko, Makromol.Chem.,182, 2109 (1980)
4. G.L. Clark, M. Kabler, E. Blaker and J.M. Ball, Rubb.Chem.Techn., 14(1), 27 (1941)
5. W.B. Wiegand and J.W. Snyder, I.R.I. Trans.,10, 234 (1934)
6. L. Mandelkern, "Crystallization of Polymers," Ch.7, McGraw-Hill Inc., New York, 1963
7. R.J. Farris, Polym.Eng. & Sci., 17(10),737 (1977)
8. P.J. Flory, J.Chem.Phys., 15(6), 397 (1947)
9. K.J. Smith, Polym.Eng. & Sci., 16(3), 168 (1976)
10. I.N. Sneddon, "The Linear Theory of Thermo-elasticity," Ch.1, Springer-Verlag, New York,1974
11. P. Debye, Wolfshehl Lectures, 1914
12. R.E. Barker Jr.,J.Appl.Phys.,38(11),4234 (1967)
13. F.H. Muller, Proc.Fifth Int.Cong.Rheol., S.Onogi, ed., Vol.1, 61, University Park Press, Baltimore, Maryland, 1969
14. H.G. Killian and G.W. Hohne, Thermochemical Acta., 69, 199 (1983)
15. F.H. Muller, "Rheology," Vol.V, 474, F.R.Eirich,ed., Academic Press, New York, 1969
16. D. Goritz and F.H. Muller, Coll.& Polym.Sci.,253, 844 (1975)
17. Yu. K. Godovskii, Coll. & Polym.Sci.,260,461 (1982)

18. R.E. Lyon and R.J. Farris, *Polym. Eng. & Sci.*, **24**(11), 908 (1984)
19. G. Gee, *Trans. Far. Soc.*, **42**(8), 585 (1946)
20. P.J. Flory, "Principles of Polymer Chemistry," Ch.9, Cornell University Press, Ithaca, 1953
21. D. Goritz and F.H. Muller, *Koll. Z u Z. Polym.*, **251**, 679 (1973)
22. Yu. K. Godovskii, *Polymer*, **22**, 75 (1981)
23. G. Gee, J. Stern and L.R.G. Treloar, *Trans. Far. Soc.*, **46**, 1101 (1950)
24. K.H. Meyer and A.J.A. van der Wyk, *Helv. Chim. Acta.*, **29**, 1842 (1946)
25. H. Reiss, "Methods of Thermodynamics," Ch.8, Blaisdell Publ. Co., New York, 1965
26. F.H. Muller and N. Weimann, *J. Polym. Sci.*, **C6**, 117 (1964)
27. N.G. Gaylord, ed., "Polyethers," Part 1, Wiley-Interscience, New York, 1963
28. R. Pivalko, *Sint. Fiz-Khim. Poim.*, **14**, 95 (1974)
29. I.J.W. Bowman, D.S. Brown and R.E. Wetton, *Polymer*, **10**(8), 715 (1969)
30. T. Stankunas, R.J. Farris and F.E. Karasz, *Bull. Am. Phys. Soc.*, **24**(3), 259 (1979)
31. E.M. Hicks, A.J. Ultee and J. Drougas, *Science*, **147**(3656), 373 (1965)
32. R.A. Gregg, "Encyclopedia of Chemical Technology," Vol.18, 614. 1969
33. J. McPherson, *Bur. Stds. J. Res. Wash.*, **8**, 751 (1982)
34. D.E. Roberts and L. Mandelkern, *J. Am. Chem. Soc.*, **77**, 731 (1955)
35. Dr. Brodt, private communication, Dupont Co. Inc., Polymer Products, Wilmington, Delaware

36. L. Jelinski, F.C. Schilling and F.A. Bovey, *Macromolecules*, 14(3), 581 (1981)
37. J. Gough, *Proc.Lit.& Phil.Soc., Manchester*, 2nd Ser., 1, 288 (1805)
38. J.P. Joule, *Trans.Roy.Soc.(London)*, A149, 91 (1859)
39. J.P. Joule, *Philos.Trans.*, 149, 91 (1859)
40. K.T. Compton and D.B. Webster, *Phys.Rev.*, 5, 159 (1915)
41. W. Swietoslowski, "Microcalorimetry," Reinhold Publ., New York, 1946
42. H. Esser, H. Cornelius and W. Banck, *Arch. Eisenhuttenw*, 9, 529 (1935)
43. H.L. Callendar and H.T. Barnes, *Phys.Rev.*, 10, 202 (1900)
44. G.I. Taylor and H. Quinney, *Proc.Roy.Soc.(London)*, A143, 307 (1934)
45. H. Quinney and G.I. Taylor, *Proc.Roy.Soc.(London)*, A163, 157 (1937)
46. F.H. Muller and A. Engelter, *Rheol.Acta.*, 1, 39, (1958)
47. A.A. Schlierermacher, *Ann.Physik.*, 34, 623 (1888)
48. L. Morbitzer, G. Hentze and R. Bonart, *Koll.Z. u Z. Polym.*, 216/217, 137 (1967)
49. H.O. Foster and R.E. Benner, *Proc.Fourth Int. Cong.Rheol., Part 2*, 121, Interscience Publ., New York, 1965
50. H.S. Carslaw and H.C. Jaeger, "Conduction of Heat in Solids," 2nd Ed., Oxford University Press, London, 1959
51. C. Price, K.A. Evans and F. deCandia, *Polymer*, 14, 339 (1973)
52. E. Calvet and H. Pratt, "Recent Progress in Microcalorimetry," MacMillan Co., New York, 1963

53. K.H. Schonborn, *Thermochemica Acta.*, **69**, 103 (1983)
54. W. Zielenkiewicz, in *Proc. First Int. Conf. Calorim. and Thermodynamics (Warsaw)*, Polish Scientific Publ., Poland, 1969
55. Yu.K. Godovskii, G.L. Slonimskii and V.F. Alekseyev *Polymer Science U.S.S.R.*, **11**(5), 1345 (1969)
57. G.W.H. Hohne, H.G. Killian and P. Trogele, "Thermal Analysis," Vol. II, 955, B. Miller, ed., John Wiley & Sons, New York, 1982
58. I.J. Duvdevani, J.A. Biesenberger and C.G. Gogos, *Polym. Eng. & Sci.*, **9**(4), 250 (1969)
59. I.J. Duvdevani, J.A. Biesenberger and C.G. Gogos, *Polym. Eng. & Sci.*, **10**(6), 320 (1970)
60. J.W. Maher, R.N. Hayward and J.N. Hay, *J. Polym. Sci., Polym. Phys. Ed.*, **18**, 2169 (1980)
61. S.B. Warner, *J. Appl. Polym. Sci.*, **29**, 219 (1984)
62. E.R.G. Eckert and R.M. Drake Jr., "Heat and Mass Transfer," 2nd Ed., McGraw-Hill, New York, 1959
63. H. Gregory and T. Archer, *Proc. Roy. Soc. (London)*, **A110**, 113 (1926)
64. R.P. Dring and B. Gebhart, *J. Heat Transf.*, **88**, 246 (1966)
65. D. Goritz, F.H. Muller and W. Sietz, *Progr. Coll. & Polym. Sci.*, **62**, 114 (1977)
66. R.E. Lyon, R.J. Farris and W.J. MacKnight, *J. Polym. Sci.: Polym. Lett. Ed.*, **21**, 323 (1983)
67. L.E. Alexander, "X-Ray Diffraction Methods in Polymer Science," p.157, Wiley-Interscience, New York, 1969
68. P. Scherrer, *Gottegen Nachrichten*, **2**, 98 (1918)
69. R. Hosemann and S.N. Bagchi, "Direct Analysis of Diffraction by Matter," North Holland, Amsterdam, 1962
70. L.E. Alexander, S. Ohlberg and G.R. Taylor, *J. Appl. Phys.*, **26**(9), 1068 (1955)

71. J.M. Goppel and J.J. Arlman, *Appl.Sci.Res.*, **A1**, 462 (1949)
72. S.C. Nyberg, *Brit.J.Appl.Phys.*, **5**, 321 (1954)
73. W.Sietz, D.Goritz and F.H.Muller, *Coll.& Polym.Sci.*, **252**, 854 (1974)
74. W. Sietz, D. Goritz and F.H. Muller, *Progr.Coll. Polym.Sci.*, **64**, 267 (1978)
75. J.C. Mitchell and D.J. Meier, *J.Polym.Sci.*, **A2(6)**, 1689 (1968)
76. F. deCandia, R. Gennaro and V. Vittoria, *Makromol. Chem.*, **175**, 2983 (1974)
77. H.G. Kin and L. Mandelkern, *J.Polym.Sci.*, **A2(6)**, 181 (1968)
78. Yu.K.Godovskii and N.P.Bessonova, *Coll.Polym.Sci.*, **261**, 645 (1983)
79. E.S.W. Kong and G.L. Wilkes, *J.Polym.Sci.:Polym. Lett.Ed.*, **18**, 369 (1980)
80. R. Bonart and E.H. Muller, *J.Macromol.Sci.*, **B10(2)**, 345 (1974)
81. L. Morbitzer and R. Bonart, *Koll.Z. u Z.Polym.*, **232(2)**, 764 (1969)
82. N. Bekkedahl, *Rubb.Chem.Techn.*, **40(3)**, 25 (1967)
83. L. Morbitzer and H. Hespe, *J.Appl.Polym.Sci.*, **16**, 2697 (1972)
84. F. deCandia, G. Romano, R. Russo and V. Vittoria, *J.Polym.Sci.:Polym.Phys.Ed.*, **20**, 1525 (1982)
85. L.R.G. Treloar, *Trans.Far.Soc.*, **43**, 277 (1947)
86. W.L.Ko and P.J.Blatz, *Proc.Fourth Int.Cong.Rheol.*, p.35, Interscience Publ., New York, 1965
87. P.H. Lindenmeyer, *J.Polym.Sci.:Polym.Phys.Ed.*, **17**, 1965 (1979)
88. P.H. Lindenmeyer, *Polym. Eng.Sci.*, **19(6)**, 386 (1979)

89. W. Strohmeier and W.F. Frank, *Coll.Polym.Sci.*, 260, 937 (1982)
90. B.T. Chu, "A Critical Review of Thermodynamics," p.299, E.B. Stuart and B. Gal-Or, eds., *Mono Book*, Baltimore, Maryland, 1970
91. P.W. Bridgman, *Rev.Mod.Phys.*, 22(1), 56 (1950)
92. H.W. Siesler, *Makromol.Chem.*, 180, 2261 (1979)
93. K.Tashiro, Y.Nakai, M.Kobayashi and H.Tadokoro, *Macromolecules*, 13, 137 (1980)
94. "Polymer Handbook," J.Brandrup and E.H.Immergut, eds., *Interscience*, New York, 1966
95. S.N. Chvalun, A.N. Ozerin, Yu.K. Zubov, Yu.K. Godovskii, N.F. Bakeyev and A.A. Baulin, *Polymer Science U.S.S.R.*, 23(6), 1529 (1981)
96. C. Gerth and F. H. Muller, *Koll.Z. u Z. Polym.*, 251, 857 (1973)
97. W.G. Perkins and R.S. Porter, *J.Mat.Sci.*, 12, 2355 (1977)
98. D. Goritz and F.H. Muller, *Coll.Polym.Sci.*, 253 844 (1975)
99. D.J. Dunning and P.J. Pennels, *Rubb.Chem.Techn.*, 40(5), 1381 (1967)
100. M. Cesari, L. Gargani, G.P. Giuliani, G. Perego and A. Zazzeta, *J.Polym.Sci.:Polym.Lett.Ed.*, 14 107 (1976)
101. M. Cesari, G. Perego, A Zazzeta and L. Gargani, *Makromol.Chem.*, 181, 1143 (1980)
102. T.L. Hill, "Thermodynamics of Small Systems," Part 1, Ch.5, W.A. Benjamin Inc. Publ., New York, 1963
103. R.E. Lyon, D.X. Wang and R.J. Farris, to be published
104. M.Cesari, G.Perego and A.Mazzei, *Makromol.Chem.*, 83, 196 (1965)

105. K. Imada, T. Miyakawa, Y. Chatani, H. Tadokoro and S. Murakashi, *Makromol.Chem.*, **83**, 113 (1965)
106. R. Bonart, *J. Macromol. Sci.-Phys.*, **B2(1)**, 115 (1968)
107. J.F.M. Oth and P.J. Flory, *J. Am. Chem. Soc.*, **80**, 1297 (1958)
108. E.H. Andrews, *Proc. Roy. Soc.*, **A277**, 562 (1964)
109. D. Luch and G.S.Y. Yeh, *J. Appl. Phys.*, **43(11)** 4326 (1972)
110. H.G. Zachman, *Koll. Z. u Z. Polym.*, **216/217**, 180, (1967)
111. H.G. Zachman, *Koll. Z. u Z. Polym.*, **231**, 504 (1969)
112. D.E. Bosley, *J. Polym. Sci.*, **C(20)**, 77 (1967)
113. C.B. Wang and S.L. Cooper, *Macromolecules*, **16**, 775 (1983)
114. S. Yoshida, H. Suga and S. Seki, *Polym. J.*, **5(1)**, 25 (1973)
115. T. Okino, M. Maruta and K. Ito., "Thermal Analysis," Vol. 1, p. 321, B. Miller, ed., John Wiley & Sons, New York, 1982
116. T. Nose, *J. Soc. Rubb. Ind. Japan*, **144**, 961 (1971)
117. F.T. Wall and D.G. Miller, *J. Polym. Sci.*, **13**, 157 (1954)
118. F. de Candia, R. Russo and V. Vittoria, *J. Polym. Sci: Polym. Phys. Ed.*, **20**, 1175 (1982)
119. R.S. Stein, S. Krimm and A.V. Tobolsky, *Text. Res. Journal*, **19(1)**, 325 (1949)
120. N.S. Schneider and C.S. Paik Sung, *Polym. Eng. Sci.*, **17(2)**, 73 (1977)
121. H. Ishihara, I. Kimura, K. Saito and H. Ono, *J. Macromol. Sci.- Phys.*, **B10**, 591 (1974)
122. D.E. Roberts, L. Mandelkern and P.J. Flory, *J. Am. Chem. Soc.*, **79**, 1515 (1957)

123. L. Mandelkern, D.E. Roberts, A.F. Diorio and A.S. Posner, *J.Am.Chem.Soc.*, **81**, 4148 (1959)
124. L. Mandelkern and D.E. Roberts, U.S. Pat.No. 3,090,735, May 21, 1963
125. R.J. Farris and R.E. Lyon, *Mat. & Soc.*, **8**(2) 239 (1984)
126. R.E.Lyon, D.X.Wang, R.J.Farris and W.J.Macknight, *J.Appl.Polym.Sci.*, **29**, 2857 (1984)
127. D.X. Wang, R.E. Lyon and R.J. Farris, presented at Twenty-second Canadian High Polymer Forum, Univ.Waterloo, Waterloo, Ontario, Canada, Aug. 10-12, 1983

